ΑΡΙΣΤΕΙΔΗΣ ΣΤΑΥΡΟΥ

ΣΧΟΛΗ ΜΗΧΑΝΟΛΟΓΩΝ ΜΗΧΑΝΙΚΩΝ

Μελέτη ημι-εμπειρικού μοντέλου εκτονωτή σε μονοφασικές και διφασικές ροές

Τομέας: Θερμότητας

Επιβλέπων: Σωτήριος Καρέλλας, Καθηγητής ΕΜΠ

Αθήνα 2020

ARISTEIDIS STAVROU

SCHOOL OF MECHANICAL ENGINEERING

Investigation of a semi-empirical expander model in single- and two-phase region

Section: Thermal Engineering

Supervisor: Sotirios Karellas, Professor

Athens 2020

Preface

I am grateful to Professor Sotirios Karellas, for giving me the opportunity to work on this very interesting subject.
I am also grateful to PhD Candidate Tryfonas Roumpedakis for his guidance and assistance during the whole period of this work. His help was the key element to successfully complete this work and I am very glad to have the opportunity to cooperate with him. I would also like to thank PhD candidate Antonios Charalampidis for his valuable help on the model development and MSc student Evropi Monokrousou for her advices on the report composition.
I thank my family for their support and encouragement during my studies.

<u>Υπεύθυνη δήλωση</u> για λογοκλοπή και για κλοπή πνευματικής ιδιοκτησίας:

Έχω διαβάσει και κατανοήσει τους κανόνες για τη λογοκλοπή και τον τρόπο σωστής αναφοράς των πηγών που περιέχονται στον οδηγό συγγραφής Διπλωματικών Εργασιών. Δηλώνω ότι, από όσα γνωρίζω, το περιεχόμενο της παρούσας Διπλωματικής Εργασίας είναι προϊόν δικής μου εργασίας και υπάρχουν αναφορές σε όλες τις πηγές που χρησιμοποίησα.

Ονοματεπώνυμο

Αριστείδης Σταύρου

Contents

Σύνοψη

Ο Οργανικός Κύκλος Rankine (ORC) είναι μια πολλά υποσχόμενη τεχνολογία για την εκμετάλλευση πηγών θερμότητας χαμηλής θερμοκρασίας με σκοπό την παραγωγή ηλεκτρικής ενέργειας. Σημείο κλειδί στη συνολική απόδοση του κύκλου αποτελεί ο εκτονωτής. Στην παρούσα διπλωματική εργασία μελετήθηκε εκτενώς η απόδοση εκτονωτών βάσει ενός ημι-εμπειρικού μοντέλου. Χαρακτηριστικά αυτού του μοντέλου είναι το χαμηλό υπολογιστικό κόστος αλλά και η προσαρμοστικότητά του σε διάφορους τύπους εκτονωτών λόγω ενός συνόλου παραμέτρων που χρησιμοποιεί. Για να έχουμε ωστόσο μια ασφαλή εικόνα και έναν ακριβή υπολογισμό της απόδοσης ενός εκτονωτή είναι απαραίτητη η δημιουργία ενός ντετερμινιστικού μοντέλου, το οποίο όμως αποτελεί υψηλό υπολογιστικό κόστος. Το ημι-εμπειρικό μοντέλο χρησιμοποιήθηκε για να συγκριθούν επιλεγμένα μοντέλα εκτονωτών της βιβλιογραφίας. Τα αποτελέσματα έδειξαν ικανοποιητική προσέγγιση της απόδοσης με μια μέση απόκλιση της τάξης του 6% για όλες τις μελέτες της βιβλιογραφίας που αξιολογήθηκαν. Επιπλέον, μελετήθηκε η συμπεριφορά του μοντέλου στη λειτουργία με διαφορετικό ψυκτικό μέσο από αυτό που ήδη χρησιμοποιούνταν στα συστήματα ORC. Λόγω των ολοένα και πιο αυστηρών περιβαλλοντικών περιορισμών στην επιλογή ψυκτικών μέσων, οδηγούμαστε σε επιλογή ψυκτικών χαμηλού GWP, με τα R1234ze(E) και R1233zd(E) να αποτελούν δύο από τις επιλογές οι οποίες μελετήθηκαν και στην εργασία. Τέλος, το μοντέλο χρησιμοποιήθηκε για εκτόνωση στη διφασική περιοχή. Τα αποτελέσματα έδειξαν ότι το μοντέλο δεν μπορεί να προσεγγίσει ικανοποιητικά τη λειτουργία του εκτονωτή, χρησιμοποιώντας σημεία λειτουργιάς διφασικής ροής για να υπολογιστούν οι παράμετροι, καθώς σημειώθηκε ένα μέσο σφάλμα ίσο με 20% και μέγιστη απόκλιση της τάξης του 52%.

Abstract

The Organic Rankine Cycle (ORC) is a promising technology to utilize low grade heat sources and generate electric power. The efficiency of the cycle is strongly connected with the expander's efficiency. In this work the prediction of the expander's performance has been studied extensively. The modelling has been conducted with a semi-empirical model which has low computational time and it is easily customizable in different types of expanders. On the other hand, a deterministic model would be much more accurate but requires high computational time. The semi-empirical model was used to compare different expander models from the literature. The prediction was satisfying with an average error between measured and predicted efficiency of 6% for both of the studied literature expander models. Also, has been evaluated the operation with alternative working fluids compared to the existing fluids that the ORC systems used. Due to EU regulations, new systems tend to be designed for low-GWP refrigerants, with R1234ze(E) and R1233zd(E) are two of the most promising organic fluids and therefore considered in this study. Finally, the semi-empirical model was evaluated in the two-phase expansion. The results have shown that the performance of the expander cannot be predicted adequately because there was a deviation which reached the value of 52% and an average error equal to 20%.

Nomenclature

A	*Area*	$[m^2]$
AU	*Heat transfer coefficient*	$[W/K]$
h	*Specific enthalpy*	$[J/kg]$
$\dot{m}$	*Mass flow rate*	$[kg/s]$
N	*Rotational speed*	*[rpm]*
P	*Pressure*	*[Pa]*
$\dot{Q}$	*Heat transfer rate*	*[W]*
r	*Ratio*	-
s	*Specific entropy*	$[J/kgK]$
T	*Temperature*	*[°C]*
T	*Torque*	$[N \cdot m]$
v	*Specific volume*	$[m^3/kg]$
$\dot{V}$	*Volume flow rate*	$[m^3/s]$
$\dot{W}$	*Power*	*[W]*
Greek Symbols		
η	*Efficiency*	-
Subscripts		
ad	*Adapted*	
amb	*Ambient*	
calc	*Calculated*	
crit	*Critical*	
ex	*Exhaust*	
exp	*Expander*	
in	*Internal*	
leak	*Leakage*	
meas	*Measured*	
n	*Nominal*	
is	*Isentropic*	
s	*Swept*	
su	*Supply*	
thr	*Throat*	
w	*Wall (envelope)*	

1. Introduction

1.1 Introduction in turbomachinery

Turbomachines are considered all devices which transfer energy to or from a continuously flowing fluid by the dynamic action of their moving blade rows. Essentially, a rotating blade row changes the stagnation enthalpy of the working fluid via positive or negative work, depending on the requirements of the machine. The two main categories of turbomachines can be divided into those which absorb energy to increase the pressure or head (if it is regarded as incompressible fluid) and those which produce energy by expanding the fluid to a lower pressure or head.

Turbomachines can also be categorized according to the flow path through the stages of the rotor. Firstly, there is axial flow turbomachines (Figure 1(a)) in which the flow is mainly parallel to the axis. Secondly, there are radial flow machines (Figure 1(c)) where the through-flow is in a plane perpendicular to the rotation axis. Also, there are the mixed flow machines (Figure 1(b)) which are widely used and the through-flow is both axial and radial to the rotation axis.

Lastly, turbomachines are classified as impulse or reaction, according to the location where the pressure alteration occurs, respectively. In an impulse machine all the pressure drop takes place in nozzles and the fluid is being directed onto the rotor. The Pelton turbine (Figure 1(d)) is a typical example of an impulse machine.

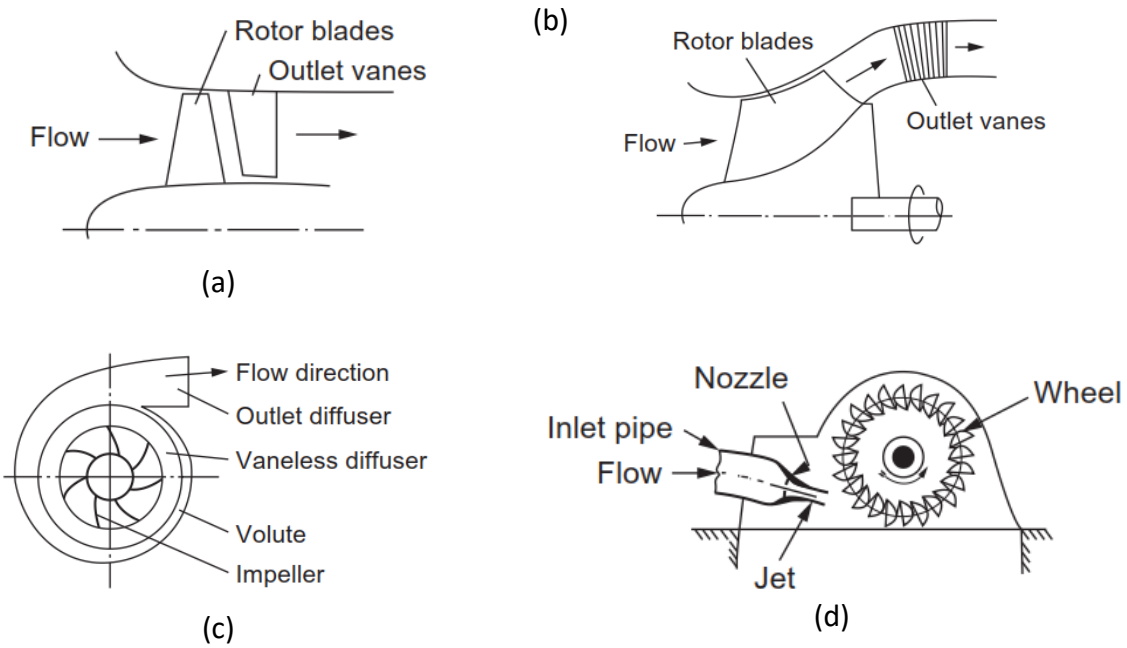

Figure 1: (a) Single Stage axial flow compressor or pump, (b) Mixed flow pump, (c) Centrifugal Compressor or Pump, (d) Pelton wheel.

1.2 Compressors

In the conventional vapor compression cycle, the compressor is used to increase the pressure of the working fluid from the evaporating pressure up to the condensation pressure as well as to circulate the fluid in the cycle. Based on the working principle, compressors are divided into two main categories: positive displacement and dynamic compressors. The main difference between the two is that, in positive displacement compressors, the work exchange takes place periodically by trapping parts of the flow in cavities, pressurizing and moving it from the inlet to the outlet of the compressor. On the other hand, in a dynamic compressor the compression takes place continuously. For small-scale applications, more favorable are considered the positive displacement compressors because of their lower design volumes, higher pressure ratios and lower rotational speed in comparison with dynamic compressors.

1.3 Expanders

The overall efficiency of the test-rig is strongly dependent on the efficiency of the expander. Expanders can be divided into two main categories; Turbines and positive displacement. Generally, axial flow machines are chosen for large-scale applications because of their high working fluid flow rates. In case of small-scale power output, the rotating speed of axial turbine increases dramatically, so radial flow machines are preferred, which have higher pressure ratios for much lower rotating speeds than turbo-machines. However, in radial flow it is difficult to assemble several stages and its operation range with high efficiency is limited. As a result, in small-scale applications positive displacement expanders are widely used, which combine the following advantages. Firstly, the rotational speed is proportional to the suction volume of the working fluid, so there is no need of a gearbox. Secondly, these expanders can operate at high pressure ratios that are directly depended by the volume ratio. In contrast with dynamic turbomachines, positive displacement expanders can work in two-phase area. The main types of positive displacement expanders are scroll, screw, piston and root (vane) expanders. In Figure 2, are presented the aforementioned categories.

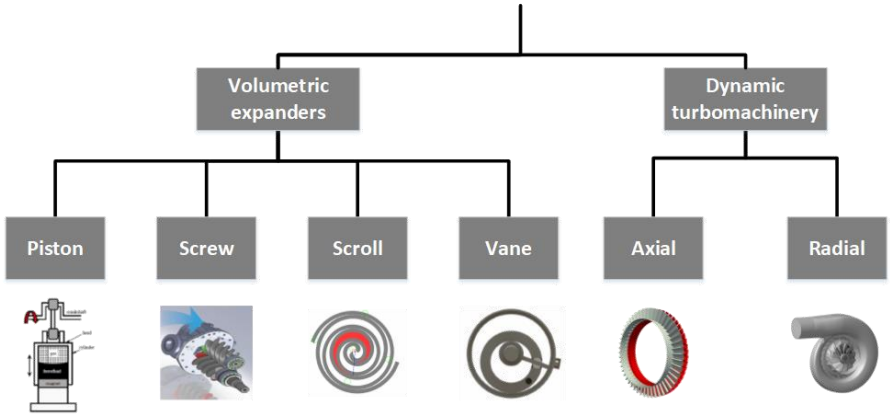

Figure 2: Types of expanders

1.3.1 Scroll expanders

In comparison with other positive displacement expanders, scroll expanders are widely used on small-scale applications, because of their high efficiency, tolerance in two-phase conditions, fewer moving parts, low cost, wide output power range and broad availability. The scroll expander shows the highest isentropic efficiency, which can reach 76% [1], compared with other displacement expanders. The scroll expander consists of two interleaving scrolls, a moving and a fixed one. The principle of the scroll expander consists of the working fluid entering at the center of the two scrolls, at high temperature and pressure, so the moving scroll is forced to move. Subsequently, the fluid moves towards areas where the volume between of the two scrolls has been increased. The majority of scroll expanders are commercial scroll compressors that have been modified and driven in reverse mode.

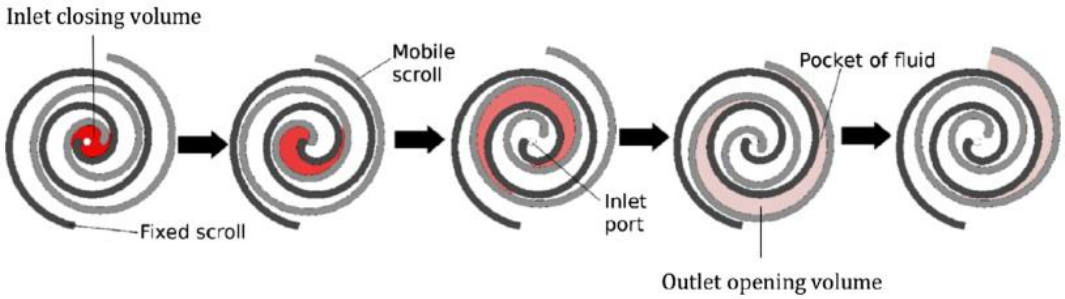

Figure 3: The principle of a scroll expander[2]

Two effects that can reduce the efficiency of the expansion process; over-expansion and more often, under-expansion. Under-expansion can occur when the pressure in the expansion chamber at the end of the expansion, is higher than the gradient pressure. In contrast, over-expansion occurs when the gradient pressure is higher than the pressure at the end of the expansion and the fluid flowing back in discharging pipe.

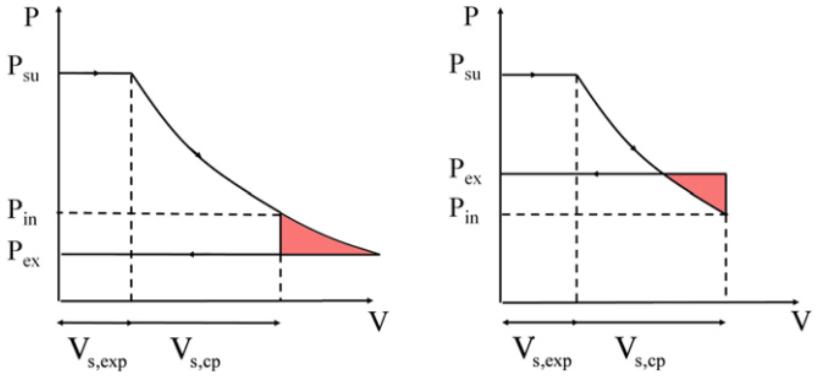

Figure 4: Pressure-volume diagram (under-expansion (left) and over-expansion (right)).

As a result, the expansion ratio constitutes a main parameter in the selection of the expander. To optimize the performance, minimizing the over-expansion or under-expansion losses, the built-in volume ratio should match with the operating conditions. The maximum shaft power and isentropic efficiency of scroll machines also depends on the selection of the working fluid, rotational speed, mechanical and leakage losses and internal heat transfer effects.

1.3.2 Screw expander

Among the different types of volumetric expanders, the screw-type presents high isentropic efficiency combined with high internal volume ratios. Similar to scroll expanders, screw-expander are also used in test-rigs with wet vapor expansion. The expander consists of a pair of meshing helical screw rotors. Its operation principle is based on changes of volumetric rates on three dimensions. The starting point of expansion take place in the top edge of the rotors, where fluid with high pressure is supplied and moves towards the rear edge by increasing its volume. In a complete revolution of the chambers, the volume of the chamber is maximum and extends along the entire length of the screws. The fluid flows from the high-pressure to the low-pressure edge and forces the helical screw rotors to move, while the axis of the main rotor is coupled to a generator, producing the output electric power.

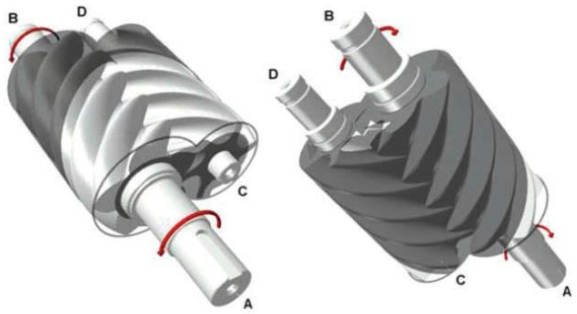

Figure 5: The principle of a scroll expander

The expander can work as compressor by changing the rotating direction, or even in the same direction by reversing the suction and discharge ports. The casing of the rotors allows this type of expanders to have negligible clearance volume at the high-pressure port, which means low leakages. Furthermore, the space between the screws is essential for the efficiency, in order to minimize the available passage of working fluid which does not produce work. An additional design approach to maximize the fluid displacement per revolution, is to enlarge the passages between the lobes as much as possible. Because of the contact between the screws, the contact forces must be taken into account due to the friction losses. Consequently, the contacts among the moving parts should be low. The lubrication of the rotor and bearing is accomplished by mixing the working fluid with oil, which is separated after the expansion in the separator tank.

Screw expanders present some advantages over other displacement expanders. Firstly, due to continuous rotation of all moving parts during the expanding process, they can reach much

higher rotational speeds. In contrast with vane expanders, screw expanders are widely used, because contact forces within them are low, making them very reliable.

1.3.3 Piston expanders

A piston expander consists of two cylinders which create four chambers. The high-pressure working fluid flows from the edge of each chamber (1, 4) towards the center (2, 3) and forces the piston to move. The efficiency is lower than the other types (always below 70% [1]) and cannot operate under high liquid fractions. Because of their operational principle, piston expanders are compatible with low displacement rates and low output power. Their advantage is that they can handle high temperatures and pressures at the suction. Also, present high volumetric ratios which are efficient for some applications. There are several investigations which improve the efficiency, such as expansion in stages with three coupled pistons, but the cost and complexity of this manufacturing is highly increased. In this case, the lubrication is performed by the oil mixed with the working fluid which is also separated after the expansion in an external circuit.

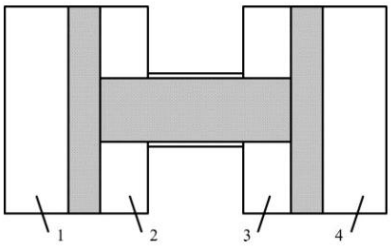

Figure 6: Piston expander

1.3.4 Other types

Another type of expander, which is a variation of piston expander, is vane expander. It consists of a chamber, cylinder shaped, in which both the suction and discharge of the working fluid are conducted. The fluid forces a rolling piston and rotates the power shaft. The efficiency of the vane type expander is about 50% [3], which is considerably low because of the high friction losses at the contact between the vane and the rolling piston.

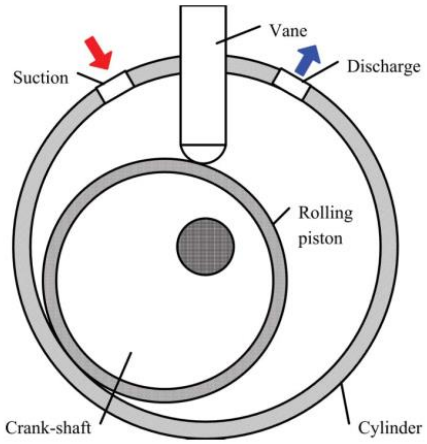

Figure 7: Vane expander

1.4 ORC technology

The environmental concerns and energy sustainability have rapidly grown the interest in the utilization of low-grade energy (80-200°C). Therefore, new solutions were needed to exploit these waste heat sources and produce electricity. The most widely used solution, is the Organic Rankine Cycle (ORC). This cycle is similar to traditional Rankine Cycle with the difference that, instead of water, it uses an organic product as working fluid. The capability to utilize low-grade energy sources is given by the lower evaporating temperature of organic fluids compared to water. The ORC solution is attractive and widely applicable in small scale decentralized systems. The heat source may be geothermal, solar energy, heat from biomass combustion, even if the waste heat from a diesel engine etc.

The main elements of the system are the pump which circulates the working fluid and supply the evaporator which is used to evaporate the working fluid by conducting thermal energy from the heating source. A key element for overall performance of the ORC system is the expander which expands the high pressure and temperature fluid to produce the useful power. The cycle completes with the condenser which is supplied with the expanded fluid and condense it to be circulated the pump.

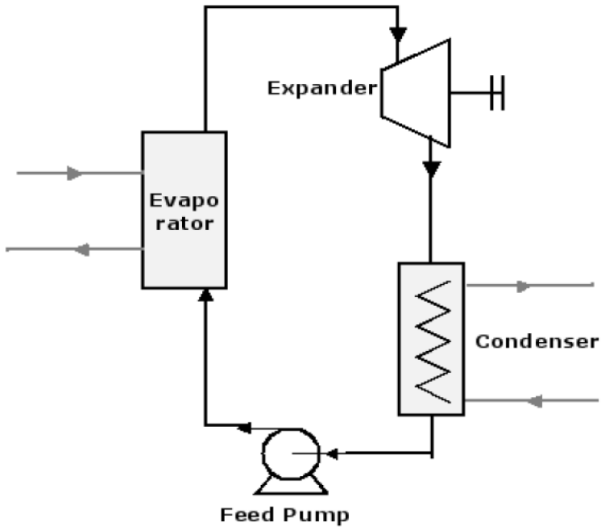

Figure 8: Schematic of ORC system [2]

In Figure 9, is presented an operation case of ORC. The process 1-2 represents the pressurization by the pump, 2-3 the evaporation and superheat, 3-4 the expansion and 4-1 the condensation of the working fluid. In recent years has been developed supercritical ORC systems with CO_2 as working fluid. Apparently, in subcritical process the fluid is preheated, evaporated and then superheated. In case of supercritical the fluid is completely out of saturation curve.

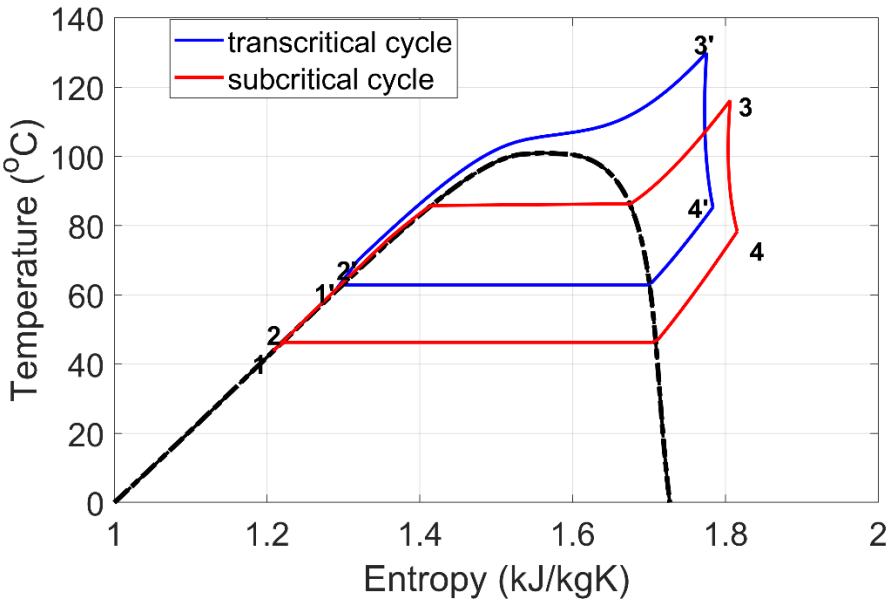

Figure 9. T-s diagram of ORC system

The ORC cycle may be modified by adding recuperator at the expander outlet which is used for utilizing the heat of the superheated vapor. Thereinto, occurs the preheat of fluid at the inlet of economizer. In Figure 10 is presented an ORC scheme with recuperator. By providing heat to the fluid, it reduces the required heat from external source, but the produced power remains at the same level, as a result increasing the efficiency of the cycle.

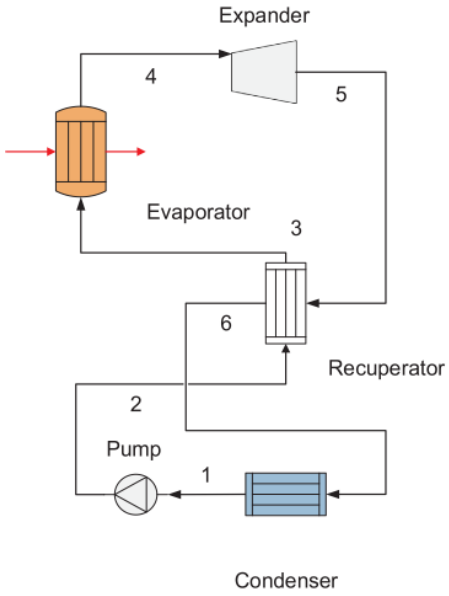

Figure 10: ORC system with recuperator [4]

In Figure 11 is illustrated the comparison between saturation temperatures and some organic fluids and it is a key criterion for selection between different organic fluids. The selection of organic fluid also based on the effect on ozone layer (ODP value) and global warming (GWP).

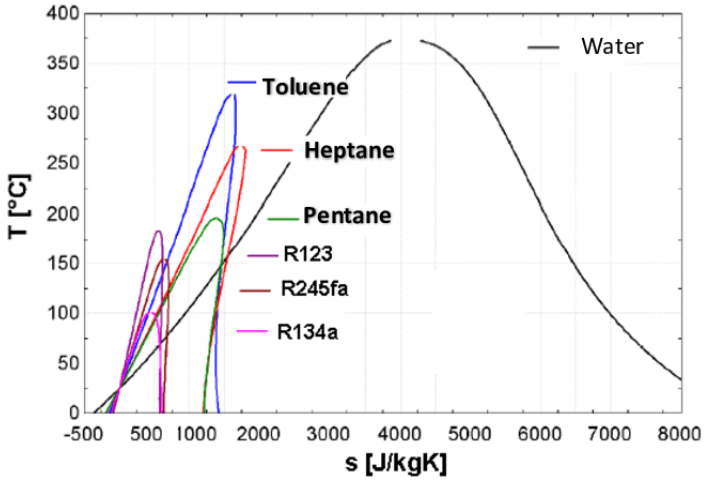

Figure 11: T-s diagram for water and organic fluids. [2]

Due to decentralized use of biomass, ORC is a promising technology for biomass utilization. This technology is ideal for producing power less than 1 MW [2], although the low electric efficiency it is preferable to be used for combined heat and power plants. A competitive technology to ORC is the gasification where the biomass transformed to H_2, CH_4, CO_2, CO and tars which removed. This technology is expensive and the high capital and operation-maintenance costs, make it unprofitable.

Geothermal sources with temperature below of 300°C can be utilized with ORC technology. Due to high capital cost for drilling and operational cost of water pump, only temperatures greater than 80°C makes the investment profitable.

The ORC technology can be supplied from solar collectors and utilize the solar radiation. It stands to reason that for small scale applications, even if for domestic use, the plant cooperates with an existing boiler. The heat that produced in summer months and not used directly, it can be exploit for cooling, with an absorption or adsorption chiller.

ORC technology can utilize waste heat from diesel engine which can be installed in industry, ships, etc. Internal combustion engines have many losses from the hot exhausts which can be in temperature 300-900°C [2] depending on type of engine. ORC supply limits make suitable technology for energy recovering from exhaust, however there is a limit on heat recovering which imposed by the dew point of gases.

Qiu et al. [5], built and tested a prototype compact organic Rankine cycle-based micro combined heat and power system for domestic use. They conducted tests to investigate the performance of micro-CHP under conditions which represent a residential application.

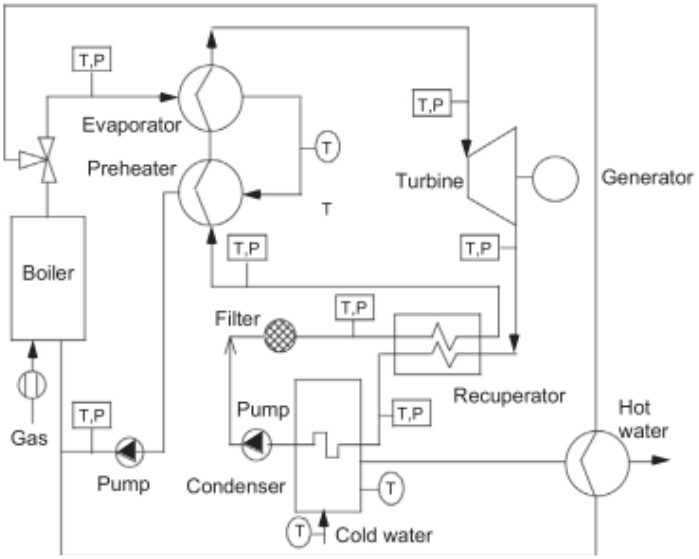

Figure 12: Schematic diagram of ORC system, Qiu et al.[5]

Figure 12, shows the diagram of the energy system which was created. There are three fluid loops, the first one recirculates water and steam to transfer the heat to evaporator which circulates, in the second loop, the organic fluid. The last loop is the cooling water one which condensates the organic fluid vapor after the expansion. The loop with the organic medium recirculates n-Pentane as working fluid. After the expansion the vapor enters in the recuperator where part of the enthalpy is recovered. The expander of the system is a semi-hermitic scroll expander (Figure 13) with obtained isentropic efficiency 75.2%. The ORC efficiency that measured was 7.7% and the electric efficiency 4.6%.

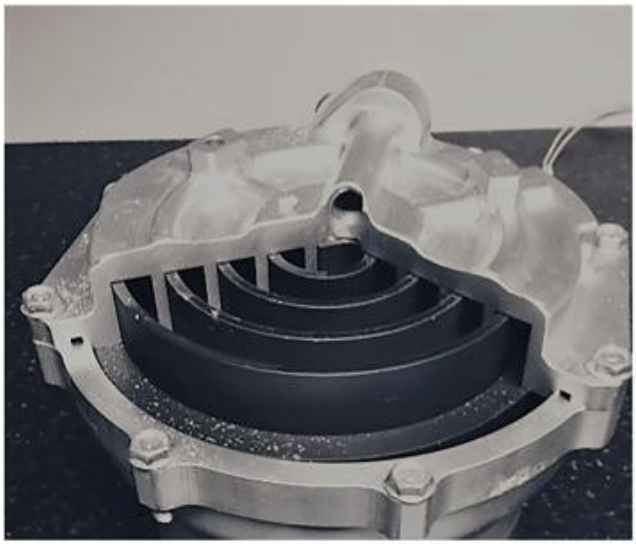

Figure 13: Photo of the scroll expander [5]

Kang et al. [6], created an ORC test-rig with two stage radial turbine coupled with a high-speed generator. This application generates electric power by using R245fa as working fluid. In Figure 14 is shown the ORC system which developed with a shell and tube type evaporator which is supplied with the water steam to transfer heat to the working fluid. Also, the two-stage turbine, with high pressure part (HPT) and the low pressure (LPT), is depicted. The condenser of working fluid is connected with the cooling tower where the latent heat is rejected from the condensation.

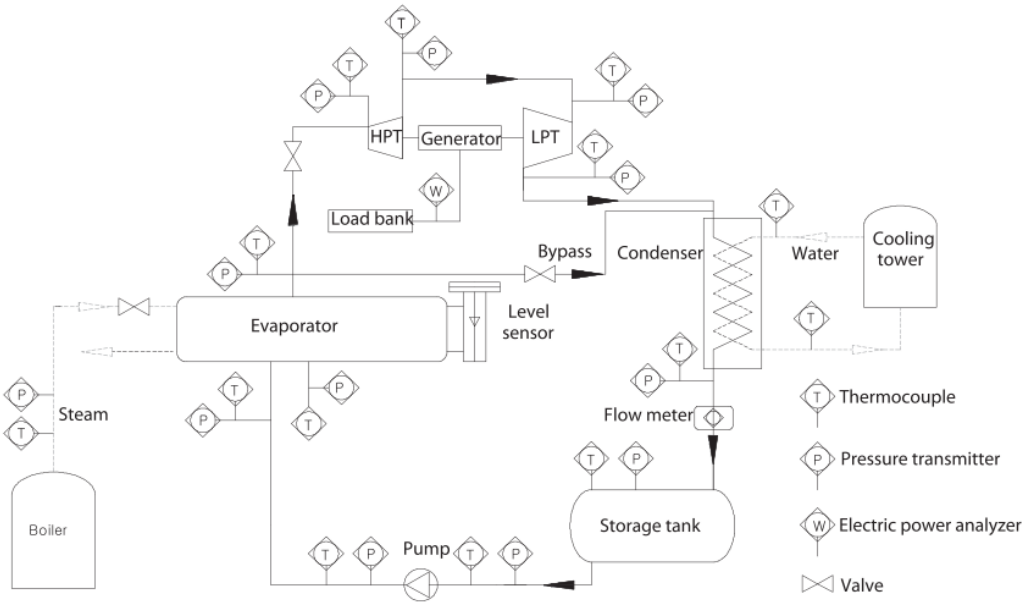

Figure 14: Schematic diagram of the designed ORC system [6]

The preliminary experimental tests are conducted to define the performance of the ORC and the turbine. In The test sets the evaporation temperatures were 113, 114, 115 and 116 °C, with proportionally increase of pressure from 17.4 to 18.6 bar. The first estimation of the isentropic efficiency of the radial expander was about 80%. In the experiment the measured values were from 63.1% to 68.5% with power and expansion ratio range between 33.439 kW and 10.9-11.6, respectively. If the power output will be taken into account, the efficiency of the turbine drops approximately to 58.4%. Overall cycle efficiency measured from 8.91% to 9.8%.

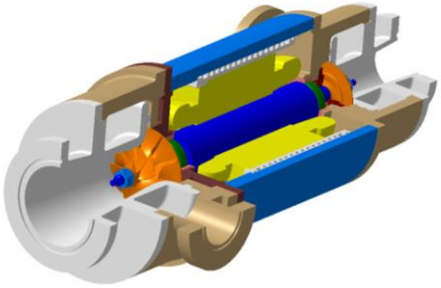

Figure 15: Two-stage radial turbine 3-D drawing.

In Figure 16 is presented the individual isentropic efficiency of the two stages of the turbine and it can be perceived the better performance of the low-pressure stage. The performance of LPT is more important because it is the part which connect with the condenser. [6]

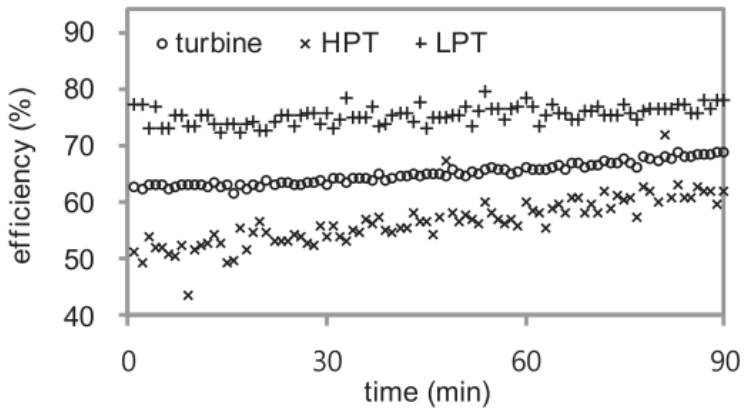

Figure 16: Isentropic efficiency of turbine as a function of time [6]

Muhammad et al. [7] designed and experimentally verified an ORC system using R245fa as working fluid with scroll expander. This system utilizes, as heat source, waste steam in pressure of 1-3 bar and supply temperature of 120°C as depicted in Figure 17.

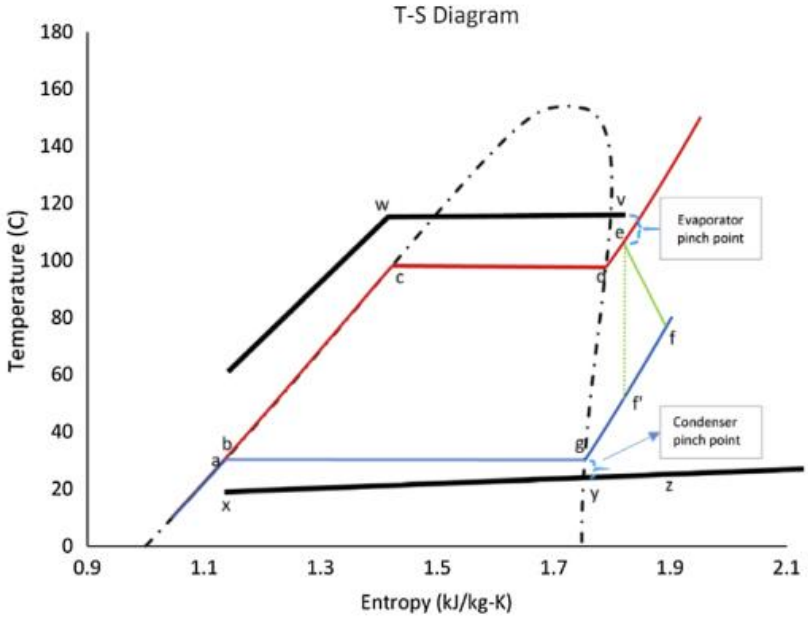

Figure 17: T-s diagram of ORC system [7]

In the components of the ORC system, except from the scroll expander with 1kW nominal power output which is coupled to an AC generator by magnetic coupling, there are two brazed plate type heat exchangers. The one is used as evaporator and the other as condenser and they are designed in worst case performance to achieve the small pinch points requirements. Working fluid pump is an important component for the ORC system and its selection is a key element for the overall efficiency due to unusual operating conditions. Ultimate solution was a gear pump

due to its ability to supply smoothly the fluid in low flow rates across high pressure differences [7]. The working fluid pump speed was set in a manner that it transferred the required mass flow, as a result when the imposed electric load was changed, the pump speed was adjusted in order to obtain the required pressure ratio.

The experimental results for generating 1kW electrical output has shown ORC thermal efficiency of 5.75% with expander's efficiency 58.8% at 3496 rpm and maximum power output. The maximum expander's isentropic efficiency that was recorded as 77.74%.

Eyerer et al. [8] investigated experimentally an ORC system and tested the operation with the working fluids R1233zd(E) and R1224yd(E) as replacement for R245fa. It has been studied both the compatibility of the materials to this replacement and the performance with the new refrigerants in a wide range of operational conditions. For the needs of this thesis it will be shown only the effect of the alteration of the working fluid on the performance of the cycle. The layout of the ORC system is a standard cycle containing a feed pump, an evaporator, a scroll expander and a condenser. The heat source is a 45kW electrical resistance heater. The expander is a semi-hermetic automotive scroll compressor modified to work as an expander. Expander has a build-in volume ratio of 2.5 and rated power of 1kW.

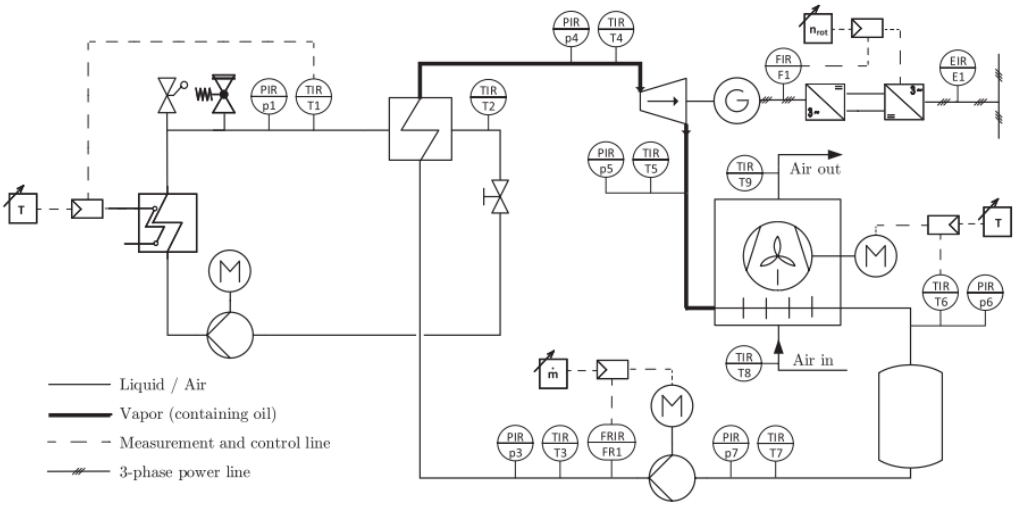

Figure 18: Schematic view of ORC system [8]

All experiments were conducted with constant heat source temperature of 120 °C. Thermal efficiency of ORC system and the expander power output are determined in a wide range of fluid mass-flow rates, rotational speed of the expander and condensation temperatures. The experimental analysis has shown that the thermophysical properties of R245fa, R12344zd(E) and R1224yd(Z) are similar. The reason why the system has different performance by changing the refrigerants are the saturation pressure, evaporation enthalpy and vapor density.

Moreover, Figure 19 shows that the values of the isentropic efficiency appear to be independent for each working fluid. In low pressure ratios the efficiency is lower due to more pronounced the loss mechanism of over-expansion. While the pressure ratio is being increased, the efficiency increases too, and then remains at a constant value because of slight under expansion occurrence.

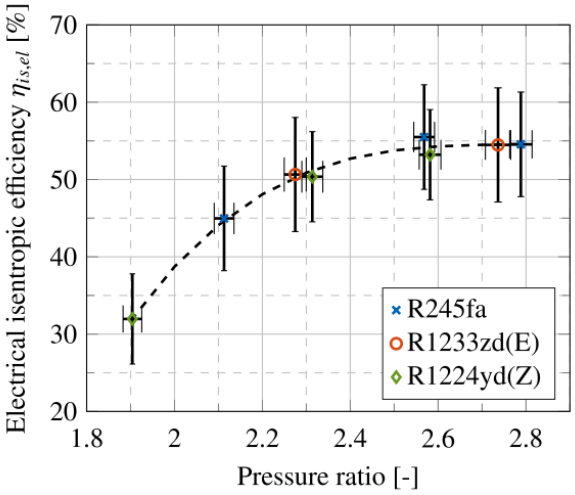

Figure 19: Electrical isentropic efficiencies as a function of pressure ratio.

As represented in Figure 20 the maximum thermal efficiency reached with R1233zd(E) and is approximately 48%. Generally, with R1233zd(E) the efficiency is 2% higher compared to R245fa. On the other hand, with R1224yd(Z) the efficiency drops about 5% compared to R245fa. For high mass flow values, R245fa and R1224yd(Z) have equal efficiencies, while with R1233zd(E) the performance dropped significantly.

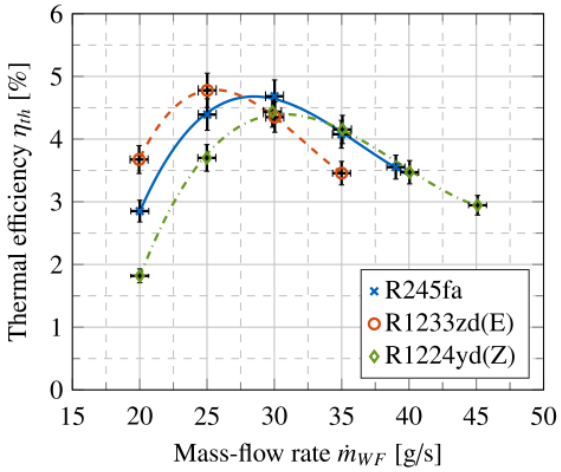

Figure 20: ORC system thermal efficiency as a function of mass-flow rate.

The expander's power output and the system efficiency defined in Figure 21. As it can be observed, the highest power output can be achieved with R245fa . When using R245fa power output is 9% higher than R1233zd(E) and 12% higher compared to R1224yd(Z).

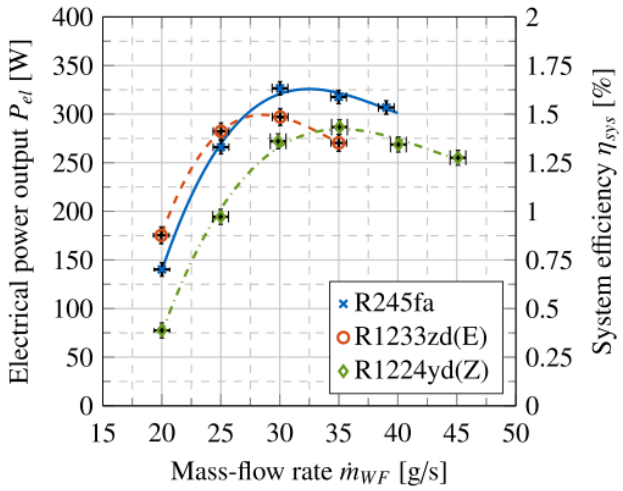

Figure 21: Electrical power output of the scroll expander as a function of mass-flow rate

Summarizing the results, the alternative refrigerants R1233zd(E) and R1224yd(Z), with reduced GWP, are appropriate to replace the R245fa with respect to overall thermal efficiency and slightly lower power output.

1.5 Literature review

O. Dumont et al. (2018) [1] tested experimentally in two ORC test-rigs, with R245fa as the working fluid, four different types of volumetric expanders (modified hermetic scroll compressor, twin-screw expander, roots and a swash-plate piston). The test-rig is constructed with a standard mass of working fluid and the parts that consists are a brazed evaporator and same type recuperator, shell and tube water-cooled condenser, gear pump and a receiver. Although these four types of expanders don't have the same nominal power, to define their performance in terms of isentropic efficiency and filling factor, this study focuses in operation limit conditions and the behavior in different operation conditions, including the nominal power. It is worth noting that test-rigs are used small-capacity expanders, less than 5 kW. The conclusion is that the scroll expander presents the highest efficiency (76%), while the piston and screw present 65% efficiency and the roots 47%. The results presented at the Table 1.

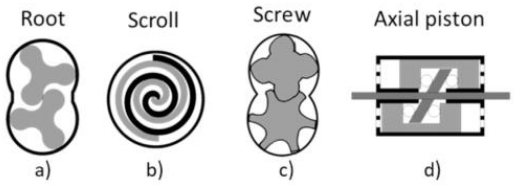

Figure 22: Types of volumetric expanders [1]

An experimental investigation of V. Lemort et al (2009) [9] is carried out on a scroll expander into an ORC system with HCFC-123 as working fluid. The expander is an open-drive oil-free air scroll compressor and the only modification were to remove the cooling fan and to insulate the machine. The expander drives an asynchronous machine and its mechanical power is determined by measuring the rotational speed and the torque developed at the torque meter shaft. The expander in this test-rig achieved maximum isentropic efficiency of 68%. This analysis pointed out that the internal leakages and, to a lesser extent, the supply pressure drop and the mechanical losses are the main losses which affecting the performance of the expander. The validated semi-empirical model was used to quantify the losses during the expansion process and to point out the design to achieve better performances. The model that presented in this paper used by Dumont [1], in an evolved version to study the different types of volumetric expanders.

Z. Miao et al. (2017) [10] tested an ORC system driven by the heat from a lubricant oil circuit. This system uses R123 as working fluid and a scroll expander to generate work. Figure 23 shows the thermodynamic cycle of the ORC, the heat source and the cooling water. In this study, are represented the effects of operational conditions on the cycle performance, such as the temperature and the mass flow of the conductive oil, the built-in volume ratio of the expander, the heat transfer area of the evaporator and the environment conditions. The thermal efficiency of this system that measured is 5.64 % and shaft power 2.65 kW, but is can improved by optimizing the match among the components. The optimum cycle that predicted presents a shaft power of 6.05kW and thermal efficiency of 10.7%. The scroll expander model is developed based on semi-empirical model proposed by Lemort et al. [9]. The mathematical model was verified based on experimental results and the maximum deviation between the tested measures and calculations by the model is 5.5%.

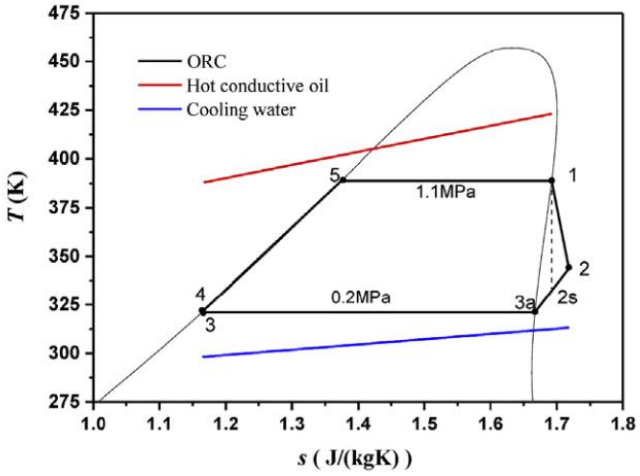

Figure 23: T-s diagram of the cycle Miao et al. [10]

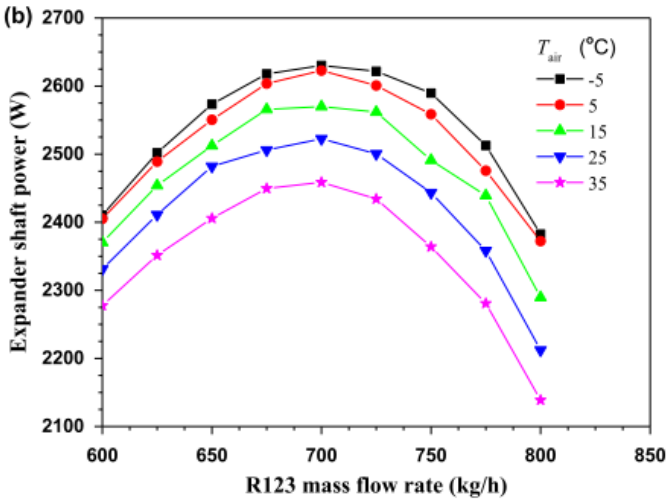

Figure 24: Expander shaft power with refrigerant mass flow [10]

An interesting observation in Figure 24 is the effect of the air temperature on the produced shaft power. The shaft power decreases gradually from 2630W to 2459W while the air temperature increases from -5°C to 35°C.

Another test-rig with an open-drive scroll expander investigated by D. Ziviani et al. (2018) [11]. This test-rig utilizes low-grade waste heat recovery (lower than 150°C) by using R245fa as working fluid. The expander which was chosen has a nominal power capacity of 5 kW with built-in volume ratio of 3.5. The model which was developed to calculate the expander is based on the semi-empirical model introduced by Lemort et al. [9]. The maximum isentropic efficiency of 58 % was measured at 1600 rpm and the maximum output power was 3.75 kW at 2500 rpm. In this study represented the following diagram (Figure 25) which calculates the isentropic

efficiency by taking into account the parameters, separately. As a result, it is apparent that the effect of pressure drop and mass flow leakage is higher than the friction and heat losses.

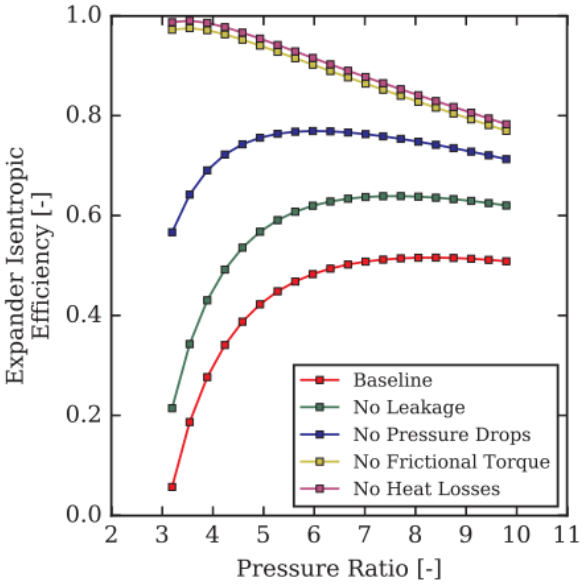

Figure 25: Expander's Isentropic Efficiency as a function of pressure ratio. (Ziviani et al. 2018) [11]

Z. Liu et al. (2018) [12] created a test-rig similar to the above mentioned, with a scroll expander, but in this case, created a FEM (Finite Elements Model) with CFD simulation results as boundary conditions to define the deformation on the scrolls because of the thermal and pressure distributions. As already mentioned, the expanders are usually commercial compressors which operate in reverse mode with some modifications. That will certainly cause a different deformation behavior of the scroll parts. In this experiment, was converted a machine from an open-drive automobile air conditioning compressor. The working fluid which was used is R123.

D. Ziviani et al. (2017) [13] investigated an ORC system with single-screw expander which presents a high internal volume ratio in combination with high isentropic efficiency. Screw expander requires lubrication during operation, so in this case, used flooded expansion and the lubrication oil separated after the expansion in an external circuit, as represented in Figure 26. In this experimental setup, compared R245fa and as replacement of R1233zd, as working fluids to investigate the benefits of flooded expansion in screw expander.

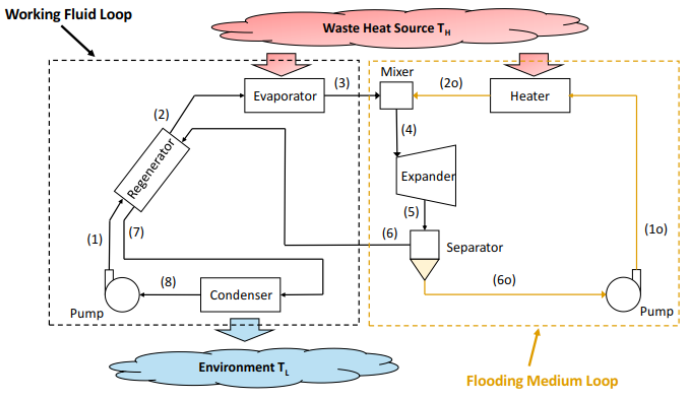

Figure 26: ORCFLE system [13]

As presented in Figure 27, screw expander can potentially reach isentropic efficiency above 80%. The optimal isentropic efficiency is depended on the pressure ratio which is proportional to the specific volume ratio.

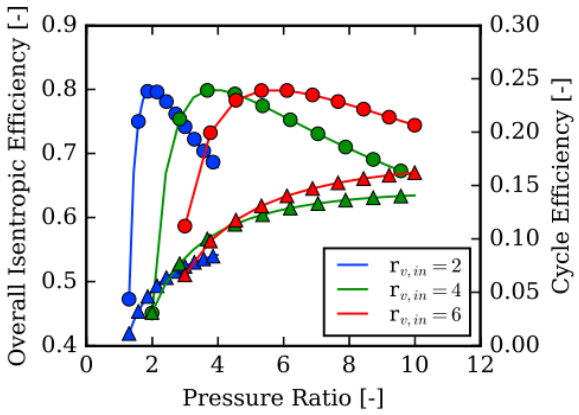

Figure 27: Influence of the expander built-in volume ratio on overall isentropic efficiency (circle markers) at different pressure ratios with R245fa

B. Lei et al (2016) [14] developed an ORC with single screw expander and R123 as working fluid. Figure 28 presents the structure of the single screw expander, where both suction and discharge of working fluid occur in radial direction. The ORC system consists of a conductive oil circuit which provides low grade heat and the working fluid circuit, as presented in Figure 29. In the experiments studied the effects of the supply pressure and the expansion ratio for different rotational speeds. The conclusion from this study was that in large expansion ratios increased built-in volume ratio suggested, by converting the expander from single stage to double stages in order to utilize the discharge velocity. The results are presented in Table 1 and it is worth noting that the shaft power was 8.35 kW and the volumetric efficiency 83%. The maximum overall efficiency of ORC system was 7.98%.

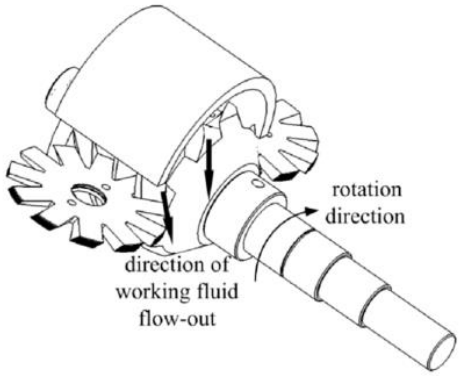

Figure 28: Structure of single screw expander and direction of working fluid. [14]

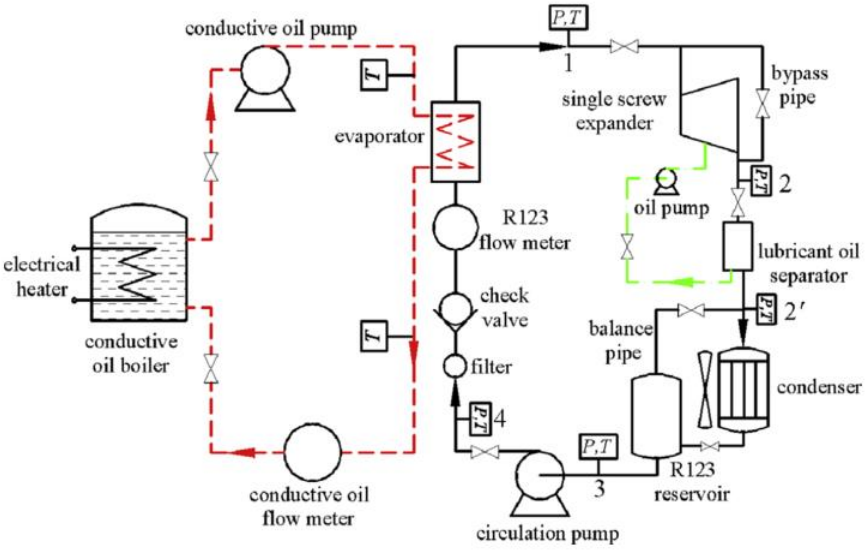

Figure 29: Diagram of ORC System [14]

F. Ayachi et al. [15] investigated a small ORC for low grade heat recovery, under different operating conditions with refrigerant R245fa as working fluid. The expander which used on the ORC system is a converted hermetic scroll compressor. The expander modeled with the semi-empirical model which imposed by Lemort et al. [9] Supply temperature ranges between 105 and 135 °C and the pressure from 10.3 to 22.5 bar. The net efficiency of the combined expander-generator is shown in Figure 30 and the maximum value is 70% for supply pressure 20 bar. According to Figure 30, the maximum measurement is equal to 2.9kW at the supply pressure of 22.5 bar, with temperature and pressure ratio at 135°C and 3.8 bar, respectively.

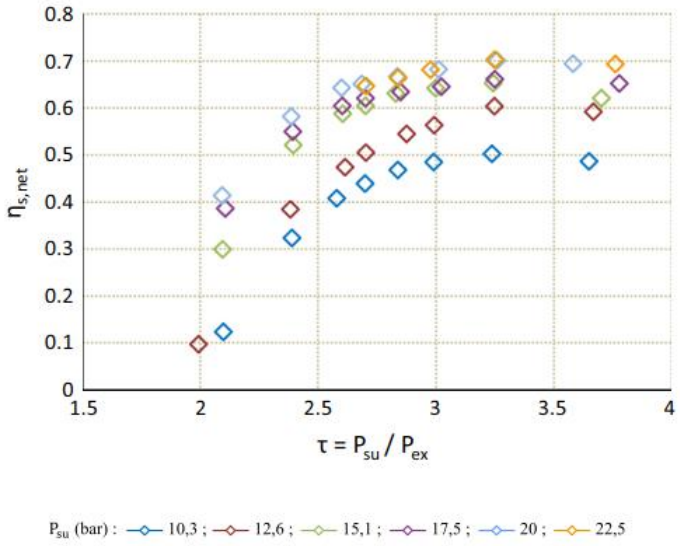

(a)

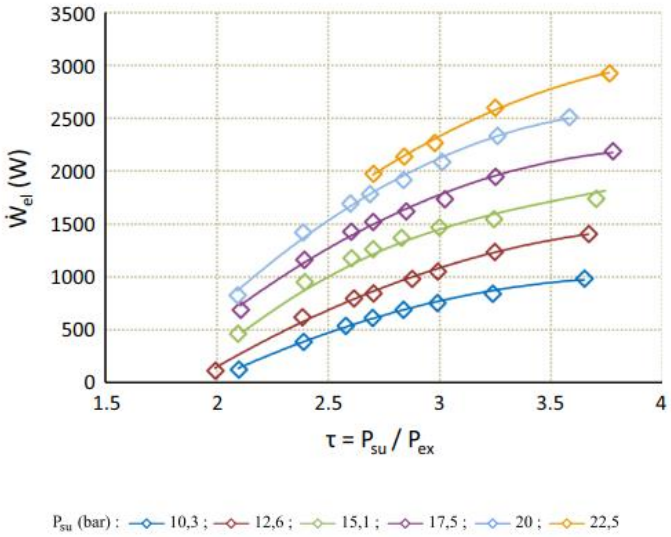

(b)

Figure 30: Evolution of (a) the net efficiency and (b) the net power output with the pressure ratio [15]

Tang et al. [16] experimentally investigated an ORC system with twin-screw expander, utilizing a geothermal source. This 200kW system was installed to extract heat from abandoned oil wells to generate electric power. These wells stored large amounts of geothermal energy in the form of hot water, in the temperature of 100 °C. The twin-screw expander of the system is an oil-free, hence a separate oil system was installed to lubricate the bearings and gearings. Experiments

conducted with supply pressure ratios in the range of 3.3-4.7 bar, which corresponds to the R123 evaporating temperatures of 65-78.4 °C. The discharge pressure is fixed at 1.4 bar. The optimal efficiency is approximately 87.5% at 4.7 bar supply pressure. The efficiency is above 80% over a wide range of supply pressure, which demonstrates that the screw expander has good energy conversion efficiency over a wide range of source temperatures.

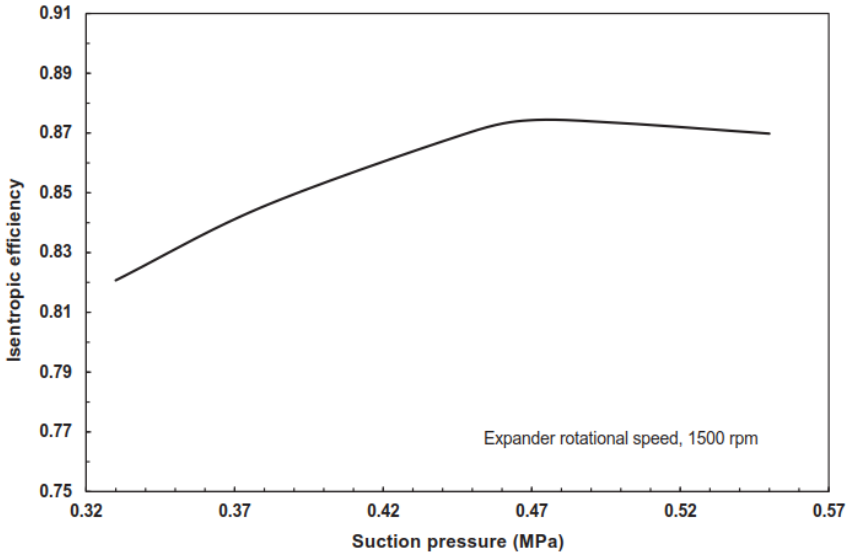

Figure 31: Isentropic efficiency as a function of supply pressure [16]

Table 1: Literature review

Inlet temperature (°C)	*Suction Pressure (bar)*	*Pressure Ratio*	*Type of expander*	*Working fluid*	*Isentropic efficiency (%)*	*RPM*	*Reference*
122-133	5.7-14.7	1.4-7.4	Scroll	R245fa	76	1137-7920	O. Dumont et al. (2018) [1]
75-130	6.4-12	1.9-4.17	Screw	R245fa	65	500-12450	O. Dumont et al. (2018) [1]
70-124.4	2.7-10	1.14-4.47	Roots	R245fa	47	1000-11000	O. Dumont et al. (2018) [1]

118-153	17.7-30.7	6.2-10.6	Piston	R245fa	53	1000-4000	O. Dumont et al. (2018) [1]
101.7-165.2	5.45-11.12	-	Scroll	HCFC-123	42.4-68	1771-2660	V. Lemort et al. (2009) [9]
142.9	7.82	3.11-5.22	Scroll	R123	70	2569	Z. Miao et al. (2017) [10]
110	13.8	5.95	Scroll	R245fa	58	1600	D. Ziviani et al. (2018) [11]
110-176.07	8.35-10	2.94-3.87	Scroll	R123	-	1986-2010	Z. Liu et al. (2018) [12]
120	-	9.34	Screw	R245fa	80	-	D. Ziviani et al. (2017) [13]
120-130	11.5	8.5	Screw	R123	73	3000	B. Lei et al. (2016) [14]
105-135	10.3-22.5	2-3.8	Scroll	R245fa	70	3000	F. Ayachi et al (2016) [15]
100	3.3-4.7	2.35-3.35	Screw	R123	87.5	1500	Tang et al. (2015) [16]

1.6 Thesis scope

As shown above, the expander is a key component of an ORC system and is of crucial importance both its manufacturing as well as its operational behavior for the long-term performance and durability of the overall system. Based on this, the scope of this study is to cover the following topics:

- How can a semi-empirical model predict the expansion process for a certain model of expander?
- How accurate can be a semi-empirical model, once calibrated against experimental data?
- Which is the variation in the expander's performance if the working fluid is changed?
- How reliable could be a semi-empirical model for two-phase expansion, once calibrated with single phase expansion measurements?

2. Expander Modelling

2.1 Model Description

The semi-empirical model that used to define the operation maps of the expander is an evolved version of the model proposed by Lemort [9]. It is based on seven main parameters which lead to reliable results. Some more advanced models take into account exhaust pressure drop, mechanical losses, additional radiative ambient losses, yet more additional calibration parameters to the model can lead to overfitting problems. The most important is that this semi-empirical model is general and can simulate many technologies of expanders.

The performance between each expander is compared by using the following parameters. Firstly, the filling factor (FF) is the ratio between the measured volumetric flow rate and the theoretical volumetric rate, which is defined by the manufacturer.

$$FF = \frac{\dot{V}_{meas}}{\dot{V}_{th}} \tag{2.1}$$

Also, the isentropic efficiency evaluated over a wide range of working conditions and is defined by the fraction of the produced shaft power divided by the power would have been produced if the expansion was isentropic without mass flow leakages.

$$\eta_{is} = \frac{\dot{W}_{shaft}}{\dot{m}_r \, (h_{su} - h_{ex,is})} \tag{2.2}$$

The semi-empirical model takes into account both heat transfers and mechanical losses. The expansion process is modeled by the following steps:

- Adiabatic supply pressure drop ($su \Rightarrow su_1$)
- Supply heat transfer at constant pressure ($su_1 \Rightarrow su_2$)
- Isentropic expansion imposed by the built-in volume ratio ($su_2 \Rightarrow ad$)
- Expansion at constant volume ($ad \Rightarrow ex_2$)
- Adiabatic mixing between the leakage flow ($ex_2 \Rightarrow ex_1$)
- Exhaust heat transfer at constant pressure ($ex_1 \Rightarrow ex$)

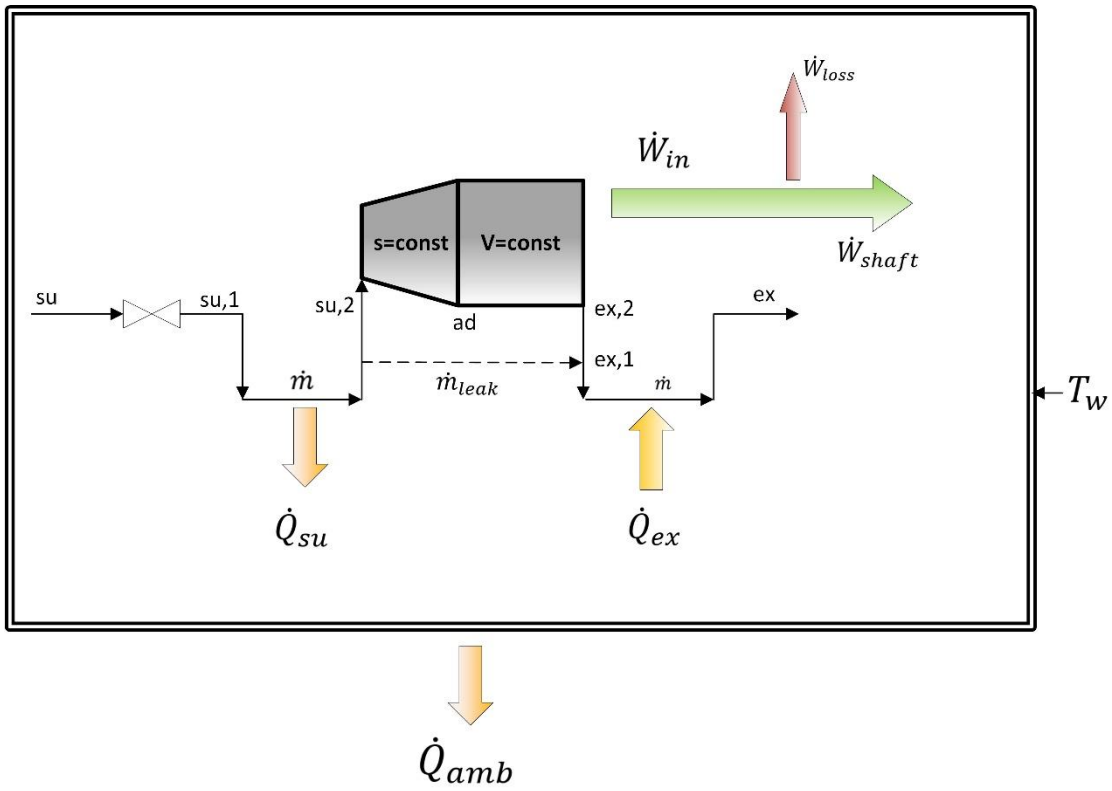

Figure 32: Schematic representation of the expander model.

In this model there are five individual variables that the user has to define as input in order to calculate the desired output data. The inputs are the rotational speed, mass flow, supply pressure and temperature as well as the pressure ratio. The model has been modified in the present work and it can be used as input either the rotational speed or the mass flow.
In the model, there are two categories of parameters. The first, defined by the manufacturer and the technical data of the expanders, and the second one, contains the calibrated parameters of the semi-empirical model based on the measurements. As a result, the comparison is not perfectly objective for all expander types, because the scroll expander is constructed many years for commercial reasons, in contrast with the screw expander which is at a prototype stage. The model which achieves an objective comparison between the volumetric expanders, initially used by Lemort [9] to predict the behavior of a scroll expander. In order to use this model for the other volumetric types, these design parameters have to been changed.

The designing parameters which were provided by the technical data are necessary for the calculations. The swept volume V_s refers to the volume of the fluid that expanded in a revolution of the shaft. In order to achieve the expansion of the working fluid, the specific volume of the fluid have to be multiplied during the expansion process. As mentioned above, the fluid may be under- or over-expanded, so to calculate the isentropic expansion, the built-in volume ratio $r_{v_{in}}$ (specific volume ratio between the start and the end of isentropic expansion) has to be known.

According to the construction material of the expander, there are upper limits for the supply temperature and pressure and a maximum value of rotational speed range.

The following parameters are crucial for the expander modelling and they are calibrated by the measurements. Firstly, the nominal flow rate $\dot{M}_n$ is a parameter that affects the heat transfer coefficients AU_{su}, AU_{ex} and AU_{amb}. The supply pressure drop which is modeled as an isentropic flow through a converging nozzle, calculated by using the cross-sectional area A_{su} of the supply port. The leakage flow, $\dot{M}_{leak}$, is defined by the leakage area, $\dot{A}_{leak}$, such as the gap area between the scrolls and the housing. Finally, the expanders' mechanical parts have a mechanical loss torque, T_{loss}, which reduces slightly the produced shaft power. A parameter which was defined in the case of piston expander, is the clearance volume V_0, due to recompression losses of the trapped fluid.

In the analysis below, in some cases the swept volume and volume ratio were considered as calibrated parameters, to have a better fitting in the measured results.

2.2 Mathematical Model

2.2.1 Supply Pressure drop

The first process (su⇒su$_1$), which was modeled as adiabatic pressure drop, accounts all pressure losses encountered at the suction line. This process is compared with the flow through a converging nozzle with cross-sectional area A_{su}, which is a manufacturing parameter. It is described as:

$$\dot{M} = \frac{A_{leak}}{v_{su}} \sqrt{2\left(h_{su} - h_{su_1}\right)} \tag{2.3}$$

By imposing the mass flow at the supply, the specific enthalpy at the nozzle throat is calculated, consequently, for constant specific volume in the nozzle, the specific entropy and the value of pressure are also estimated.

2.2.2 Supply heat transfer

The heat transfer mechanisms inside the expander occur in the expander shell and the expansion chamber between supply or exhaust flow and between the expander's shell and ambient. The losses that occurred at the supply, described as:

$$\dot{Q}_{su} = \dot{M}\left(h_{su_1} - h_{su_2}\right) \tag{2.4}$$

By considering the shell's metal mass with temperature T_w, the supply heat transfer is given by:

$$\dot{Q}_{su} = \left(1 - e^{\frac{AU_{su}}{\dot{M} \cdot cp}}\right) \cdot \dot{M} \cdot c_p\left(T_{su_1} - T_w\right) \tag{2.5}$$

Where, AU_{su} is the heat transfer coefficient at supply suction. In the same way, the exhaust heat transfer calculated as:

$$AU_{su} = AU_{su_n} \cdot \left(\frac{\dot{M}}{\dot{M}_n}\right) \tag{2.6}$$

2.2.3 Internal Leakages

There are two main internal leakages paths into the expanders. The first is between the moving part (which can be scroll, screw etc., according type of the expander) and the shell. The second, is the path between the multiple moving parts, such as the gap between the screws. These areas are defined as A_{leak} and calculated by the equation:

$$\dot{M}_{leak} = \frac{A_{leak}}{v_{su_2}} \cdot \sqrt{2\left(h_{su_2} - h_{leak}\right)} \tag{2.7}$$

2.2.4 Internal mass flow rate

The internal mass flow rate, $\dot{M}_{in}$, is the difference between the flow rate entering the expander and the leakage flow rate. This rate is generating the power at the expansion process and is calculated by the following equation.

$$\dot{M}_{in} = \frac{N \cdot V_s}{v_{su_2}} \tag{2.8}$$

The equation above is used not to calculate $\dot{M}_{in}$ because it has already been calculated by the difference with the overall flow rate. This equation is useful to calculate the rotational speed *N* of the shaft.

2.2.5 Power

The following equations that calculate the power which is produced in individual parts of the expander, derived from the energy balance.

Firstly, the internal power is defined by the following equation:

$$\dot{W}_{in} = \dot{M}_{in}\left[\left(h_{su_2} - h_{ad}\right) + v_{ad} \cdot \left(P_{ad} - P_{ex}\right)\right] \tag{2.9}$$

The adiabatic point is calculated by the multiplication of specific volume at the suction throat with the built-in volume ratio.

The power of losses caused by the friction between the moving parts (scrolls, screw) and the bearings. It is proportional to friction losses T_{loss} which is defined by the manufacturer.

$$\dot{W}_{loss} = 2\pi \cdot N \cdot T_{loss} \quad (2.10)$$

The shaft power is the difference between the internal power and the loss power:

$$\dot{W}_{shaft} = \dot{W}_{in} - \dot{W}_{loss} \quad (2.11)$$

2.2.6 Energy balance of the expander

Finally, the ambient losses are calculated and their value corresponds to the heat transfer between the expander and the ambient because of the temperature difference.

$$\dot{Q}_{amb} = AU_{amb} \cdot (T_w - T_{amb}) \quad (2.12)$$

So, the energy balance of the expander is defined by:

$$\dot{W}_{loss} - \dot{Q}_{ex} + \dot{Q}_{su} - \dot{Q}_{amb} = 0 \quad (2.13)$$

The equation above is used as convergence criterion of the semi-empirical model.

2.3 Calibration of the parameters

As referred above, except for the manufacturer properties, some parameters calibrated by the model (heat transfer coefficients, supply and leakage area, torque loss, nominal mass flow rate, swept volume). The input variables are unchanged and to calculate the output variables (output power, exhaust temperature, mass flow rate), the model necessitates all the parameters. Initial values are given to the parameters which are not provided by the manufacturer and subsequently calculated by the model. The calibration process is carried out by minimizing the objective function which is the global error between the calculated and measured values. This error is calculated by:

$$error = \frac{1}{3} \cdot \sqrt{\left(\sum_{1}^{N_{tests}} \left(\frac{\dot{m}_{calc} - \dot{m}_{meas}}{\dot{m}_{meas}} \right) \right)^2} + \frac{1}{3} \cdot \sqrt{\left(\sum_{1}^{N_{tests}} \left(\frac{\dot{W}_{shaft_{calc}} - \dot{W}_{shaft_{meas}}}{\dot{W}_{shaft_{meas}}} \right) \right)^2} + \frac{1}{3} \cdot \sqrt{\left(\sum_{1}^{N_{tests}} \left(\frac{T_{ex_{calc}} - T_{ex_{meas}}}{T_{ex_{meas,max}} - T_{ex_{meas,min}}} \right) \right)^2} \quad (2.14)$$

The calibration process is described by the following flow chart:

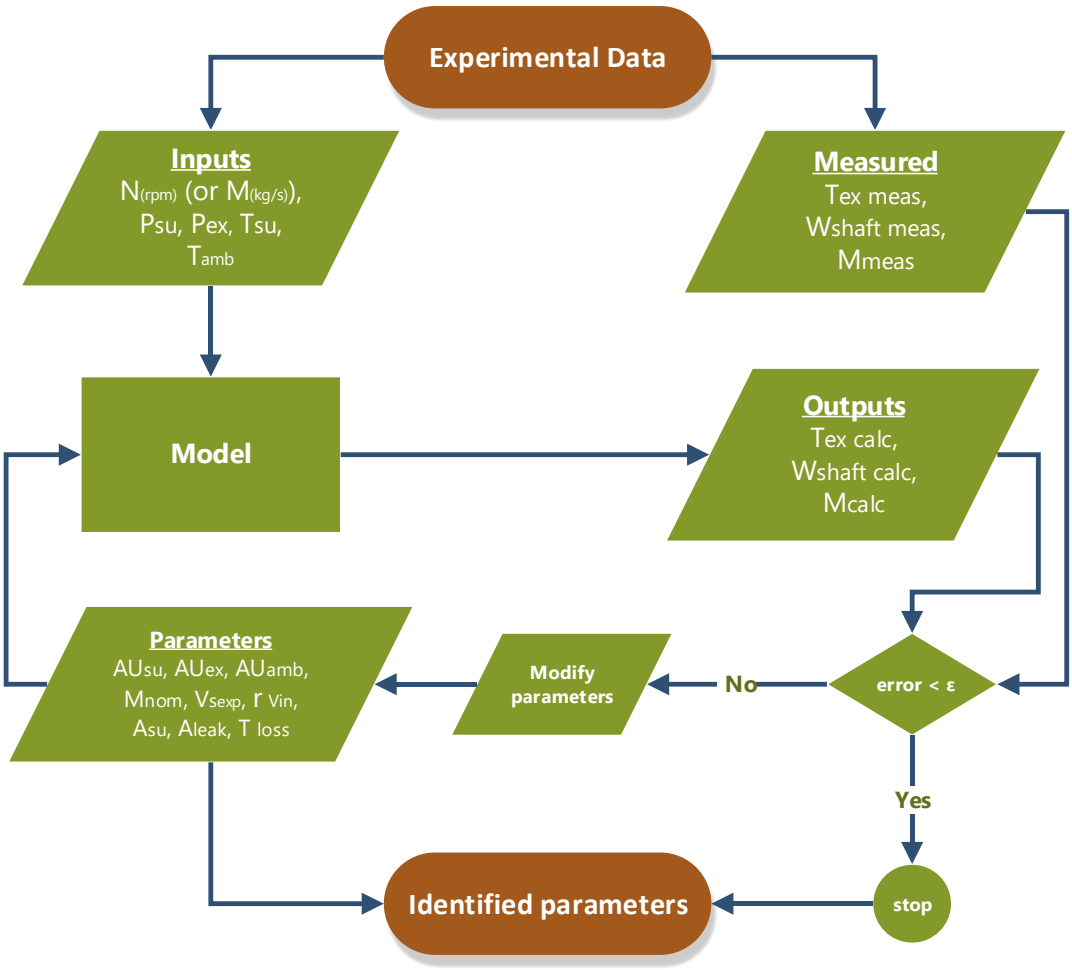

Figure 33: Flow chart of the parameter calibration process.

2.4 Comparison with literature measurements

2.4.1 Comparison with Lemort et al. [9]

As referred above, the model that is used to calculate the properties of the expander introduced by Lemort et al. [9]. In this test-rig experiments carried out on an open-drive oil-free air scroll compressor that used as expander. In a given range of supply conditions the output properties were calculated, subsequently the geometric parameters of expander were calibrated, based on measurements of experiments.

In this publication, figures are given with the evolutions of main values, such us isentropic efficiency, filling factor, shaft power and exhaust temperature. Although, in tests it is not determined the exact value of supply temperature. In order to have a good estimation for the supply temperature which have been used, an assessment between the tests was carried out, with the supply pressure and specific volume to be determined.

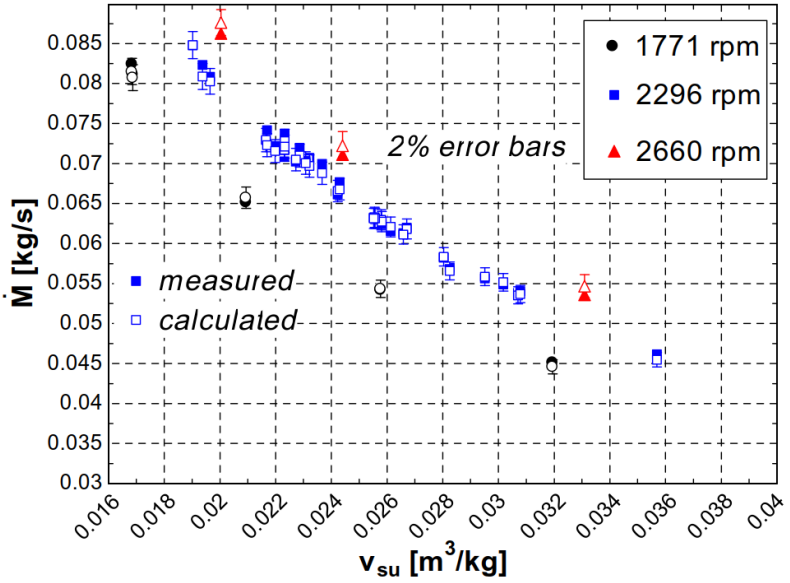

Figure 34: Evolution of the mass flow rate as a function of specific volume at the supply [9]

In this paper, the correlation between the exhaust temperature and the mean temperature of the supply and exhaust is presented by the following diagram (Figure 35). In order to match the points of the tests, the calculated supply and the measured exhaust temperatures were used.

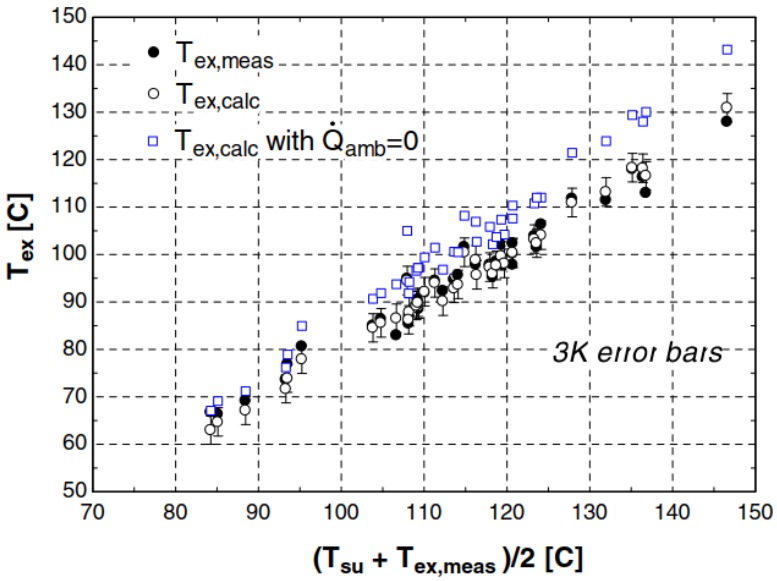

Figure 35: Evolution of the exhaust temperature as a function of the mean fluid temperature between supply and measured exhaust. [9]

Firstly, all these operation points are checked with the model that developed on this thesis. It was used paper's [9] geometrical parameters. This check is carried out to calculate the global error between measured and calculated values.

For the analysis, 21 operation points were deployed from the experiments since some points have been removed in 2660 rpm. The same experimental supply conditions were used in order to have a reliable comparison.

In calibration, the values that have been taken into account are the mass flow, exhaust temperature and shaft power.

$$error = \sqrt{\sum_{1}^{N_{tests}} \left(\left(\frac{\dot{m}_{calc} - \dot{m}_{meas}}{\dot{m}_{meas}} \right)^2 + \left(\frac{T_{ex_{calc}} - T_{ex_{meas}}}{T_{ex_{meas,max}} - T_{ex_{meas,min}}} \right)^2 + \left(\frac{\dot{W}_{shaft_{calc}} - \dot{W}_{shaft_{meas}}}{\dot{W}_{shaft_{meas}}} \right)^2 \right)}$$

Table 2 presents the comparison between the identified parameters from the paper and the parameters which calculated from the calibration.

Table 2: Calibrated parameters based on the measurements.

	Lemort et al.2009 [9] Parameters	*Calibrated Parameters*	*Units*
$r_{v_{in}}$	4.05	3.465063	$(-)$
$AU_{amb,n}$	6.4	3.90725	(W/K)
$AU_{su,n}$	21.2	20.278125	(W/K)
$AU_{ex,n}$	34.2	18.513751	(W/K)
A_{leak}	4.6E-06	4.57823E-06	m^2
T_{loss}	0.47	0.401675	$N \cdot m$
$V_{s_{exp}}$	3.65E-05	3.72273E-05	m^3
A_{su_n}	2.743E-05	2.12E-05	m^2
M_{dot_n}	0.12	0.104375	kg/s

The error between measured and calculated data by Lemort et al. is $3.03 \cdot 10^{-2}$ and after the calibration the error has the value of $8.056 \cdot 10^{-5}$.

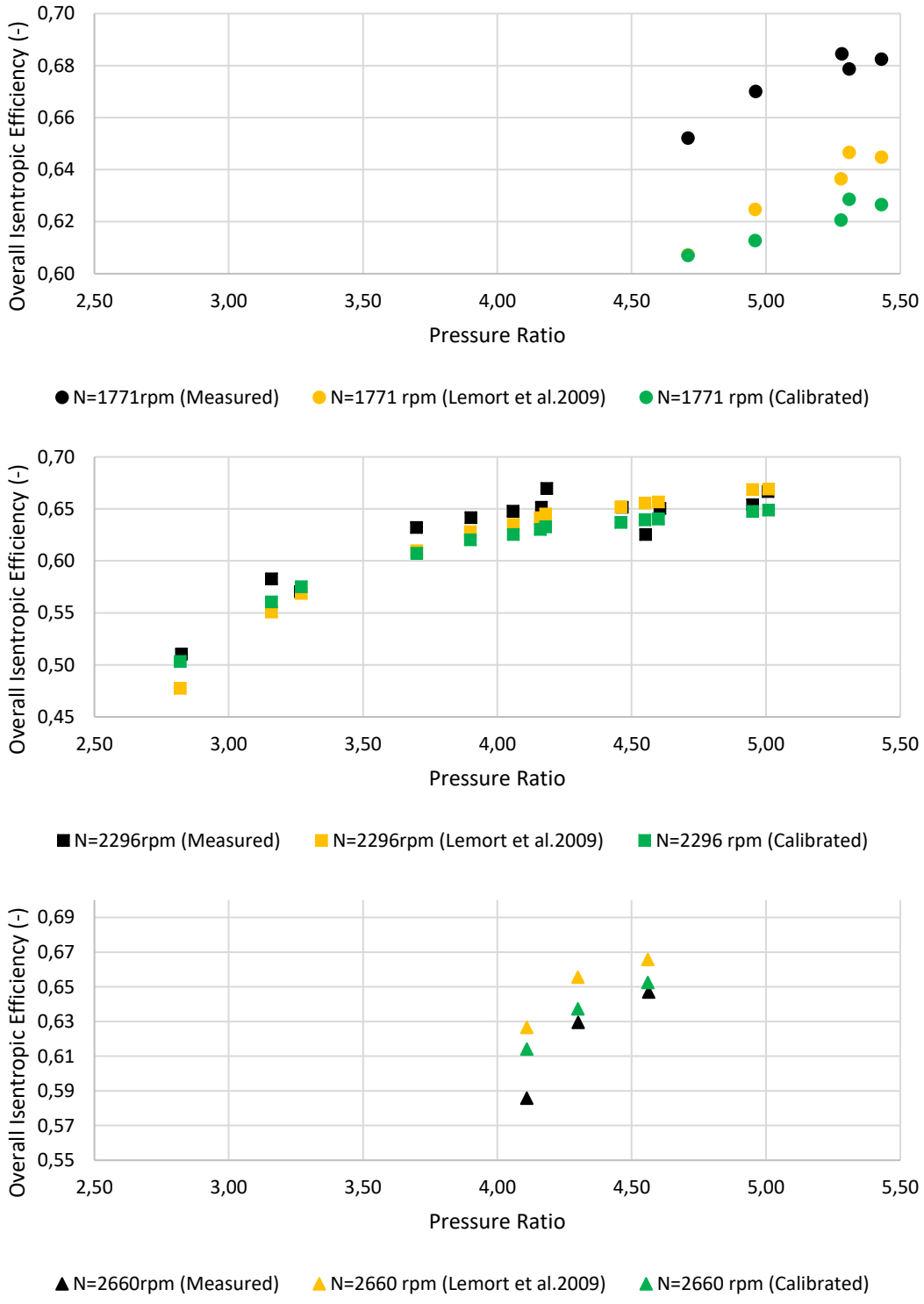

Figure 36 : Overall isentropic efficiency as a function of pressure ratio and rotating shaft speed for each investigation.

In Figure 36 the evolution of isentropic efficiency was compared for the measured data, the data that calculated with publication's parameters and with green points the calibrated data. In the range of 4-5 pressure ratios, the fitting of calibrated to measured data is reliable. Although in very low and very high pressure ratios the error is increased. In contrast with the measured data where the peak efficiency recorded at 1771 rpm, in both calculated sets of data the peak was at 2296 rpm. Generally, the measured data has shown better performance than the predicted by model. The maximum isentropic efficiency relative error between the measured and calibrated values is 9.34% at 5.28 pressure ratio (1771 rpm). The minimum observed at pressure ratio 3.27 (2296 rpm) and the value of deviation is 0.85%.

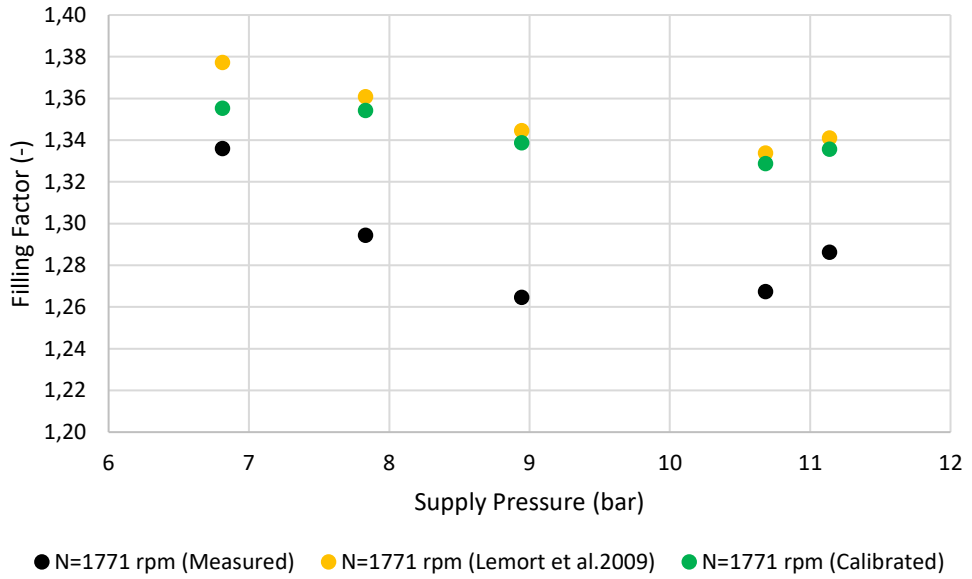

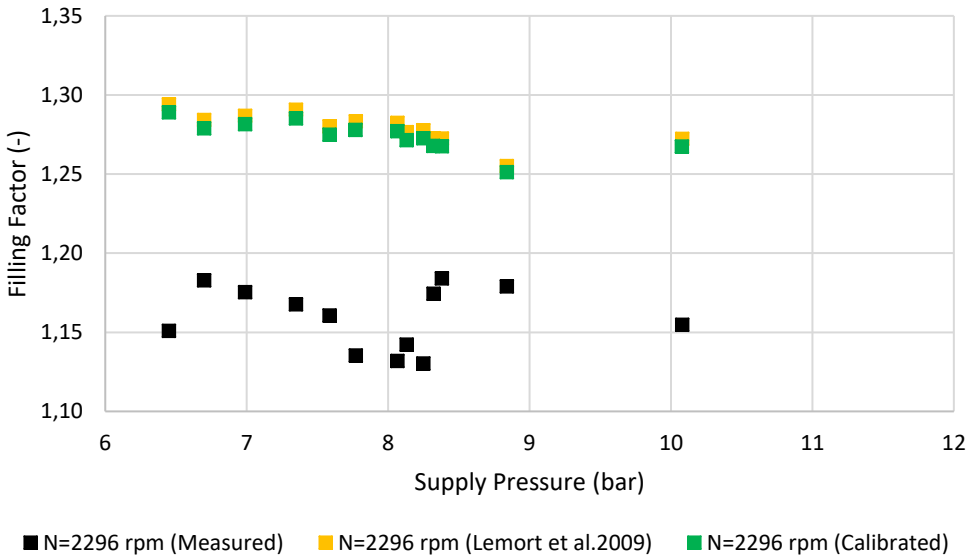

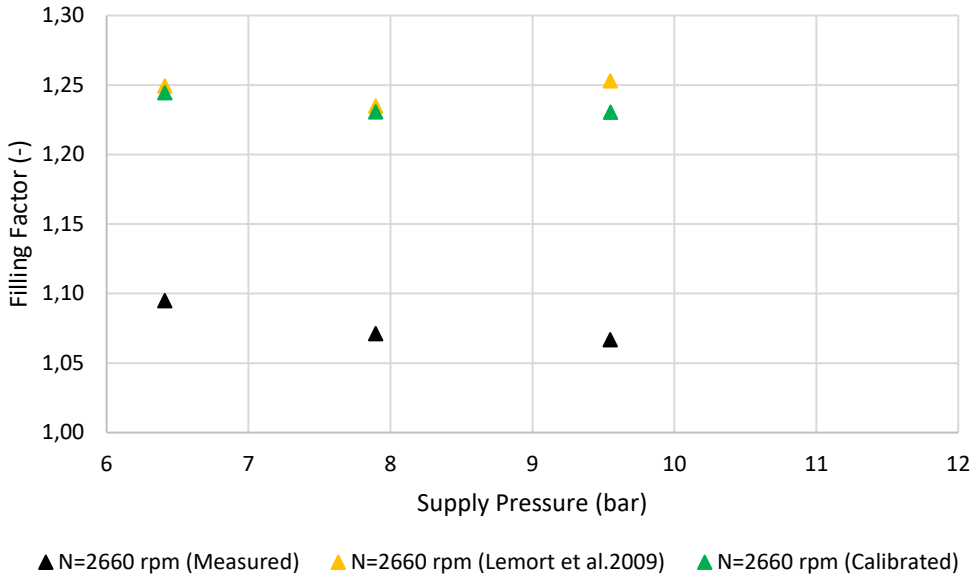

Figure 37 : Filling factor with the supply pressure separated according to rotating speed.

According to the comparison of the filling factor which is given in Figure 37, it is apparent that there is a remarkable deviation between the measured and predicted by the model data. The maximum and minimum error was calculated at the supply pressure of 9.55 and 6.81 bar, with values of 15.35 % and 1.45%, respectively. Also, it could be expected an increase in the filling factor by increasing the pressure, however the trend is balanced by the effect of the supply pressure drop. In both data sets it is clear that the filling factor is decreasing by increasing the rotational speed.

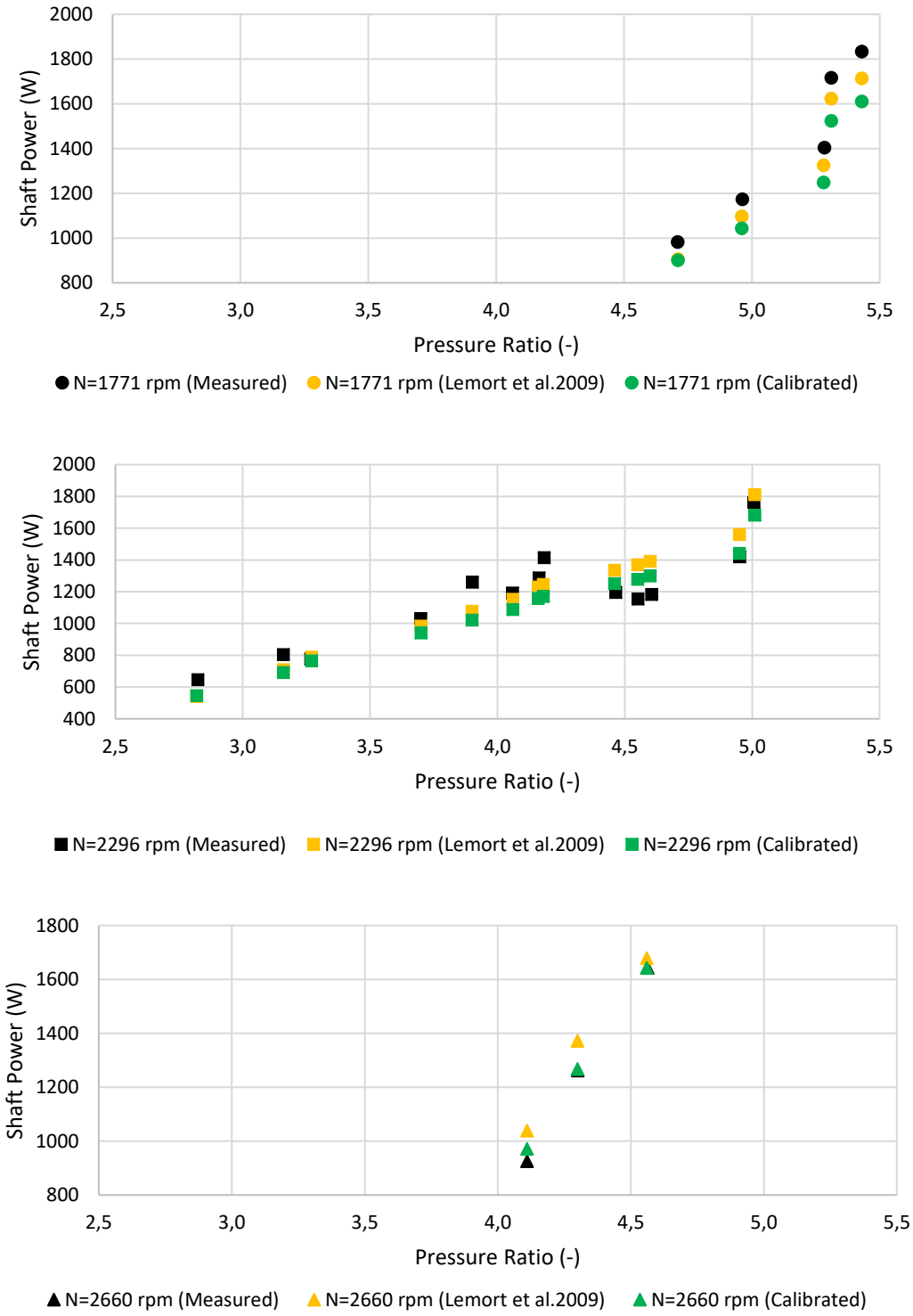

Figure 38 : Evolution of shaft power with pressure ratio

The fitting between measured and calculated data which is given in Figure 38 is acceptable. The prediction in low and high pressure ratios are worse than in the interim values. The maximum error between the measured and calculated is 19% at pressure ratio 3.9 (2296 rpm) and the minimum 0.002% at 4.56 (2660 rpm). It is clearly visible that in the range of 4.50 to 5.5 pressure ratio recorded the peak shaft power. In this range it could be the optimal operation of the expander because has the peak efficiency in combination with peak shaft power. In general, as it was expected, the shaft power increased linearly with the pressure ratio.

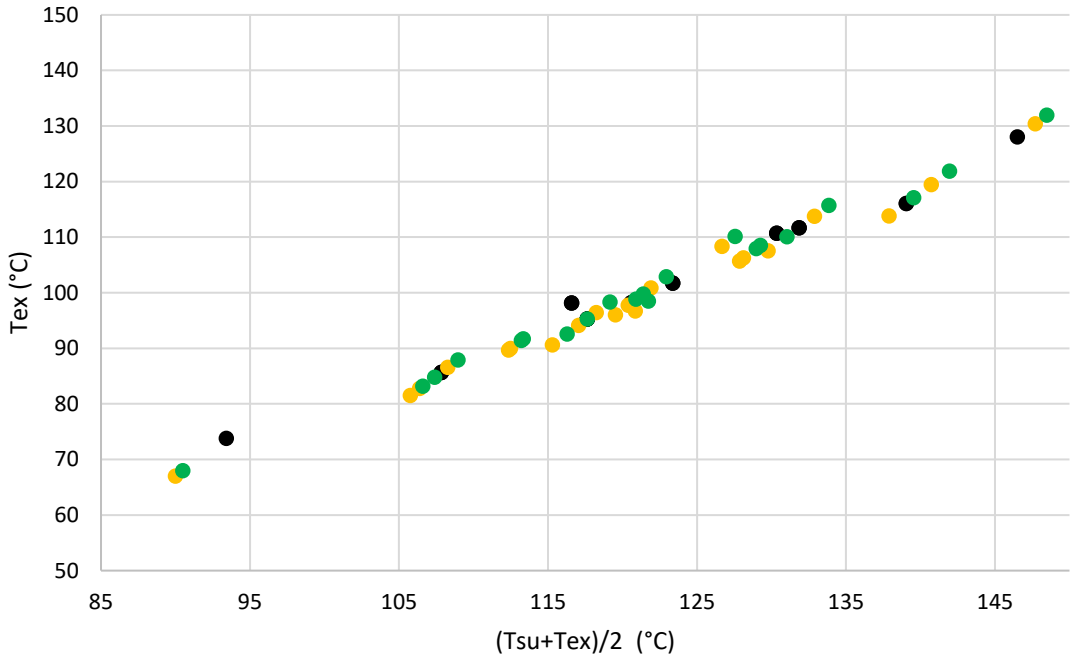

Figure 39: Exhaust temperature with mean temperature between supply and exhaust.

2.4.2 Comparison with Miao et al. [10]

In 2017, Miao et al. [10] conducted an experimental investigation with a scroll expander using R123 as working fluid. In this publication is given extensively the values of the measurements, including supply and exhaust pressure as well as temperatures and produced mechanical power. The mathematical model which used was a semi-empirical based on Lemort et al. [9], with the geometrical parameters to have been calibrated. Although, it is not given the values for supply, exhaust and ambient heat transfer coefficient and the nominal mass flow.

By using the modeled data, a first estimation was calculated only for the parameters that are unknown. In order to optimize the whole set of parameters, with the calibration process which has been described in paragraph 2.3, were used the values measured in tests. The first case will

be referred as modeled and the optimized one, will be referred as tested. Table 3 below, presents these operation data points which were defined in the paper and used for the analysis.

Table 3: Comparison of tested and modeled results Miao et al. [10]

Parameters	Value								
m (kg/h)	Control	656	653	653	650	650	650	648	648
N_t (rpm)	Control	2569	2156	1782	1498	1215	1075	940	831
$T_{exp.in}$ (°C)	tested	142.93	141.14	137.79	132.47	124.65	121.6	120.3	121.29
	modeled	143.54	141.75	136.46	131.90	124.62	120.40	119.63	124.08
$P_{exp.in}$ (kPa)	tested	781.92	848.33	928.53	1008.27	1091.58	1133.33	1168.26	1212.58
	modeled	750.00	820.00	910.00	1000.00	1100.00	1150.00	1180.00	1290.00
$T_{exp.out}$ (°C)	tested	119.5	112.5	105.3	96.43	86.17	81	74.6	66.7
	modeled	118.68	112.60	103.45	95.78	85.04	78.86	69.98	72.98
$P_{exp.out}$ (kPa)	tested	251.29	248.33	246.33	243.22	238.7	236.97	233.95	232.01
	modeled	254.66	251.17	247.59	243.60	240.09	237.76	234.15	234.45
$T_{con.out}$ (°C)	tested	18.15	18.25	18.23	17.84	17.91	18.01	17.3	17.27
	modeled	19.74	19.55	19.29	19.06	18.98	18.86	18.61	18.55
$P_{con.out}$ (kPa)	tested	144.01	143.61	142.16	140.51	139.53	139.44	137.93	137.84
	modeled	149.90	147.53	145.14	142.47	140.66	139.40	137.91	137.21
$T_{evp.in}$ (°C)	tested	19.43	20.13	20.09	19.9	19.74	19.91	19.48	19.07
	modeled	20.74	20.55	20.29	20.06	19.98	19.86	19.61	19.55
$P_{evp.in}$ (kPa)	tested	799.64	866.54	940.77	1019.29	1100.63	1140.80	1180.36	1219.52
	modeled	770.00	840.00	930.00	1020.00	1120.00	1170.00	1200.00	1320.00
W_{exp} (W)	tested	1395	2036	2414	2650	2651	2553	2399	2297
	modeled	1474.05	1975.97	2325.36	2505.24	2572.49	2552.13	2407.45	2465.35

The error objective function for the modeled results was $2.14 \cdot 10^{-2}$ and for the tested measurements $2.53 \cdot 10^{-2}$, respectively

In Table 4 are presented the parameters which were calculated by the calibration process.

Table 4: Calibrated parameters

	Parameters based on modeled results	*Parameters based on tested results*	*Units*
$r_{v_{in}}$	2.27	2.27	$(-)$
$AU_{amb,n}$	19	29.95	(W/K)
$AU_{su,n}$	39.905	49.33	(W/K)
$AU_{ex,n}$	33.42188	4.91	(W/K)
A_{leak}	7.00E-06	7.00E-06	m^2
T_{loss}	5.5	4.267	$N \cdot m$
$V_{s_{exp}}$	1.19E-04	1.19E-04	m^3
A_{su_n}	6.10E-05	6.10E-05	m^2
M_{dot_n}	0.0613	0.0601	kg/s

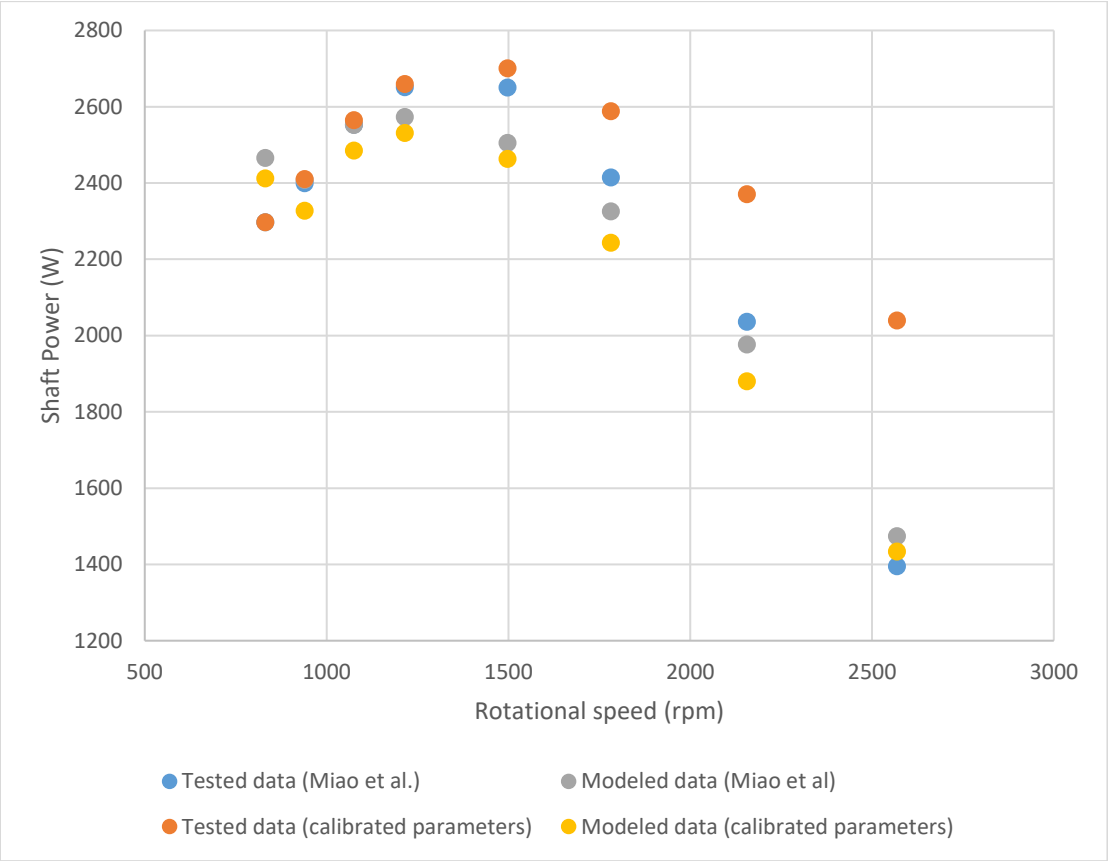

Figure 40: Shaft power with rotational speed.

Figure 40 presents the produced shaft power as a function of the expander's rotational speed and the fitting between tested and modeled data for pressure ratio in range of 7.5-13 bar. The mass flow between these points is approximately constant, in the small range of 648-656 kg/h. Thus, operational points with high supply pressure correspond to low rotational speed and for low supply pressure to high rotational speed. There are trends both for data which recorded in publication and data calculated by the calibration process. As it can be observed the maximum shaft power obtained in range 1000-1500 rpm and for greater rotational speed reduces. The minimum shaft power relative error in tested data between the published and calculated data is zero, for rotational speed 831 rpm and the maximum 46.2% for rotational speed of 2569 rpm. In modeled data the errors are much less and moreover, the maximum error is 4.8% at 2156 rpm and the minimum 1.6% at 1215 rpm.

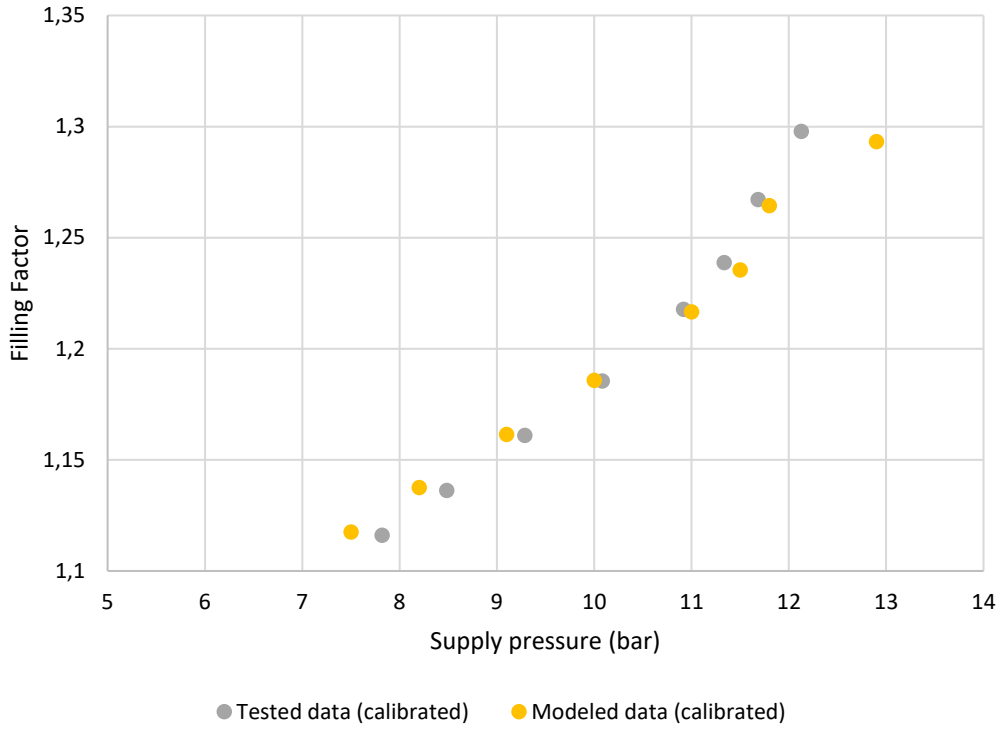

Figure 41: Filling Factor as a function of supply pressure

In Figure 41 is represented the trend of filling factor with the supply pressure. It has been calculated both for modeled and tested data, considering the calibration of parameters by the semi-empirical model. As it can be observed, the filling factor increases with increasing the supply pressure and decreasing the rotational speed.

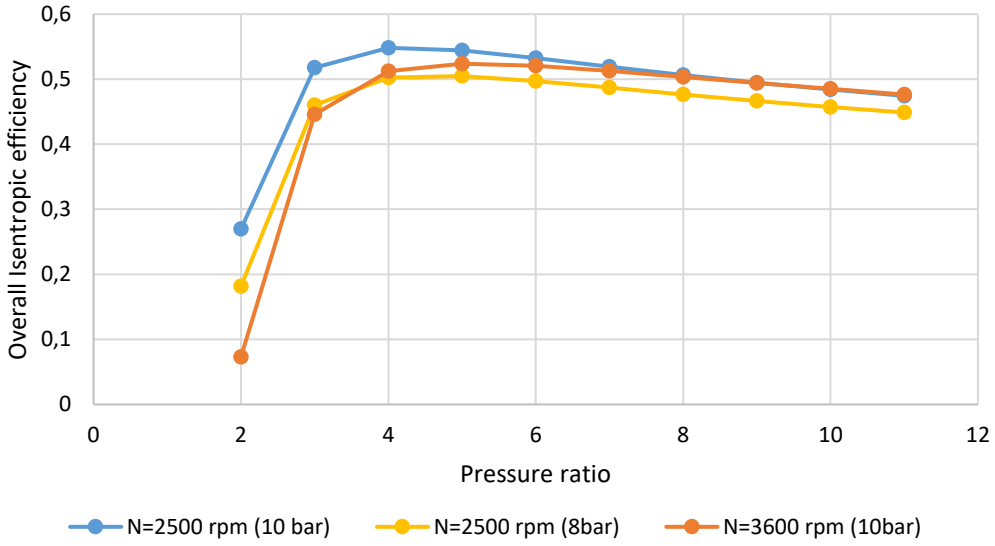

Figure 42: Isentropic efficiency with pressure ratio

In Figure 42 is presented the performance of the scroll expander as a function of pressure ratio and each curve has fixed supply pressure and rotational speed. Apparently, the isentropic efficiency increases when increasing the pressure ratio until a certain value and then slightly decreases.

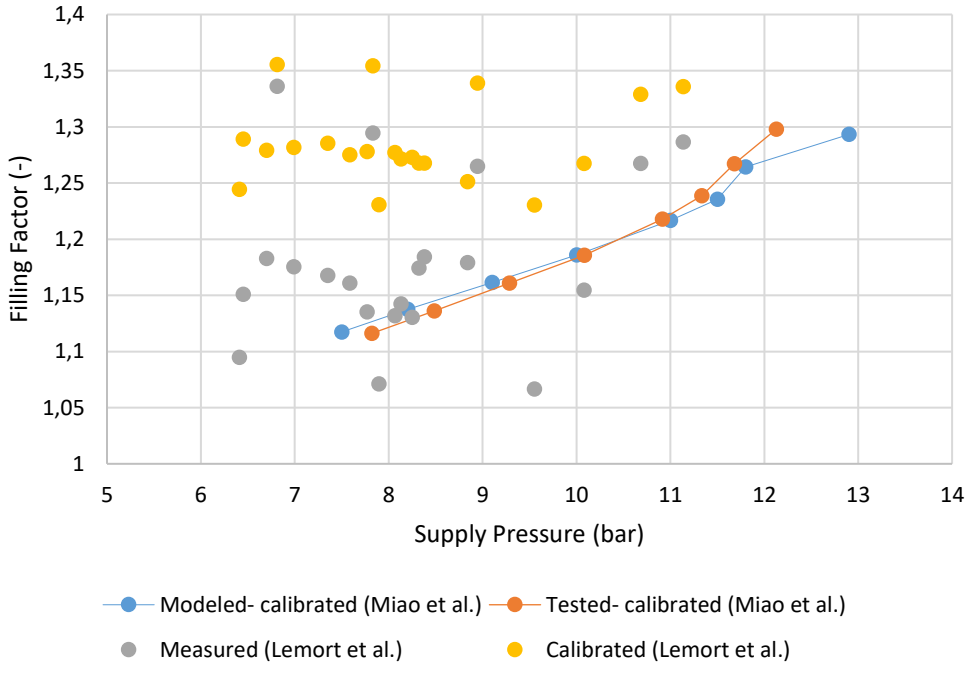

Figure 43: Comparison with Lemort et al. expander model filling factor.

Figure 43 presents a comparison to filling factor between Miao et al. [10] expander and Lemort et al. [9]. In Miao's model there is a constant increase in contrast with Lemort's where it cannot be observed a clear trend. This is caused due to a wide range of mass flow values; in fact, in Lemort measurements the mass flow range is 0.045-0.09 kg/sec in contrast with Miao et al. where is approximately constant.

2.4.3 Comparison with Ziviani et al. [11]

In this work, both the semi-empirical model and an ANN model used to determine the optimal set of parameters in expander modeling. For this comparison will be used the set that came up from the semi-empirical model. The objective function that defined for the calibration process has been modified as:

$$error^2 = \sum_{1}^{10}\left(\left(\frac{\dot{m}_{calc}-\dot{m}_{meas}}{\dot{m}_{meas}}\right)^2+\left(\frac{T_{ex_{calc}}-T_{ex_{meas}}}{60}\right)^2+\left(\frac{\dot{W}_{shaft_{calc}}-\dot{W}_{shaft_{meas}}}{\dot{W}_{shaft_{meas}}}\right)^2\right)$$

It is not used all the experimental data points but it is considered a set of 10 randomly points to optimize the parameters. The range of supply pressure was between 1.5-20 bar and the mass flow 0.05-0.15 kg/s R245fa.

In the publications, there is a clear separation in two categories of figures according to supply temperature, for 85 °C and 110 °C. In order to make the comparison, has been used the case of 85 °C, with 18 experimental points and its data exported from paper's electronic annex [11]. In contrast with the paper's study, in this thesis are used all the experimental points in calibration process.

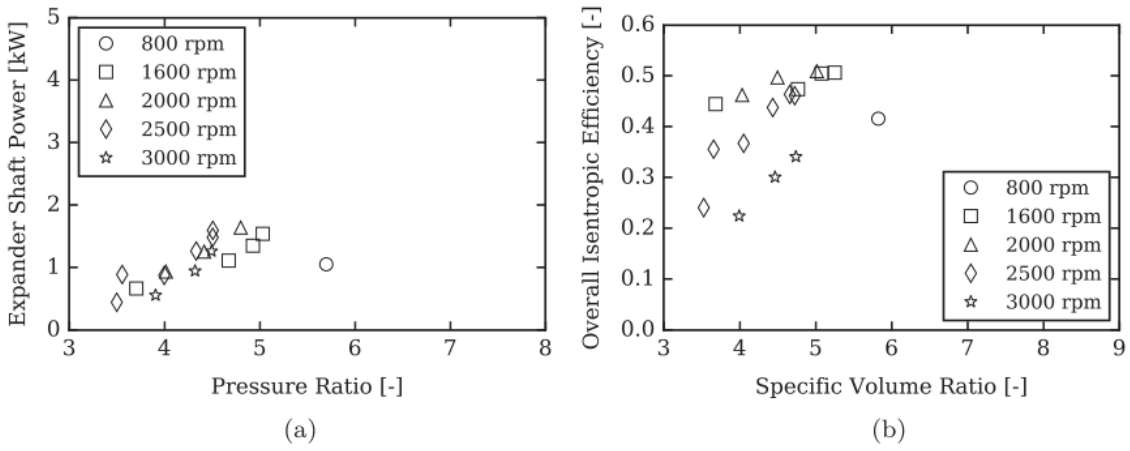

Figure 44: (a) Shaft Power with pressure ratio and (b) Isentropic Efficiency with pressure ratio [11]

In Figure 44 (a) that presented in Ziviani et al. [11], can be seen that the produced power increases with increasing pressure ratio. The measurements are divided by the rotational speed and it can

be observed that the peak power was measured at 2000 rpm. Also, as being represented in Figure 44 (b) the peak efficiency observed at 2000 rpm, for a specific volume ratio is about 5.

Table 5: Calibrated Parameters

	Parameters in Ziviani et al. [11]	*Calibrated Parameters*	*Units*
$r_{v_{in}}$	3.3009	3.3	$(-)$
$AU_{amb,n}$	6.1725	6.000007	(W/K)
$AU_{su,n}$	28.3949	21.36	(W/K)
$AU_{ex,n}$	11.7066	19.999943	(W/K)
A_{leak}	7.43E-06	7.50E-06	m^2
T_{loss}	2.2968	4	$N \cdot m$
$V_{s_{exp}}$	8.10E-05	8.00E-05	m^3
A_{su_n}	4.01E-05	4.00E-05	m^2
M_{dot_n}	0.138	0.120	kg/s

Table 5 presents the calibrated parameters of the semi-empirical model. In first column is the data calculated in paper [11] and the global error that was calculated by the equation in paragraph 2.3 and the value was 0.369888. It is worth noting that in the paper is referred that the value of objective function was 0.282 but it has been used the modified equation for 10 experimental points. In the second column of Table 5, the data calculated after the calibration process according to semi-empirical model is presented. The result for the global error was 0.202422.

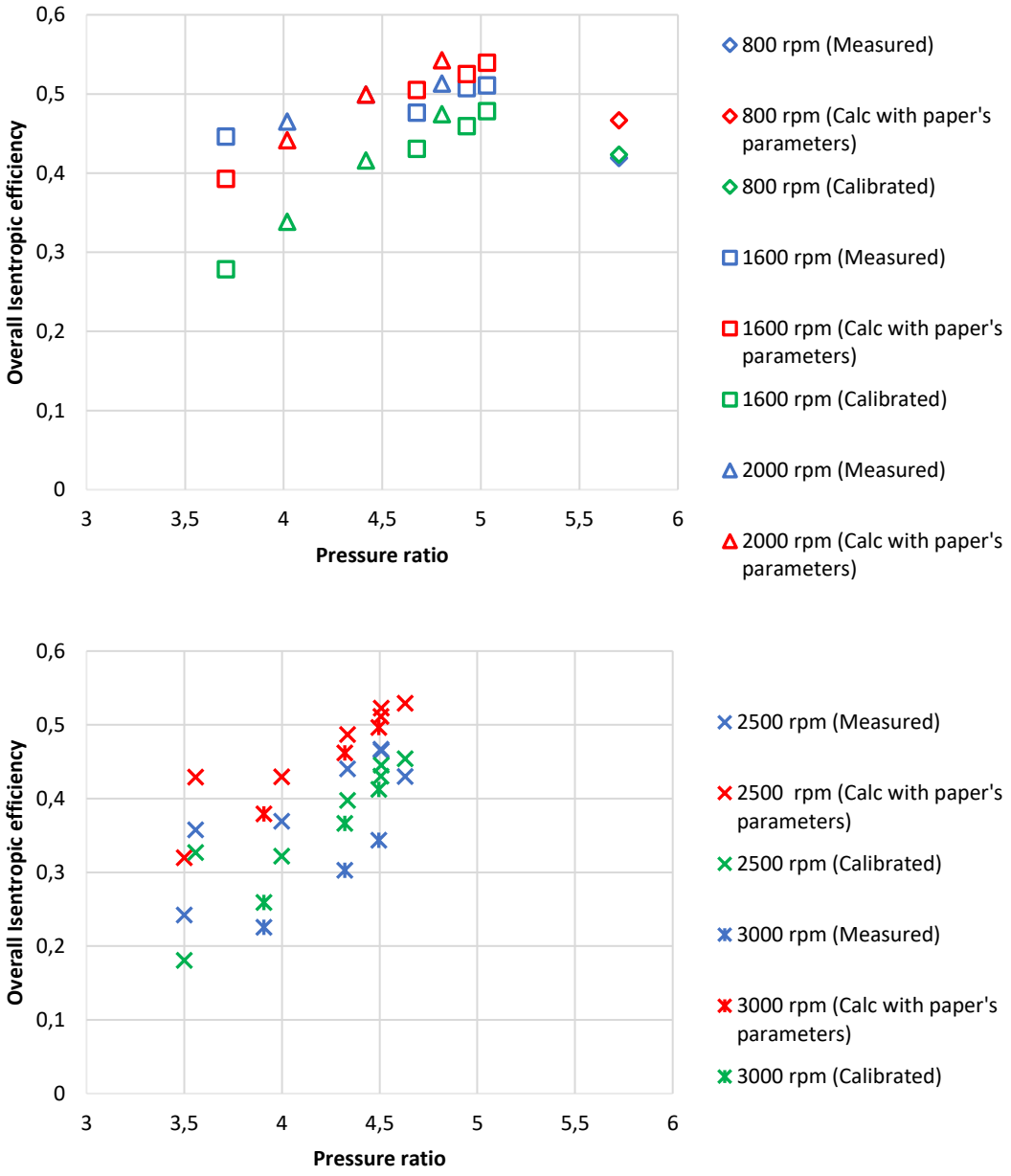

Figure 45 (a), (b): Expander's isentropic efficiency with pressure ratio.

In Figure 45 is presented the isentropic efficiency of the expander as a function of the pressure ratio for different rotational speeds. The first set of data points (blue color) depicts the measured values from the experiments. The second one (red color) refers to the calculated by the model of this thesis by using the first set of parameters as defined by Ziviani et al. [11]. Finally, the green points on figure calculated using as inputs the data of the experimental points and with the calibrated parameters which defined in Table 5. It is clear that the points with calibrated parameters fit better on measurements. The maximum error between measured and calibrated is 37.6% at 3.7 pressure ratio (1600 rpm) and the minimum is 1.002% at 5.7 (800 rpm).

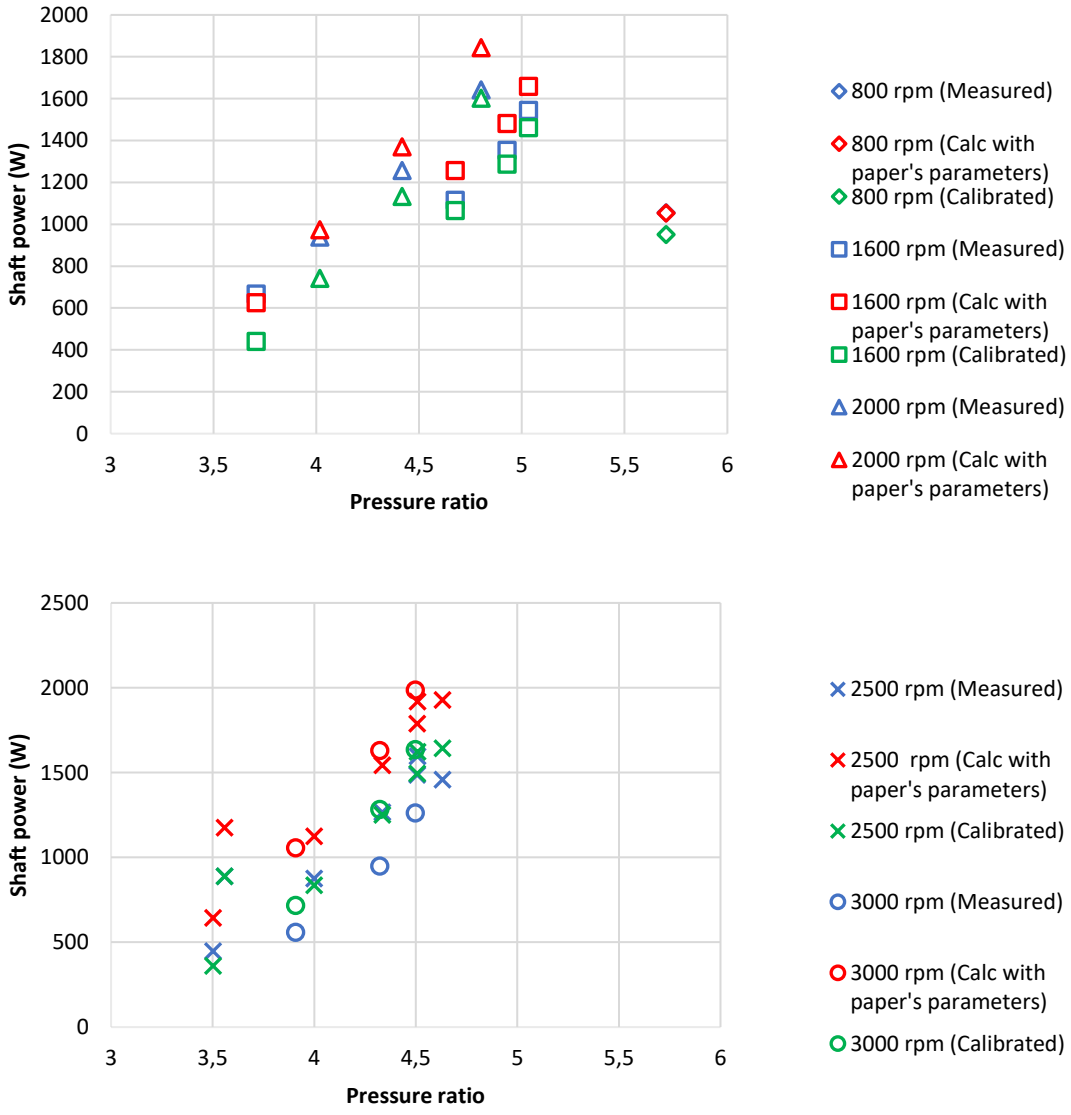

Figure 46 (a), (b): Expander's shaft power as a function of pressure ratio.

In a similar way, in Figure 46, represented the expander's output power as a function of pressure ratio. As previous, the data that have been calculated with calibrated parameters approaches more the measurements. Moreover, the maximum error is 35.27% at 4.32 pressure ratio (3000 rpm) and the minimum 0.1% at 3.56 (2500 rpm).

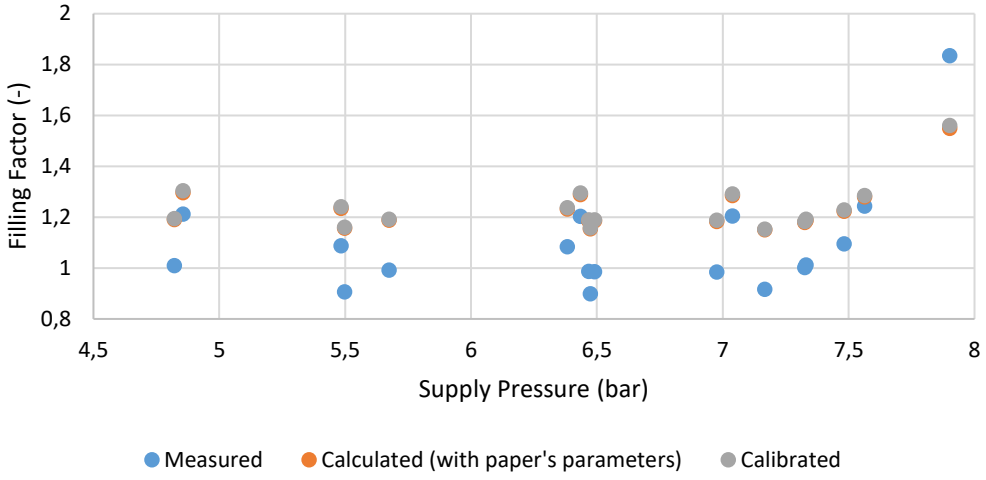

Figure 47: Filling Factor as a function of supply pressure

In Figure 47 is presented the filling factor as a function of supply pressure both of measure, model calculated and calibrated data. It is obvious that the error between measured and calibrated parameters is remarkable with an average error of 16.65%.

2.4.4 Comparison of the expanders' performance.

Except from the papers compared above, in paragraph 2.4, the data of Dumont et al. [1] has been considered but it was not possible to do the calibration due to insufficient experimental points. There is an extensive report for the isentropic efficiency and filling factor of the expanders, nevertheless no values are provided for the exhaust temperature and shaft power apart from a working range. Consequently, the output values calculated only for the parameters which were identified on paper, in order to add them in performance comparison.

Figure 48, presents the performance curve for the expanders which were studied above. For each curve, the rotational speed has adjusted for maximum of overall isentropic efficiency. Also, for the curve calculation the calibrated parameters were used (except from Dumont et al. [1]). In parenthesis are defined the supply pressure for each case; all calculations were conducted for 25°C ambient temperature.

All the curves with solid lines are for scroll expanders, while the dashed-line for screw model of Dumont et al. [1]. As it can be seen, in all cases, the efficiency has a significant value for pressure ratios larger than 3, because for lower ratios, the losses are comparable to shaft power. The peak efficiency is observed for pressure ratio approximately 5 and followed by a small reduction.

This is due to the limitations of the expander shaft speed at high pressure. The best performance was reported by scroll expander with calibrated data from Lemort et al. [9]. Also, in this figure it can be observed that scroll expanders can operate in wide range of pressure ratios, without significant decrease of efficiency, in contrast with screw expander which despite the high peak efficiency, have sharper decrease with increasing pressure ratio.

Similar to Figure 48, in Figure 49 there is a comparison in performance of literature's expanders but in this case is compared the produced mechanical power. As it was expected, there is a monotonic increase in shaft power by increasing the pressure ratio. It is worth noting that the performance above is plotted for really high-pressure ratios which cannot be achieved in complete test-rigs, due to pumps limitations. The highest pressure ratios which recorded in the investigated studies, was 5-6.

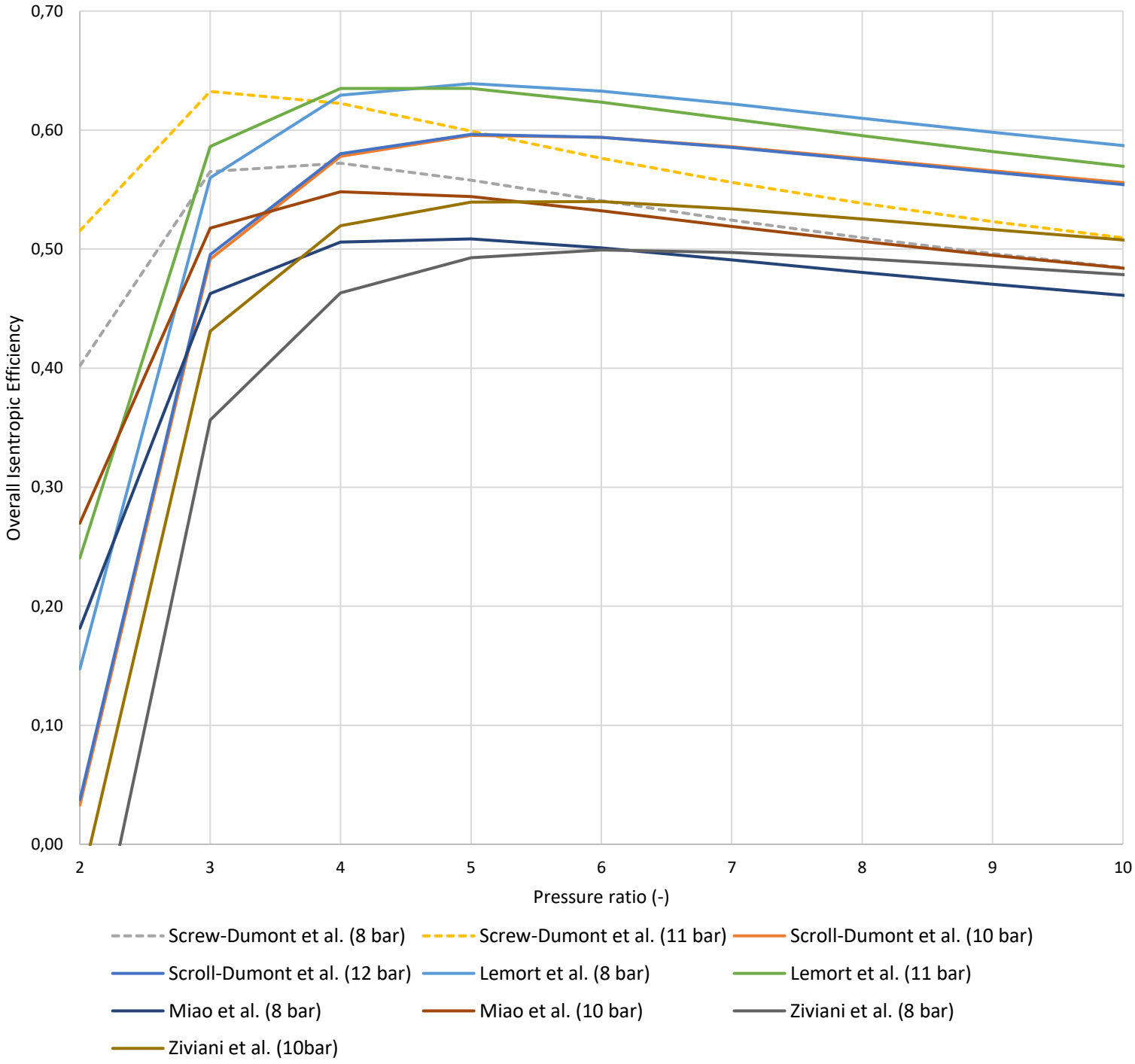

Figure 48: Optimal efficiency curve for the compared expanders.

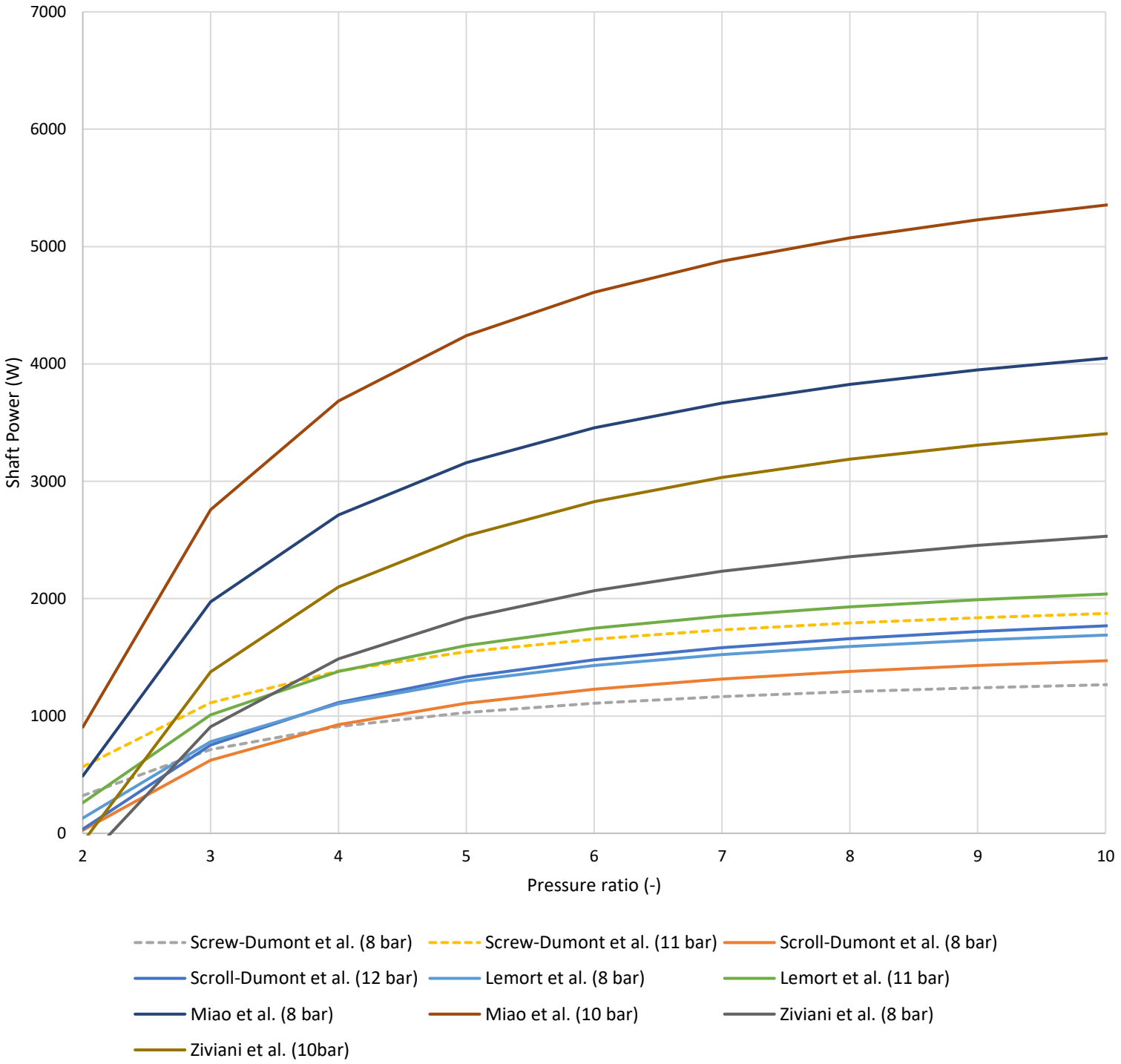

Figure 49: Shaft power as a function of pressure ratio.

3. Expanders' operation with low-GWP refrigerants

3.1 Review of refrigerants R1234ze(E) and R1233zd(E)

Due to Regulation EU No 517/2014, there is a growing trend to replace refrigeration and air conditioning systems with new systems that use environmentally friendly refrigerants [17]. The global warming potential (GWP) limits must be very low, so refrigerants R1234ze(E) and R1233zd(E) are two of the most promising, due to present good environmental properties. In a few years, a lot of studies have been conducted to characterize these refrigerants, to be correctly designed in R1234ze(E) and R1233zd(E) systems.

Table 6 and Table 7 present the main properties of R1234ze(E) and R1233zd(E) and it can be seen the really low GWP and the zero ODP values.

Table 6: Main Properties of R1234ze(E) [18]

Property	Value
Group	HFO
Chemical formula	trans-$CF_3CH = CHF$
Molar mass, kg/kmol	114
Critical temperature, °C	109.36
Critical pressure, bar	36.4
Critical density, kg/m^3	489.2
Normal boiling point, °C	−19.3
Triple point, °C	−104.53
ODP (ozone depletion potential)	0
GWP_{20} (global warming potential) 20 years	4
GWP_{100} (global warming potential) 100 years	1
Atmospheric lifetime of individual components, days	16.4

Table 7: Thermo-physical comparison of R1233zd(E) and R245fa [19]

Parameters	R1233zd(E)	R245fa
Chemical formula	$CF_3CH{=}CHCF_3$	$CF_3CH_3CF_2$
P_c (kPa)	3570	3650
T_c (°C)	165.6	154.01
Boiling point (°C)	17.97	14.81
Latent heat at boiling point (kJ/kg)	195.52	196.23
Mol.w. (kg/kmol)	130.5	134
Slope	dry	dry
ODP	0.00034	0
GWP_{100yr}	7	1030
Atmospheric life time	7.7	0.07
Flammability	Non-flammable	Non-flammable
ASHARE Std 34 safety class	A1	B1
Decomposition temperature(°C)	> 250	n.a.

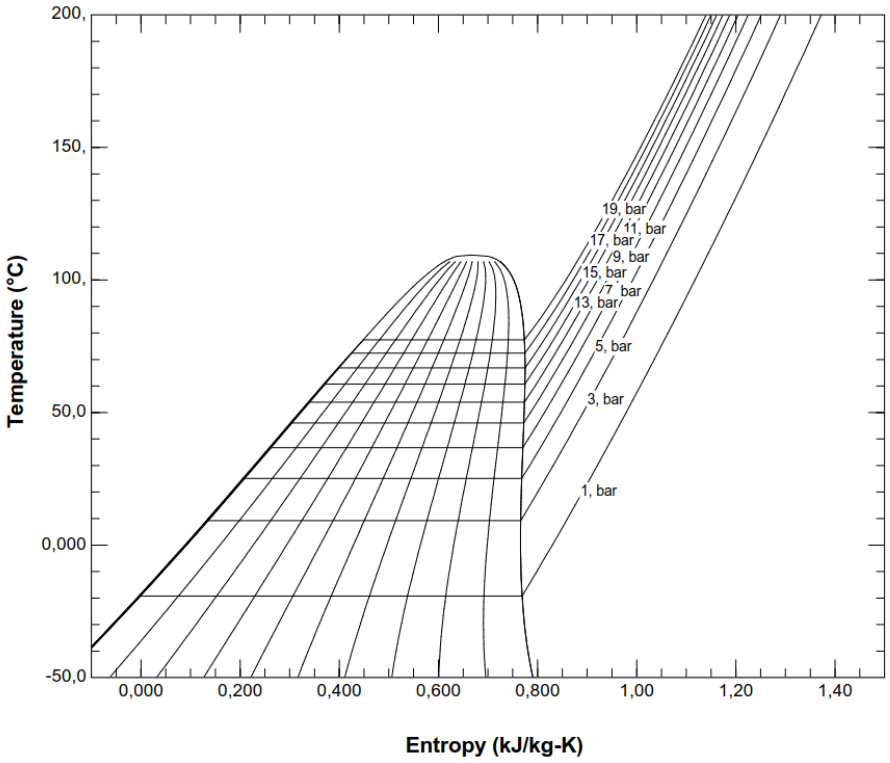

Figure 50: T-s diagram of R1234ze(E) [20]

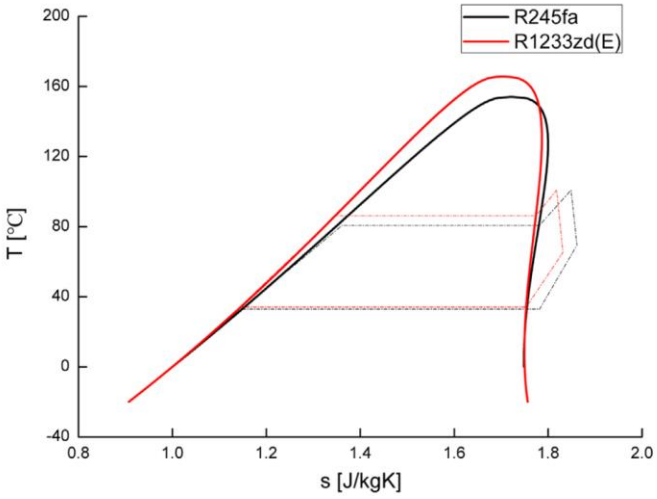

Figure 51: T-s diagram of R245fa and R1233zd(E) [19]

3.2 Expanders operation with refrigerant R1234ze(E) and R1233zd(E)

All the expander models that have been calibrated in paragraph 2.4, will be recalculated with working fluids R1234ze(E) and R1233zd(E) in order to check the response of the semi-empirical model. Both fluids will be tested for the same supply conditions as checked above.

3.2.1 Lemort et al. model operation with refrigerants R1234ze(E) and R1233zd(E)

The operation conditions used on Lemort's tests have a range of supply temperature 101.7-165.2°C. As can be seen in the T-s diagram in Figure 50, the critical point of R1234ze(E) is 109.37°C. The maximum temperature that CoolProp library can calculate the properties is 147°C. Because of the fact that some points exceed the limit, such as supply temperature, in the case of R1234ze(E), is used the saturated temperature at each pressure increased by the superheating which was applied in the case of R123. The superheating range in operation with R123 was in range 7-70°C. The new supply temperatures range between 52-107.5°C. Also, imposed the same rotational speed as input and calculated again the mass flow rate. For the case of R1233zd(E) the supply conditions are identical with the case of R123 in paper's review.

In figures below are shown the calculated data with refrigerant R123 and with the calibrated parameters, as well as the results of R1234ze(E) and R1233zd(E) calculated with the same calibrated parameters.

In Figure 52 (a), (b), (c), are presented the efficiency with pressure ratio, for the various refrigerants. Figures are divided based on the expander's rotational speed. It can be observed that the highest error is for 1771 rpm rotational speed and for the case of R1234ze(E), with the relative error ranges in 0.3%-1.9%. Similarly, in operation with R1233zd(E) the error is about 1.3%-2.4%. In higher rotational speeds, the relative error does not exceed the values of 1% and 1.1% for each refrigerant, respectively. This effect can be explained by the lower density of two low-GWP refrigerants which causes higher flow velocities and in turn higher losses in the expander which is more intense in low rotating shaft speeds. To sum up, the efficiency's deviation from operation with R123, decreases both by increasing pressure ratio and rotational speed.

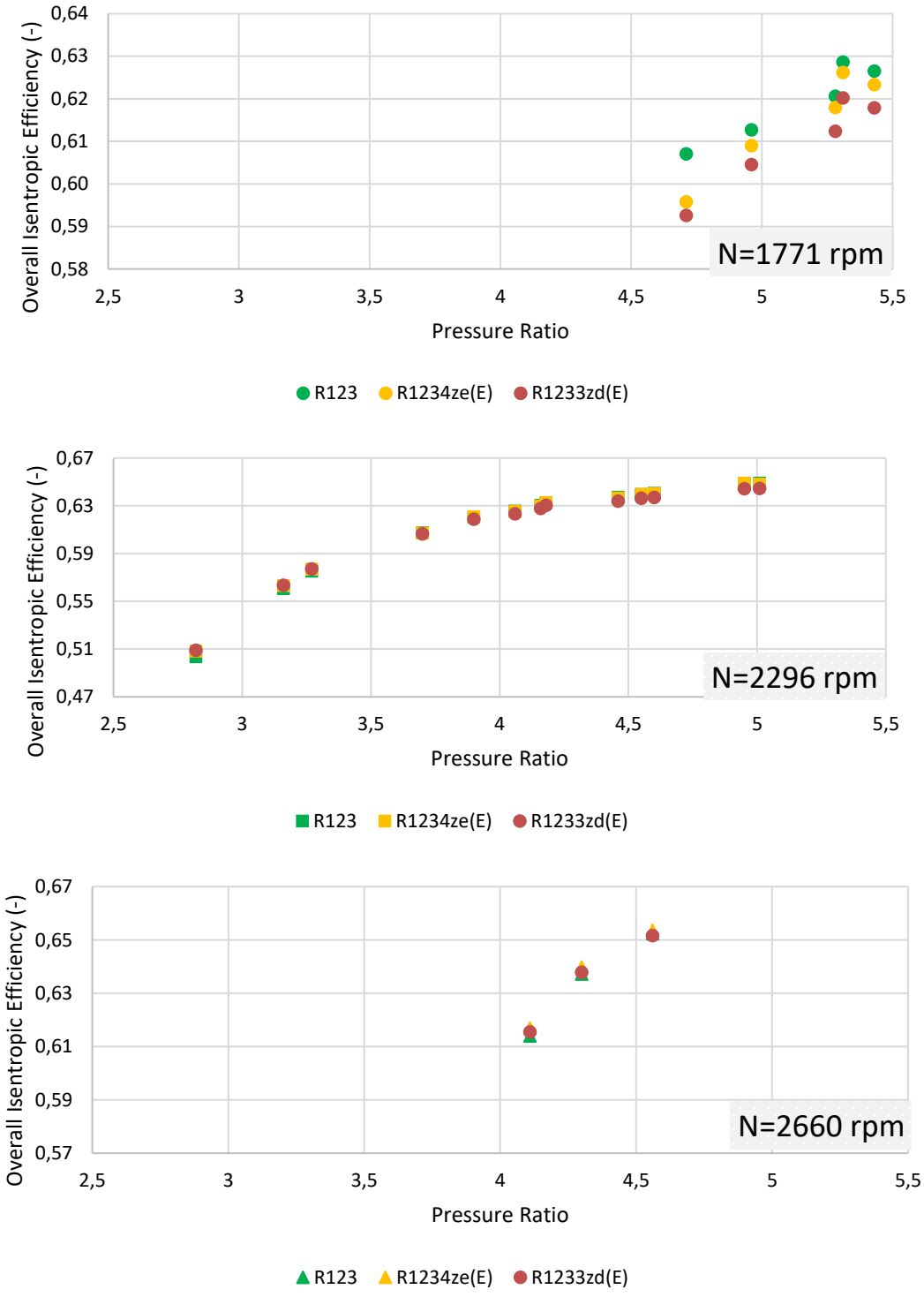

Figure 52: Isentropic efficiency for refrigerants R123, R1234ze(E) and R1233zd(E)

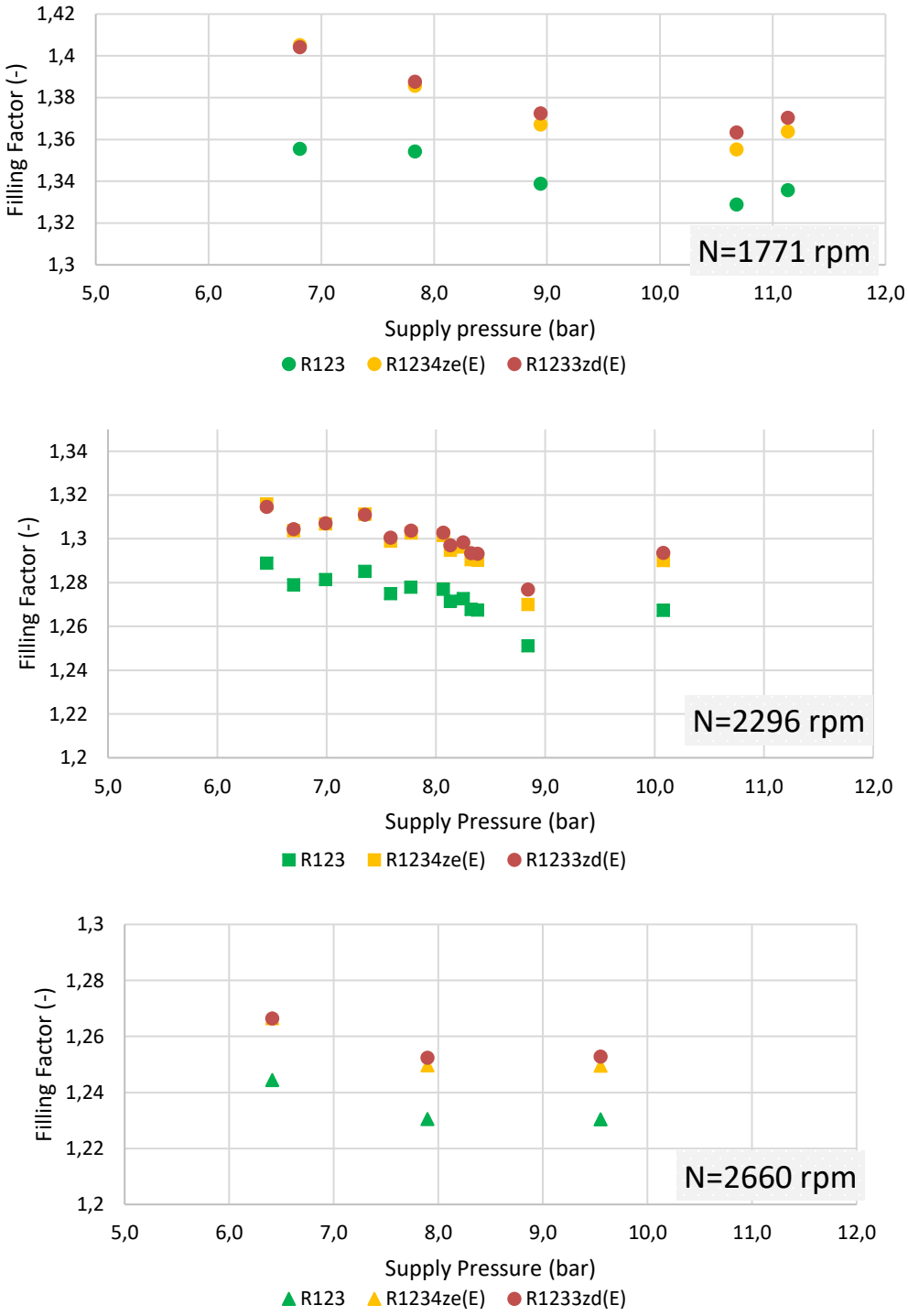

Figure 53: Filling factor for refrigerants R123, R1234ze(E) and R1233zd(E)

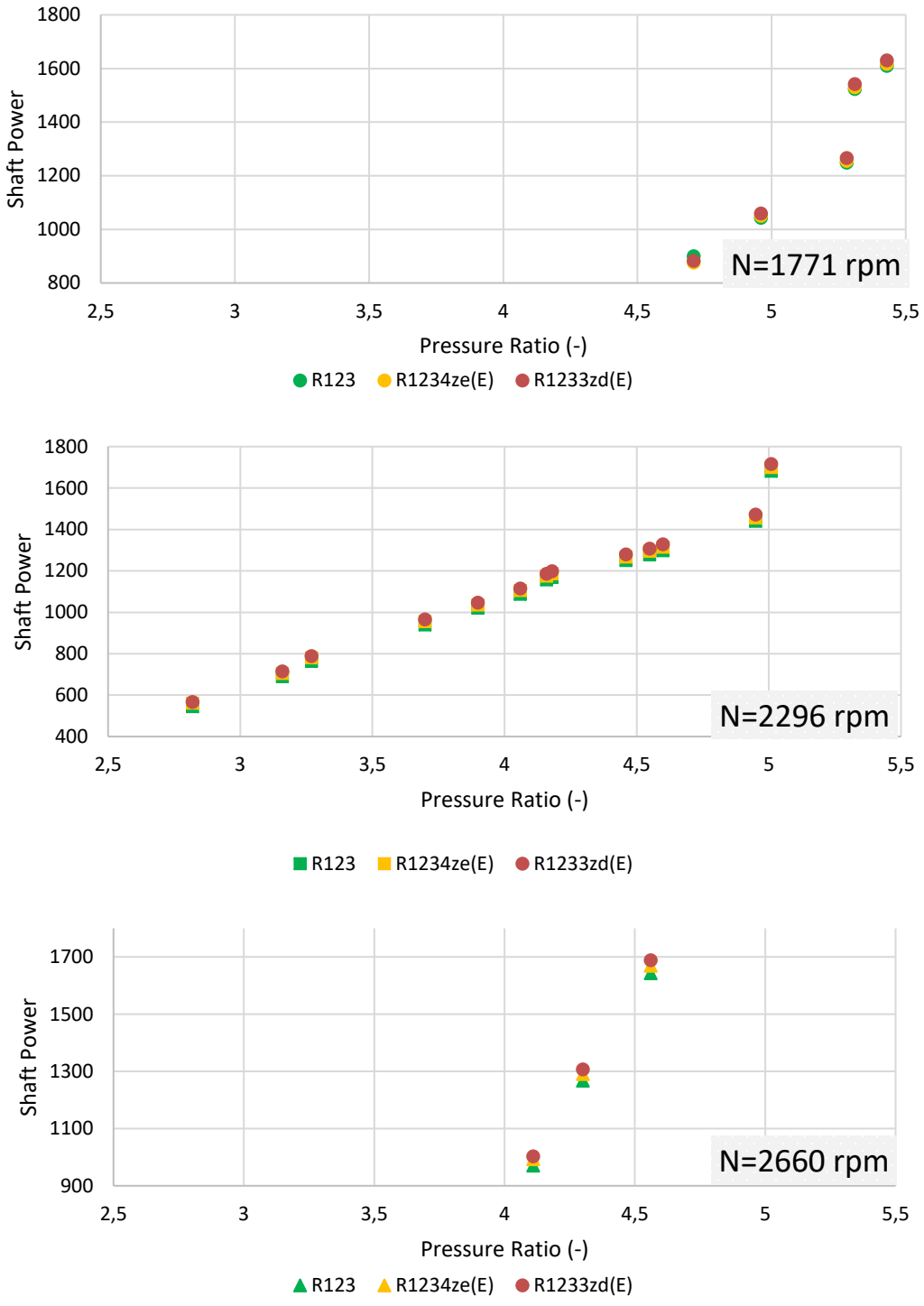

Figure 54: Produced Shaft Power for refrigerants R123, R1234ze(E) and R1233zd(E)

In Figure 54(a), (b), (c), it can be seen that the produced shaft power for R1233zd(E) is higher than R1234ze(E). The operating point with highest error between R123 and both others is in 2296 rpm for 2.92 pressure ratio. Specifically, the operation with R1234ze(E) produces 3% more power and with R1233zd(E) 4.2%, respectively, compared to R123. In general, for constant rotational speed the deviation decreases by increasing the pressure ratio. By increasing the rotational speed, the deviation from initial operation with R123 increases, too.

As it is observed in Figure 53 (a), (b), (c) the deviation of filling factor value is higher for lower rotational speeds and low pressure ratios and has the value of 3.7% with R1234ze(E) and 3.6% with R1233zd(E). On the other hand, increasing the shaft speed and the pressure ratio, the values are closer to initial operation and the difference does not exceed 1.8% with both low-GWP refrigerants.

An interesting observation from Figure 55 is that the difference between initial operation with R123 and the operation with low-GWP refrigerants is equal in all operation points. The new points (operation with R1234ze(E) and R1233zd(E), respectively) are shifted slightly, due to higher produced shaft power.

Also, it can be seen in this figure that the mass flow is lower for equal shaft power with new refrigerants, but this is caused due to lower density of the fluids compared to R123 and not to expander's model.

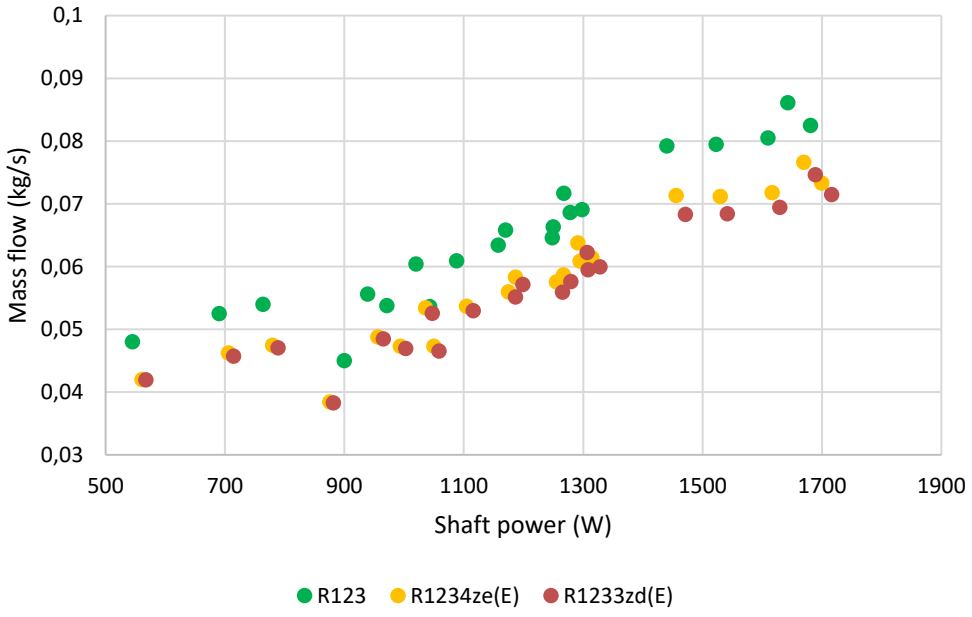

Figure 55: Mass flow as a function of produced shaft power.

3.2.2 Miao et al. model operation with refrigerants R1234ze(E) and R1233zd(E)

In this publication the results are divided in two main categories, the first one for tested data and the second for the modeled data. In figures below, represented the categories for the data which calculated with calibrated parameters both for R123, R1234ze(E) and R1233zd(E). In this comparison, were used identical supply conditions for all the operation points.

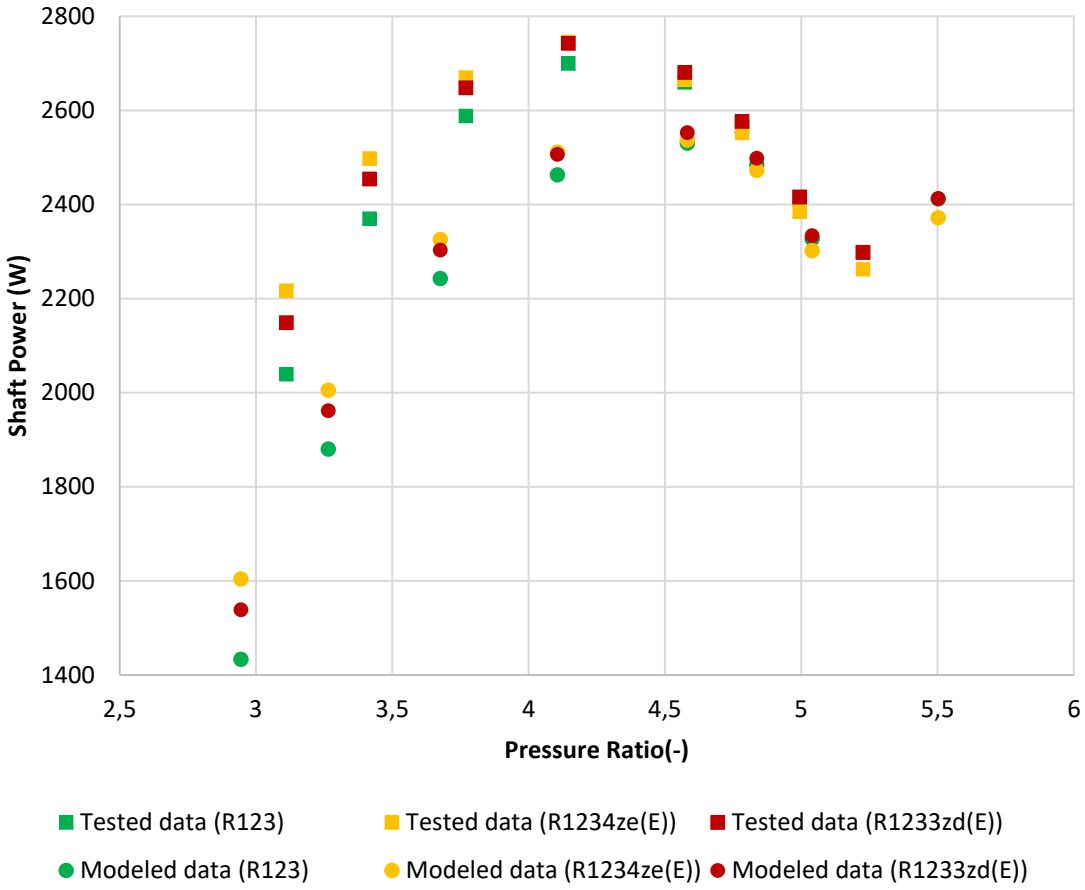

Figure 56: Shaft power with pressure ratio for refrigerants R123, R1234ze(E) and R1233zd(E)

As is shown in Figure 56 in low pressure ratios, less than 4, the highest shaft power achieved with R1234ze(E). In case of tested data for pressure ratio 3.11 when the expander operates with R1234ze(E) produces 8.7% more power than with R123, while in modeled data the increase is 11.9%. For higher pressure ratios, it seems that the effect is reversed and the shaft power with R1234ze(E) is up to 1.5% lower than R123. The operation with R1233zd(E) as working fluid presents a slight increase on shaft power compared to R123. More specifically, for low pressure ratios the increase is more intense and is about 5.4% and for the highest tested pressure ratio 0.5%. An analogous trend occurs in modeled data with the maximum increase at 7.3% and minimum 0.46%.

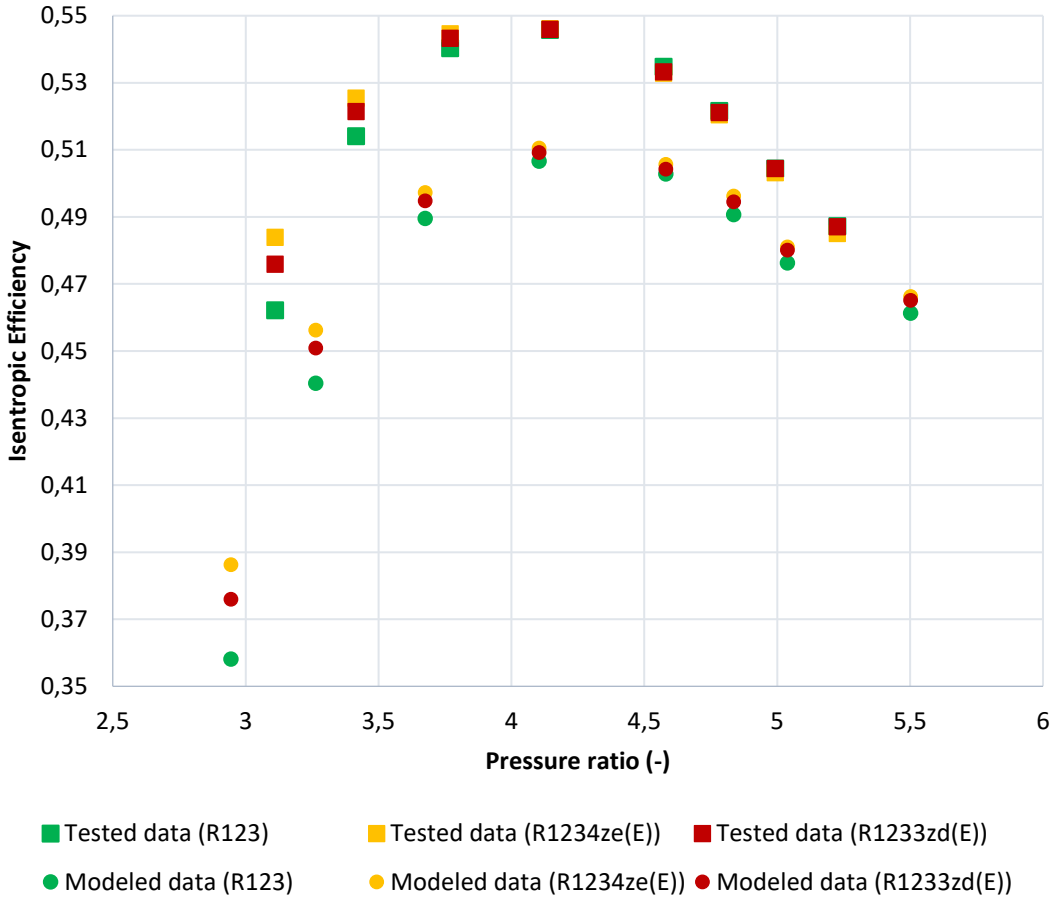

Figure 57: Isentropic Efficiency with pressure ratio for refrigerants R123, R1234ze(E) and R1233zd(E)

In Figure 57 is shown the comparison of the efficiency between operation with the refrigerants R123, R1234ze(E) and R1233zd(E). As it can be observed, the deviation from initial operation with R123 is higher for low pressure ratios. In fact, in pressure ratio 3.1 with R1234ze(E) the efficiency is 4.7% (relative error) higher than R123 and with R1233zd(E) is 2.97% higher. By increasing the pressure ratio, the deviation decreases and the values are 0.04% and 0.03% for R1234ze(E) and R1233zd(E), respectively.

Figure 58 presents the evolution of filling factor as a function of supply pressure. Increasing the supply pressure, the deviation between operation with different fluids increases, too. On the first operating point for pressure 7.8 bar the relative difference is 2.2% for R1234ze(E) compared to R123 and 0.98% for R1233zd(E). On the last point, with pressure 12.13 bar, the difference increases to 7.87% and 3.1% for R1234ze(E) and R1233zd(E), respectively.

To sum up, in this expander by replacing R123 with R1234ze(E) the efficiency will be slightly higher, with more increase in low pressure ratios. The produced power will be also higher, but

in high pressure ratios is a bit lower. For R1233zd(E) both the efficiency and the shaft power are higher, thus is considered an appropriate replacement to R123.

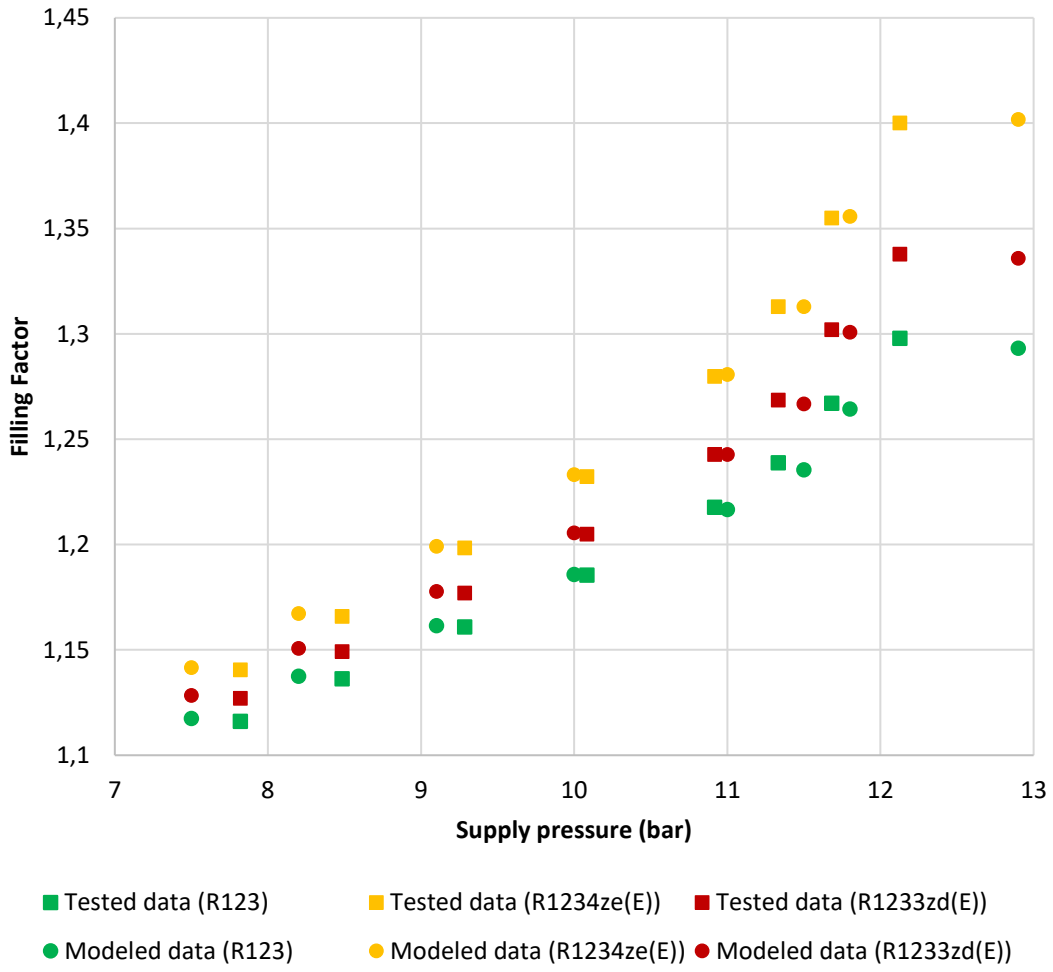

Figure 58: Filling Factor as a function of supply pressure for the refrigerants R123 and R1234ze(E)

3.2.3 Ziviani et al. model operation with refrigerants R1234ze(E) and R1233zd(E).

In this comparison, has been studied the case with operation points which supply temperature is in range of 77-85°C hence in R1234ze(E), identical supply conditions with the paper's tests were used. In case of R1233zd(E), due to lack of properties, an extra constant superheating of 10°C is added.

In Figure 59 (a), (b) it can be seen the expander's isentropic efficiency as a function of pressure ratio and classified by rotational speed. In the first figure it is observed that for low rotational speed as increasing the pressure ratio the deviation from operation with R245fa increases, too. More specifically, for pressure ratio 5.7 and 800 rpm shaft speed the operation with R1234ze(E) is 4.1% less effective than R245fa and in pressure ratio 3.7 at 1600 rpm the efficiency is 1.68%

lower. In all internal tested operation points the efficiency of R1234ze(E) is lower than R245fa as working fluid. The same trend is shown with R1233zd(E) where in maximum pressure ratio the efficiency is 1.7% less than R245fa and for minimum pressure ratio has a difference of 0.045% for low rotational speed (Figure 59 (a)). On higher rotational speed (Figure 59 (b)) observed more deviation in low pressure ratio, about 0.8% and for high pressure ratio the operation with R1233zd(E) is 0.15% more efficient compared to R245fa.

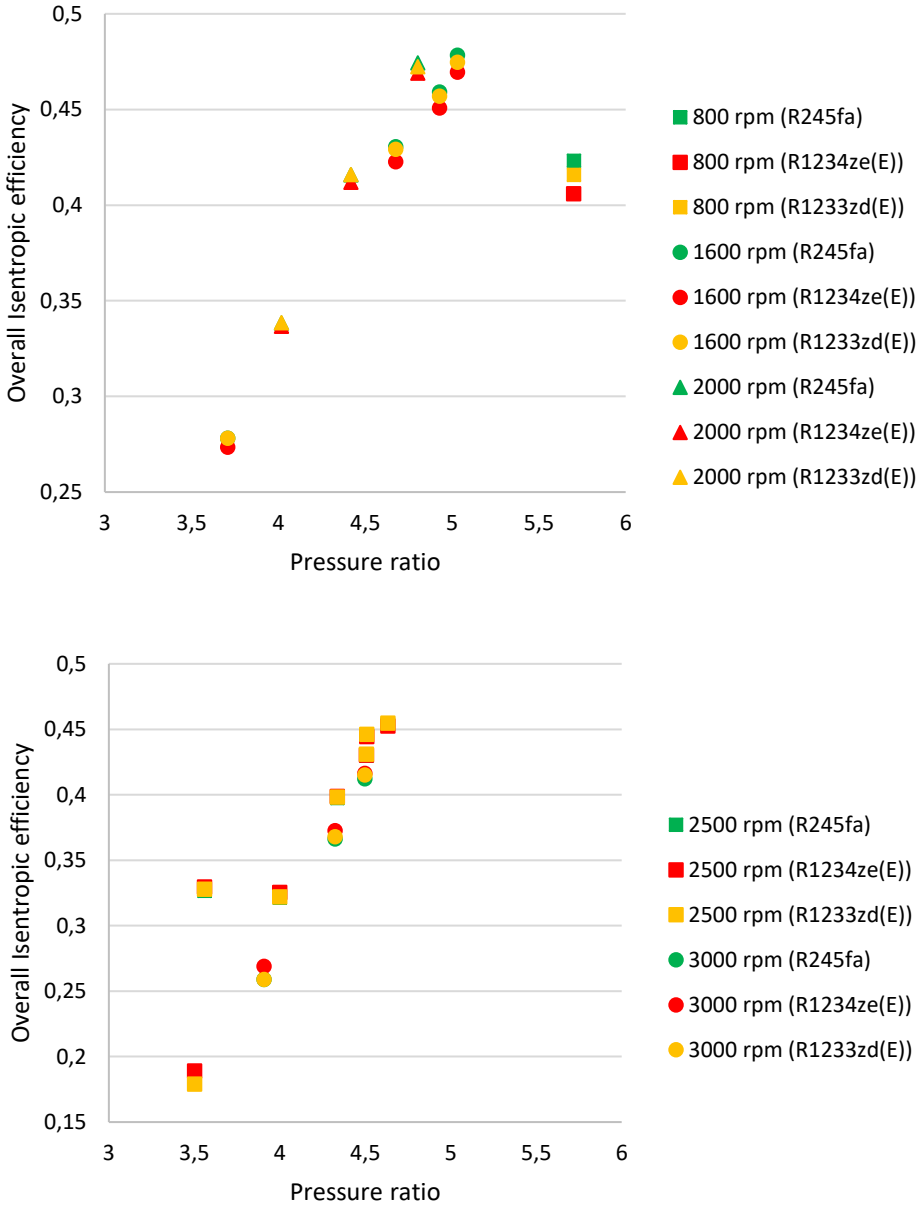

Figure 59: Isentropic efficiency with pressure ratio for the refrigerant R245fa, R1234ze(E) and R1233zd(E)

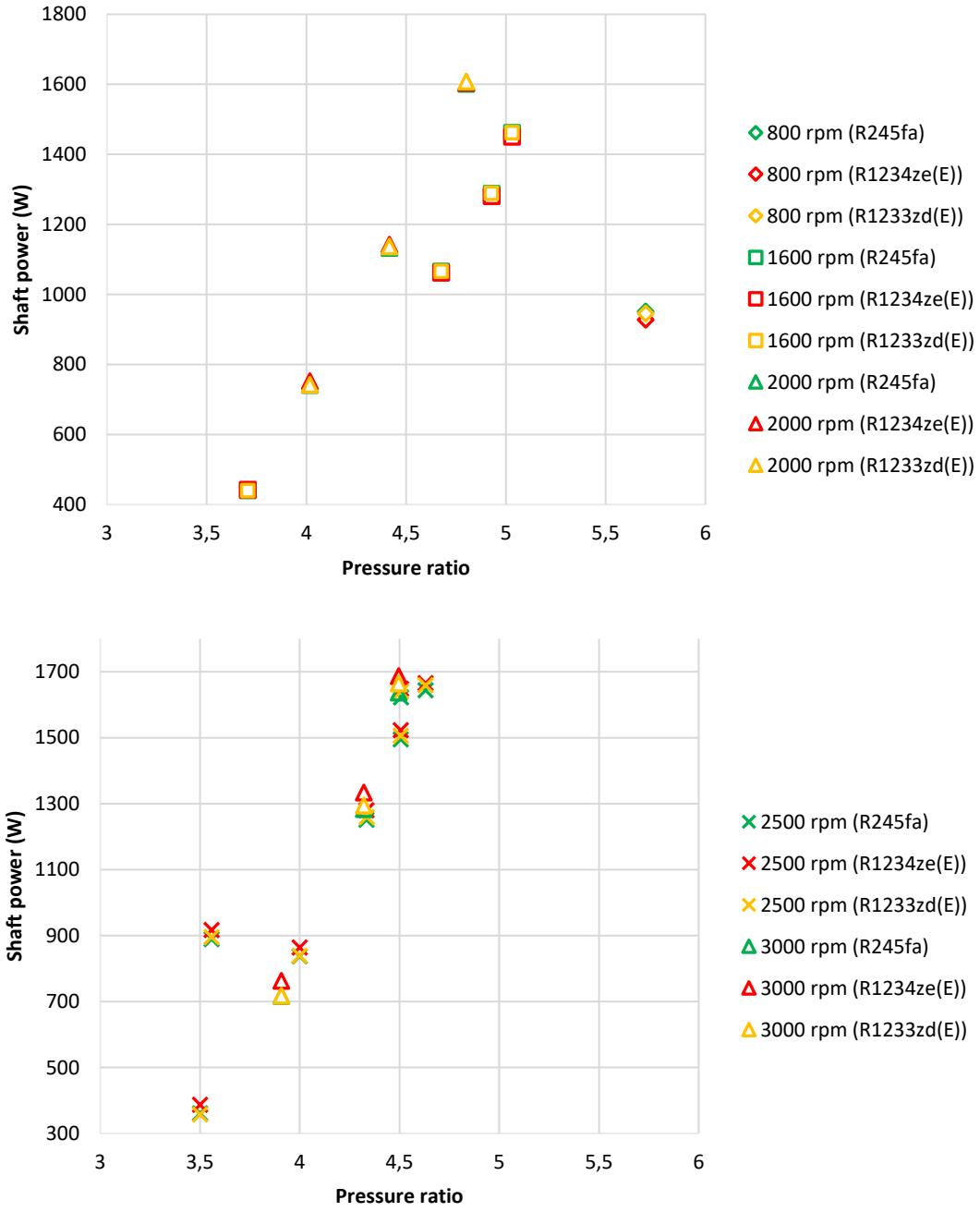

Figure 60 (a), (b): Produced mechanical power as a function of pressure ratio for refrigerants R245fa, R1234ze(E) and R1233zd(E).

In Figure 60 (a), (b) is presented the evolution of produced shaft power as a function of pressure ratio. According to Figure 60 (a), for the highest pressure ratio the shaft power with R1234ze(E) is 2.5% less than R245fa and in lowest pressure ratio 0.3% higher. In case of R1233zd(E) the

difference to operation with R245fa in low pressure ratio is 0.2% less powerful and in high pressure ratio 0.6% lower. In higher shaft speeds -Figure 60 (b)-, the shaft power is generally higher with low-GWP refrigerants compared to R245fa, except from the lowest pressure ratio point with R1233zd(E) where it is 1.1% lower. With the same refrigerant, in high pressure ratio, the power is 0.9% more than R245fa. For R1234ze(E) the deviation ranges between 1.28%-7% and is inversely proportional to pressure ratio.

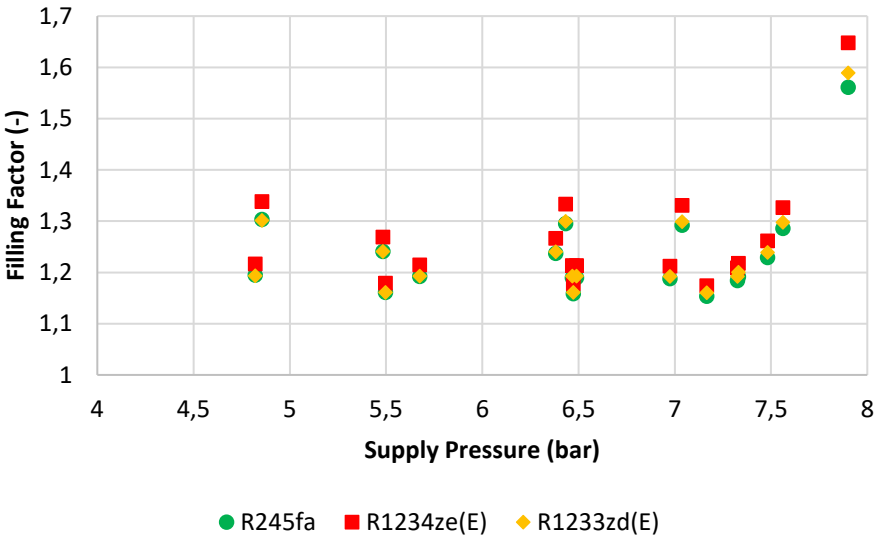

Figure 61: Filling factor as a function of supply pressure for refrigerants R245fa, R1234ze(E) and R1233zd(E).

According to Figure 61, where represented the filling factor with supply pressure for different refrigerants, it can be observed that when operates with R1234ze(E) there is the highest deviation from the initial operation with R245fa. Specifically, in highest supply pressure 7.9 bar and corresponding shaft speed 800rpm, the filling factor is 5.5% higher than R245fa. For constant rotational speed, as increasing the supply pressure, the deviation increases, too. In lowest supply pressure the filling factor of R1234ze(E) is 1.6% higher compared to operation with R245fa. On simulations with R1233zd(E) the filling factor is even closer to initial operation and is 1.8% higher in maximum supply pressure and 0.15% lower in minimum pressure.

4. Expansion in two-phase region

Even though many ORC systems have been investigated in the last years, there is not any experimental data for wet expansion. In terms of this thesis, it will be checked the reliability of semi-empirical model proposed by Lemort et al. [9] in two-phase conditions. Due to a lack of experimental measurements and because it has not developed a test-rig yet, the expander models used previously will be evaluated. It will be simulated the effect of wet expansion to overall expander's efficiency, to the produced mechanical power and finally the effect to filling factor.
As described above, the mathematical model has as independent variable the refrigerant mass flow or the rotating shaft speed. So, both cases have been studied for a better overview.

4.1 Wet expansion simulation on literature models

4.1.1 Lemort et al. model

In this test rig was investigated a scroll expander with R123 as working fluid. On the calculations for the wet expansion were used the same pressure values for inlet and outlet with the difference that the expansion starts at a fluid quality 70% or 60%. In the first case imposed the same rotational speed with initial superheated operating points.

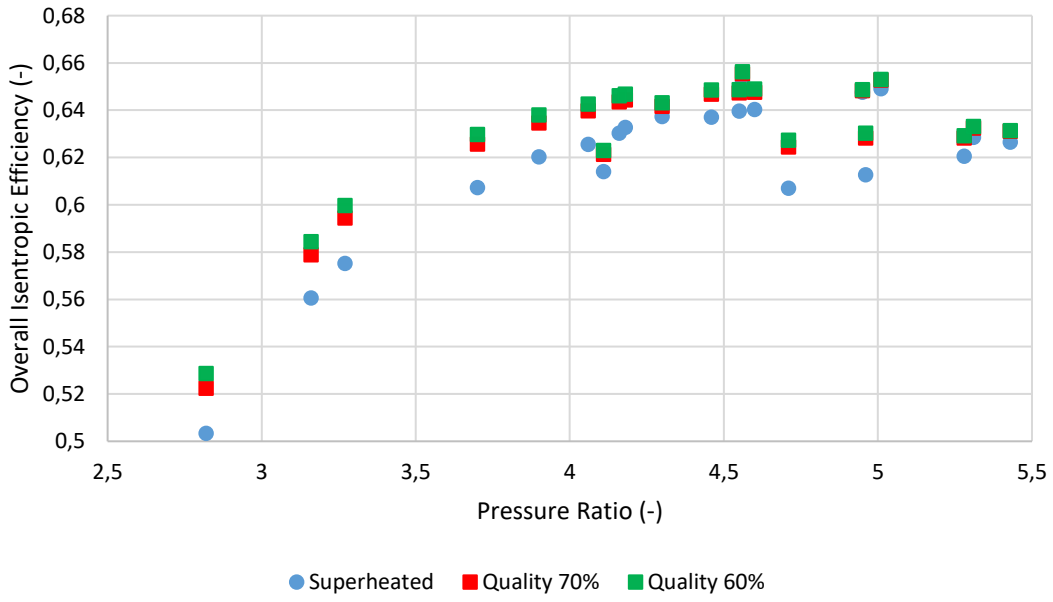

Figure 62: Isentropic efficiency with pressure ratio on wet expansion

Figure 62 represented the evolution of isentropic efficiency as a function of pressure ratio in wet expansion. It has been calculated for supply quality 70% and 60%. It can be observed that in all points the efficiency is larger as the vapor quality drops. In the lowest pressure ratio for supply vapor 70% the efficiency is 3.8% higher than superheated operation and for supply 60% is 5% higher. As an increasing pressure ratio, the deviation from initial operation decreases and for pressure ratio 5.43 the efficiency is 7.3% and 7.9%, respectively. However, it cannot be concluded that with the wet expansion the efficiency increases because it has not studied the mass flow of these points. This investigation will be addressed in next figures.

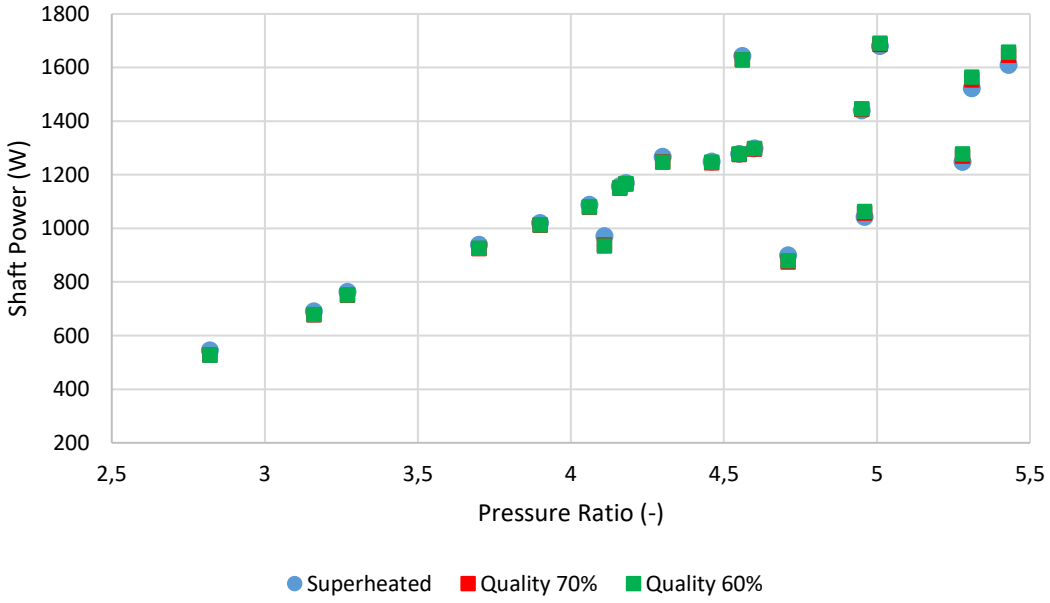

Figure 63: Shaft power with pressure ratio on wet expansion

In Figure 63, it can be observed that shaft power is almost equal to initial superheated operation and the deviation does not exceed 4% in both cases. This evolution of produced power suggests that the mass flow may be changed significantly from initial operation. This claim is confirmed by Figure 64 where it can be observed the gradual increment of mass flow, while the vapor quality decreases. The increase of mass flow, in case of 70% vapor quality at inlet, is 35%-60% compared to initial operation and in the case of 60% quality, the corresponding increase is 50%-80%. Given that the mass flow is not equal no reliable conclusions can be deducted towards the overall performance.

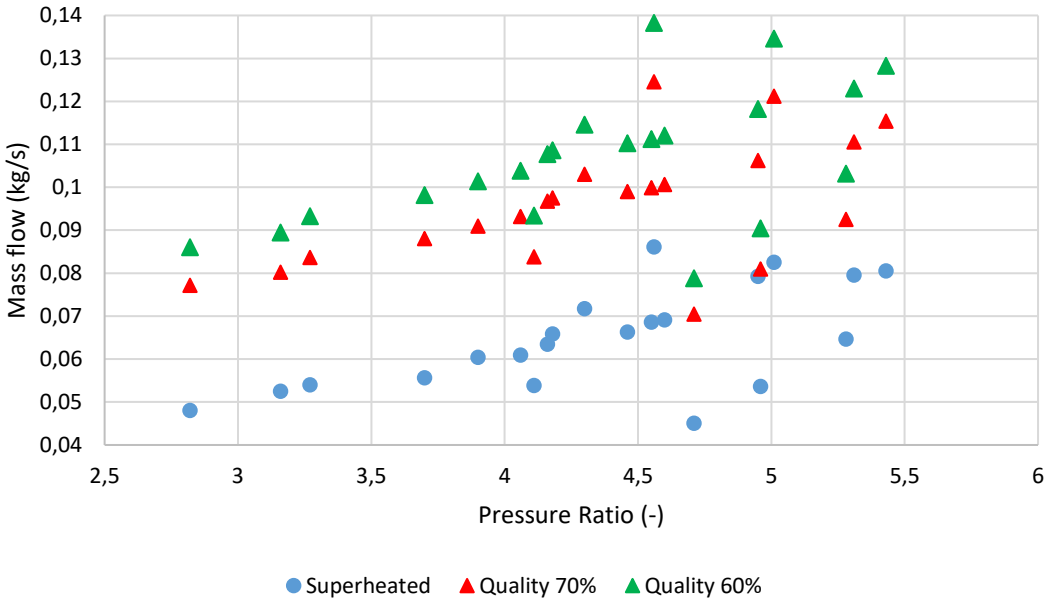

Figure 64: Mass flow comparison between wet and superheated expansion

In the second case, was imposed the mass flow equal to the initial operation and the rotational speed, along with the rest variables, obtained by the model.

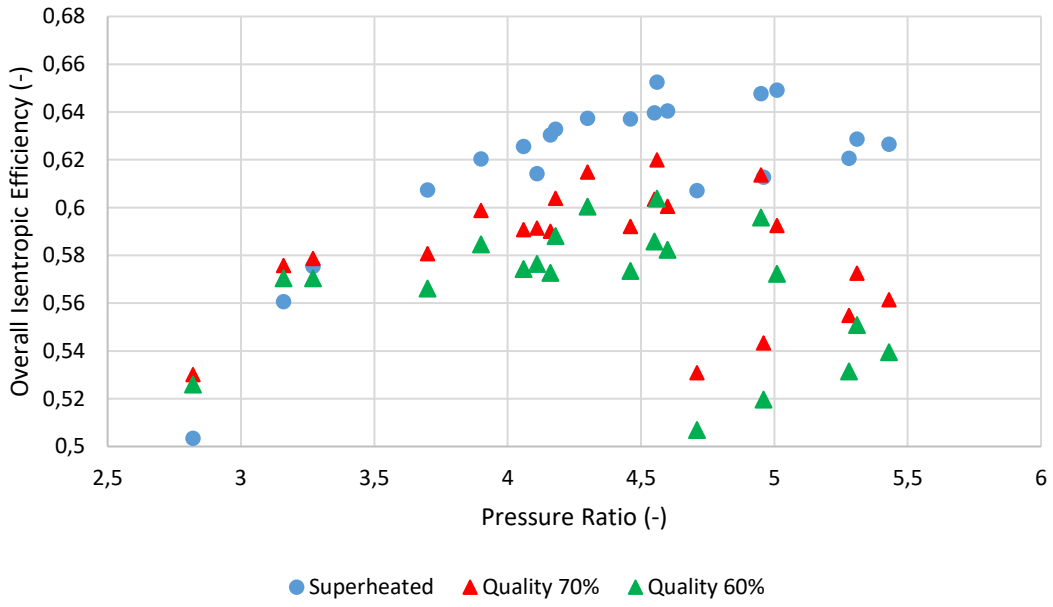

Figure 65: Overall isentropic efficiency with pressure ratio for wet expansion

Above, in Figure 65, is presented a comparison of the expander's overall isentropic efficiency between wet expansion and expansion of superheated vapor. It is clear that the efficiency is lower at initial operation, except from lowest pressure ratios and as the vapor quality at the inlet of the expander decreases the efficiency drops, too. By increasing the pressure ratio, the deviation generally also increases with some exceptions. In the lowest pressure ratio, in case of 70% vapor quality, the efficiency is 5.3% higher, and in case of 60% inlet vapor quality is 4.5%. In the highest pressure ratio the efficiency is lower and the deviation increases to 10.4% and 13.9%, respectively. Although the peak deviation recorded to pressure ratio 4.71 and is equal to 12.5% in first case and 16.5% in second case. With these values of isentropic efficiency, the vapor quality does not drop lower than 80% in case of 70% inlet and 72% in case of 60% inlet.

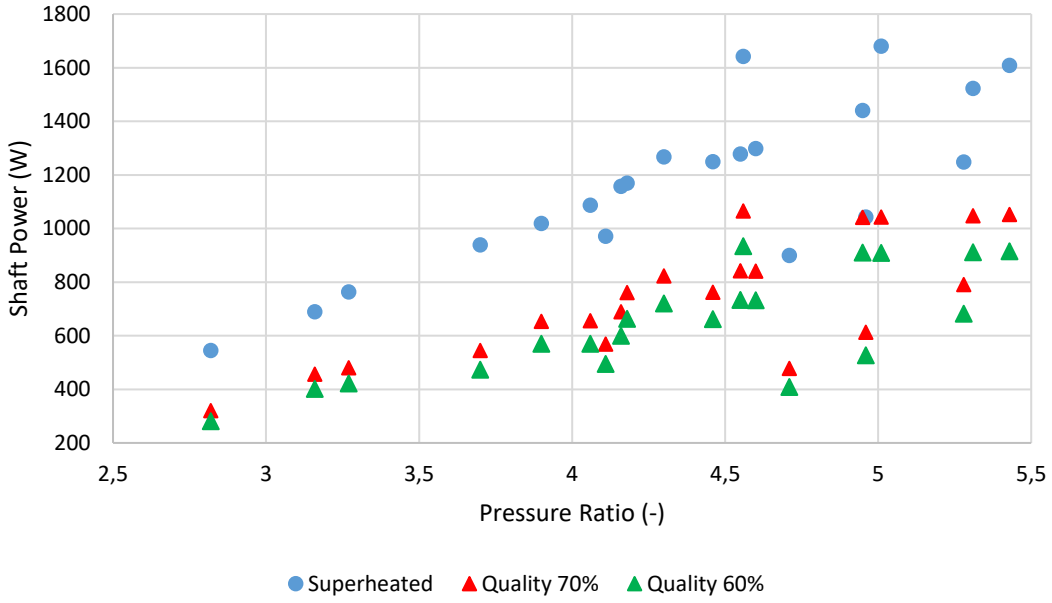

Figure 66: Produced shaft power with pressure ratio for wet expansion

As represented in Figure 66, the shaft power has a similar trend, and, in fact, for lower vapor qualities the shaft power decreases, too. In the lowest pressure ratio, the shaft power is 41% lower in case of 70% quality at inlet than an operation with superheated vapor and 48% lower in case of 60% quality at the inlet. In the highest pressure ratio, the deviation is 34.6% and 43.1%, respectively.

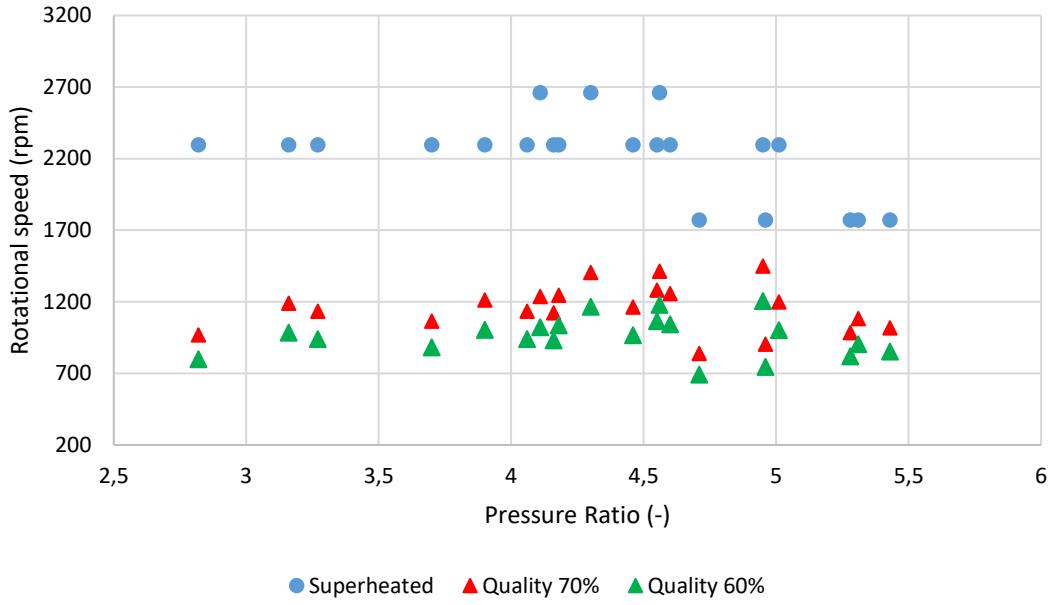

Figure 67: Comparison of obtained rotational speed between superheated and wet expansion

As referred above, it was imposed equal mass flow with superheated vapor and the rotational speed were determined by the semi-empirical model. In Figure 67, are presented the effects of wet expansion in rotational speed. It can be observed that as decreasing the vapor quality, the shaft speed decreases, too.

4.1.2 Miao et al. model

In this publication was investigated experimentally an ORC system, in which both of modeled and tested results are notified. As previously, it were studied both cases of constant rotational speed and constant mass flow as independent variables.
In figures below, is presented the operation with tested data and for equal rotational speed to the initial operation. Figure 68 presents the evolution of isentropic efficiency for operational scenarios. Decreasing the vapor quality, the efficiency decreases, too. Specifically, in case of 70% quality at inlet, efficiency records a decrease in range of 2%-4% and in case of 60% quality at inlet, 3%-6%, respectively.

In Figure 69, the shaft power as can be seen, is too close to initial operation. In lowest pressure ratio for 70% supply quality the shaft power is 8% less than initial operation and for 60% is 10.3% less, respectively. Increasing the pressure ratio, the deviation decreases and has values less than 0.5% for both categories.

This effect occurs due to mass flow increase which is depicted in Figure 70. In case of 70% inlet quality, the mass is increased by 49.7% for a low pressure ratio and 32.7% for the highest pressure ratio, while in case of 60% the increase is in range of 49%-67%.

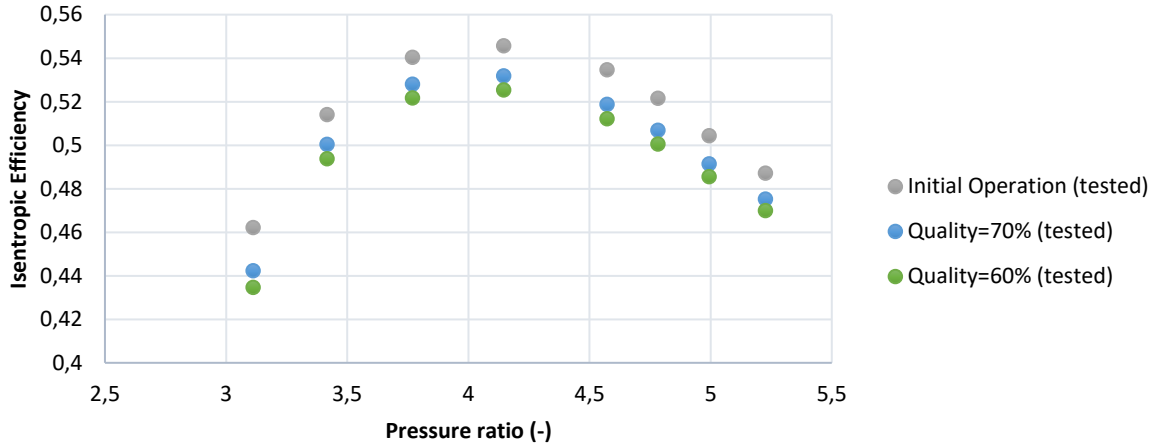

Figure 68: Isentropic efficiency as a function of pressure ratio for wet and superheated expansion.

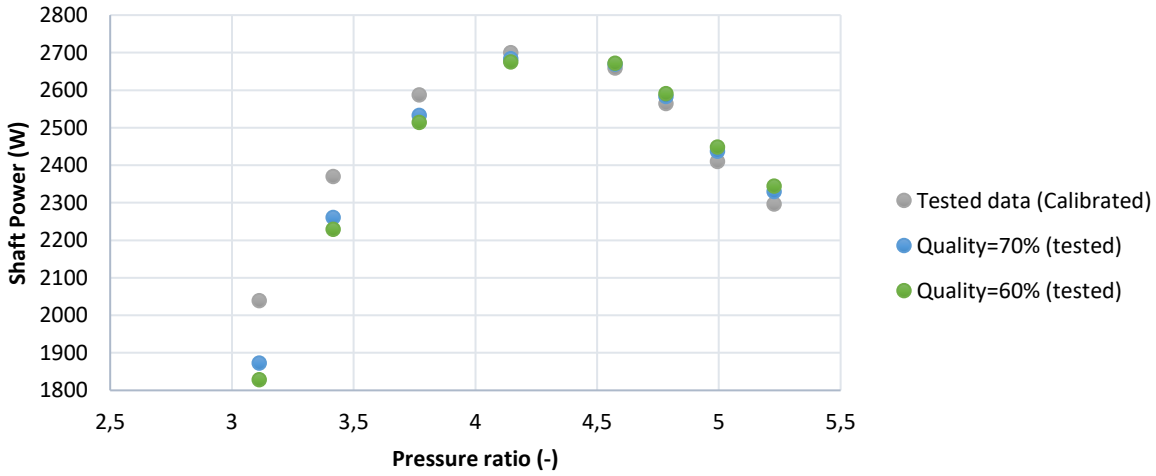

Figure 69: Shaft power as a function of pressure ratio for wet and superheated expansion.

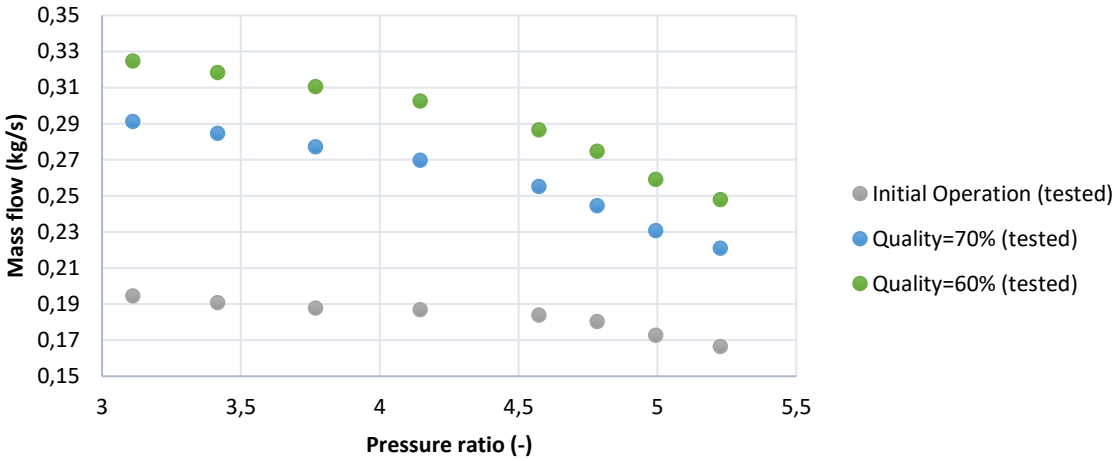

Figure 70: Mass flow comparison between wet and superheated expansion

In case of wet expansion with equal mass flow to initial operation the results represented in figures below.

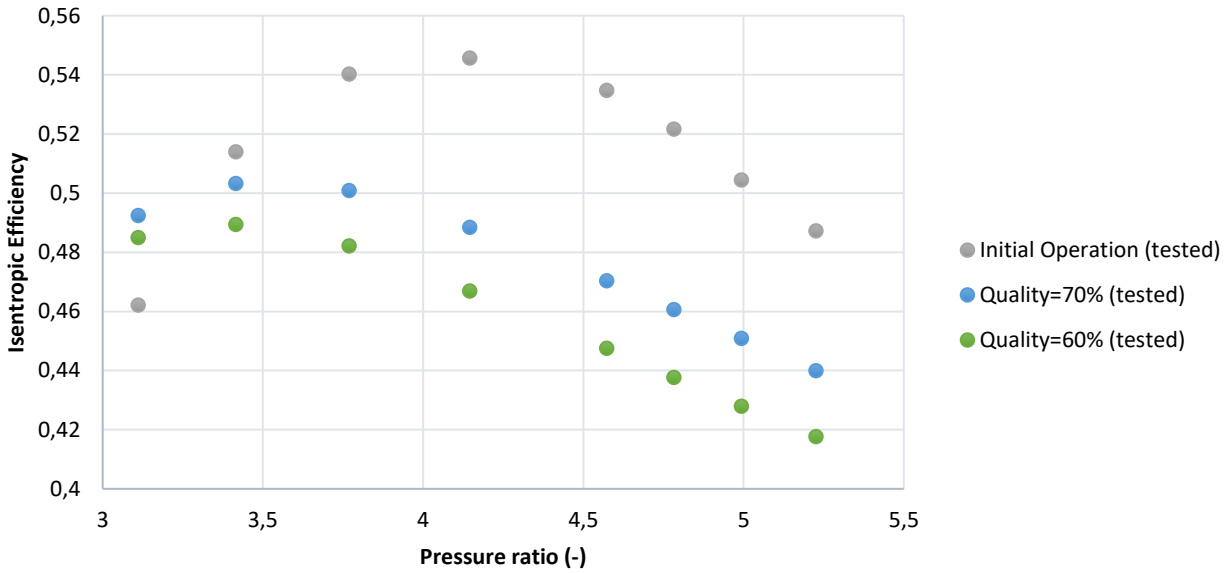

Figure 71: Evolution of isentropic efficiency as a function of pressure ratio

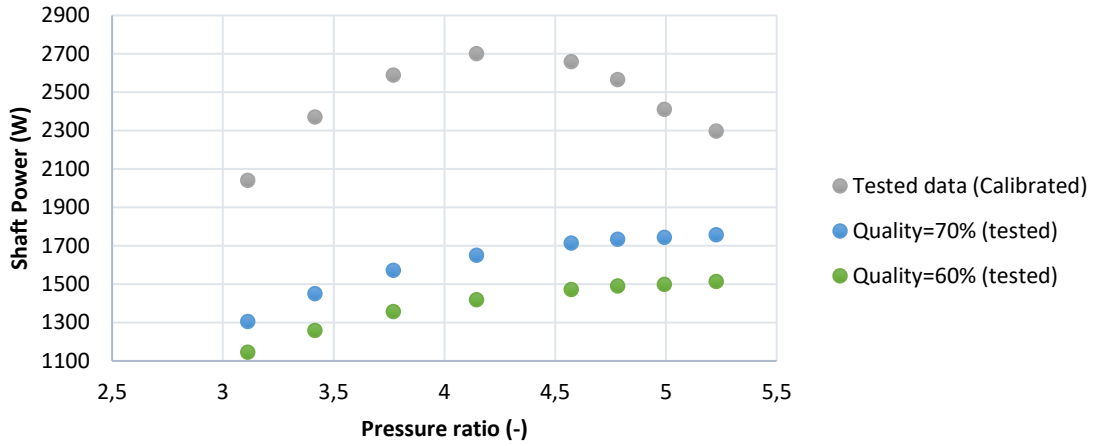

Figure 72: Evolution of shaft power as a function of pressure ratio

As can be seen in Figure 71, the efficiency decreases by decreasing the inlet vapor quality. The deviation is higher than the previous case with equal rotational speed at dry expansion. In lower pressure ratios the efficiency is 6.5% higher, in case of 70% inlet quality, compared to expansion with superheated vapor and 4.9% higher, in case of 60% inlet quality. This increase is not representative of performance due to too low-pressure ratios and superheated which is not exploited at all. In higher pressure ratios, the deviation increases and the efficiency decreases significantly. In operation with 70% inlet vapor quality, the deviation of efficiency increases to 12% and, in case of 60% quality, the efficiency is 16% lower compared to dry expansion. An analogous trend is presented on shaft power, in Figure 72, in which for a wet expansion with 70% quality the produced power is 23.5%-39.2% less than dry expansion, while in case of 60% vapor quality, the decrease is in range of 34%-47.5%.

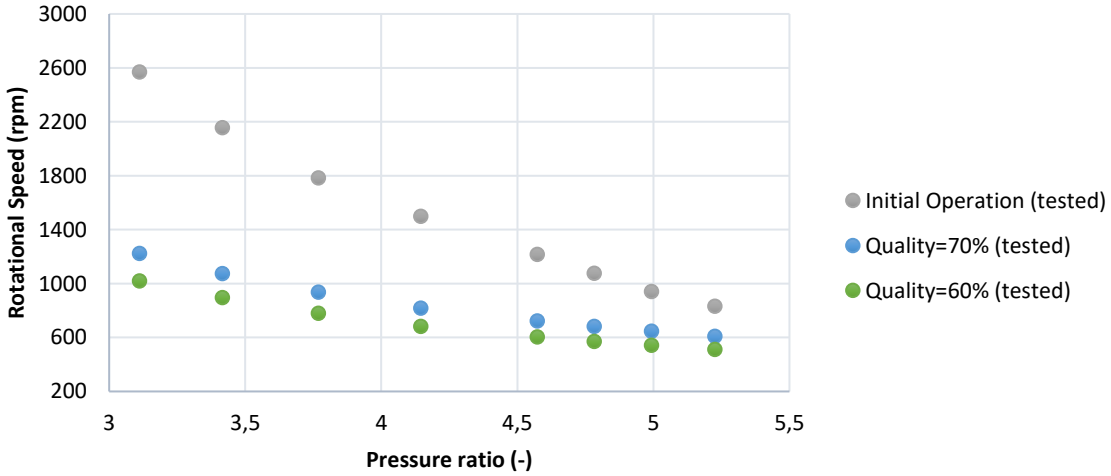

Figure 73: Comparison of rotating shaft speed between dry and wet expansion

Figure 73 represents the decrease of rotational speed with decreasing the quality of vapor. It is remarkable that in lower pressures the deviation ranges between 52%-60% and in the higher pressure ratios the deviation drops to 26.8%-38.4%.

4.1.3 Ziviani et al. model [11]

In this study there is a clear separation in measurements according to heat source temperature. Firstly, will be studied the case with heat source temperature of 85°C with equal rotational speed to initial operation with superheated vapor.

Figure 74, presents the performance of expander in dry or wet expansion. There is no clear trend whether the efficiency is higher or lower than initial operation due to the fact that the selection of operating points has different supply pressures and rotational speeds. In case of 60% vapor quality at inlet, it can be observed that in low pressure ratios the efficiency is 10% lower than dry expansion, while in high pressure ratios the efficiency is 4.8% higher. In operation with 70% vapor quality at inlet, the deviation ranges between 0.1% to 8.3%.

A similar trend can be observed in Figure 75, in which the shaft power is slightly lower in low pressure ratios and is higher in high pressure ratios compared to dry expansion. For both cases of vapor's inlet quality, the deviation is in range of 0.2%-14.8%.

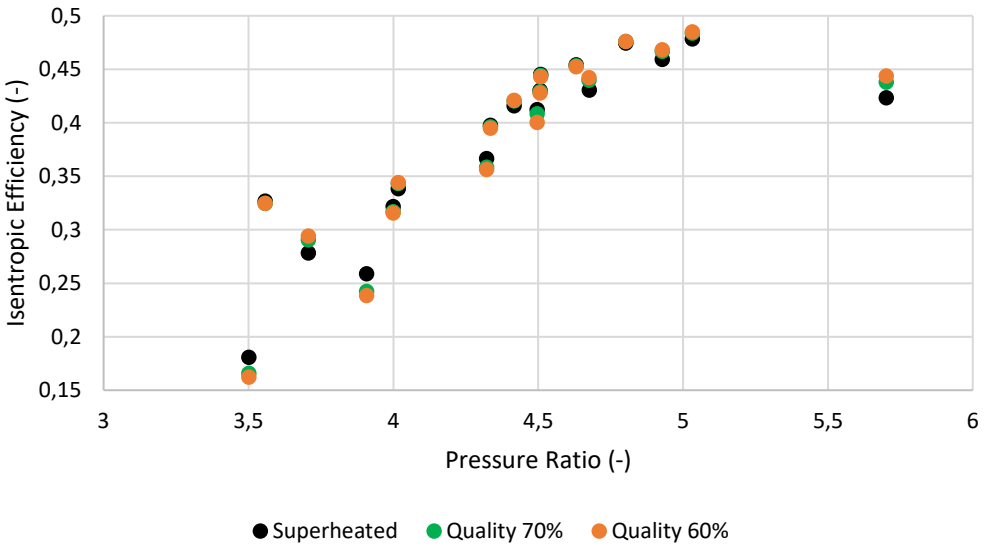

Figure 74: Evolution of isentropic efficiency as a function of pressure ratio for wet and dry expansion

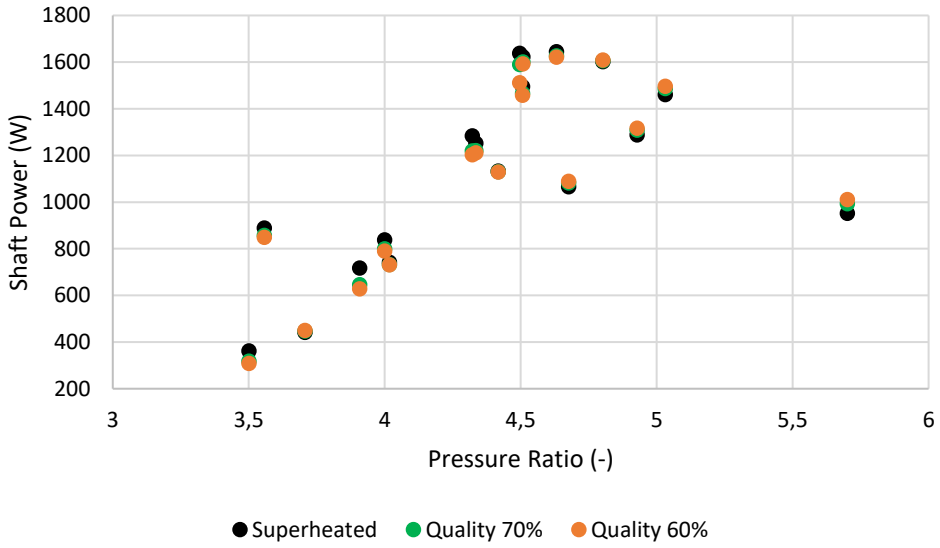

Figure 75: Produced shaft power as a function of pressure ratio for wet and dry expansion

As described above, in calculations were used identical rotational speeds and calculated the refrigerant mass flow. Figure 76 represents the effect of decreasing vapor quality on mass flow. It is obvious that as decreasing the vapor quality, the required mass flow increases. The deviation between the operation points is approximately constant and in operation with 70% vapor intake quality, the mass flow is 30-40% increased compared to initial operation, while in case of 60% quality the deviation increases to 45-60%.

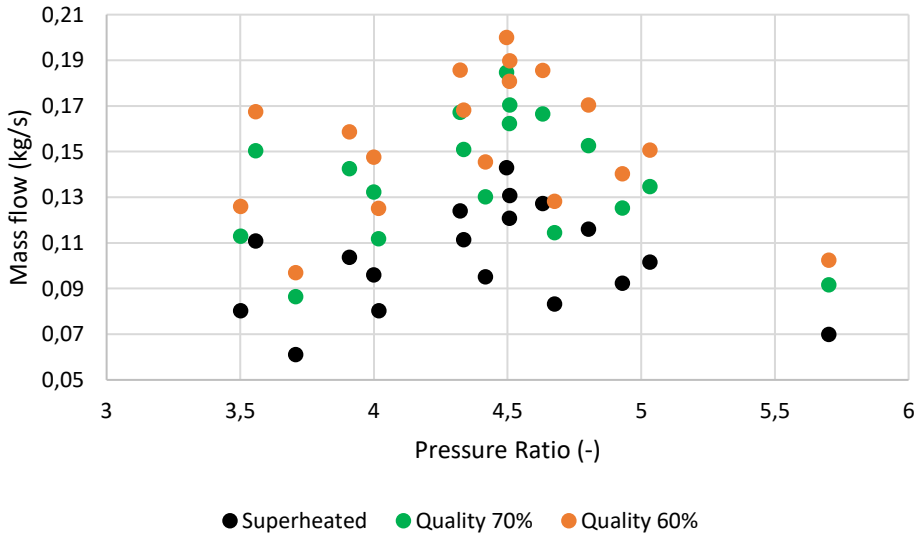

Figure 76: Comparison of mass flow between for wet and dry expansion as a function of pressure ratio.

In order to make a complete investigation, the case will be recalculated with equal mass flow rate to initial operation. The results are presented in figures below.

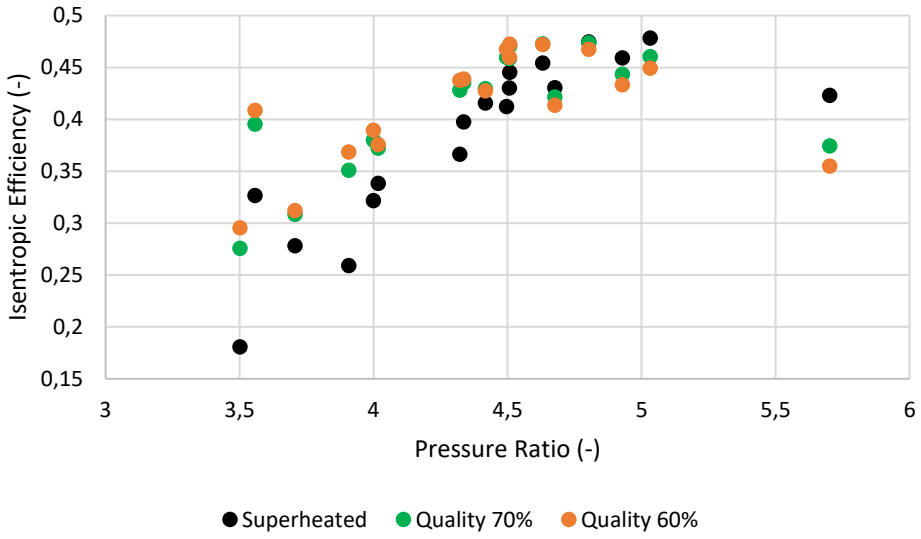

Figure 77: Evolution of isentropic efficiency as a function of pressure ratio for dry and wet expansion.

In Figure 77 can be observed that in wet expansion the efficiency in low pressure ratios is higher, while in higher pressure ratios turns lower than dry expansion. In very low pressure ratios, the superheated vapor cannot be expanded at all, in contrast with wet vapor where only a part is exploited for production of power.

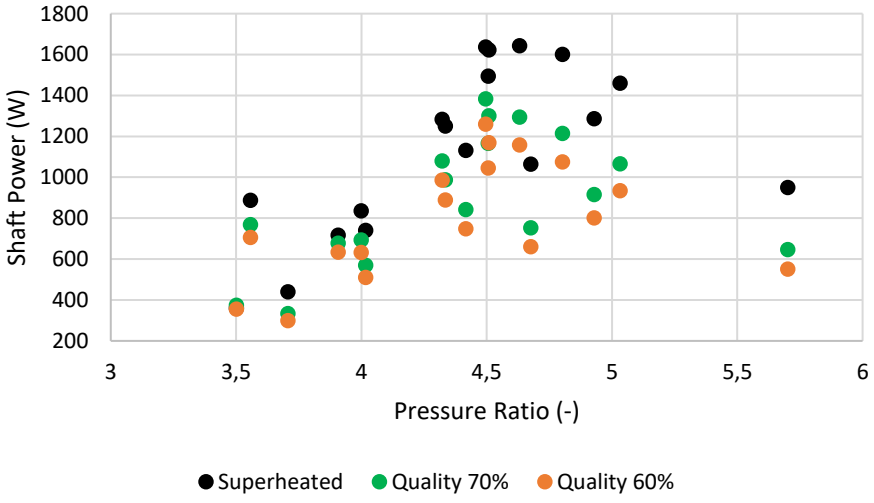

Figure 78: Produced shaft power as a function of pressure ratio for wet and dry expansion.

In Figure 78 is presented the effect of decreasing quality at the inlet on the shaft power. At wet expansion, the produced power is lower and as the pressure ratio increases the deviation increases, too. For a pressure ratio 3.5 the shaft power is 1.3% lower than initial operation with vapor quality 60% and with vapor quality 70% is 3.9% lower. This effect can be explained by the mass fraction of vapor because in so lower pressure ratios only a portion of the vapor mass can be exploited. As pressure increases the deviation of the power reaches at 32% and 42% for vapor intake quality 70% and 60%, respectively. In these pressure ratios all the mass of vapor is expanded so in case of wet expansion the beneficial vapor is less.

In Figure 79, it can be seen the effect on shaft speed by decreasing the quality of inlet vapor. The deviation of shaft speed is larger in low pressure ratios than in higher ratios. In lowest pressure ratio the calculated shaft speed is 52.1% less in case of 60% quality at supply and 42.3% lower in case of 70% quality. As the pressure ratio increases the deviation drops to 48.6% and 37.6%, respectively.

Ziviani et al. [11], investigated the case of the heat source to be in temperature of 110 °C. The comparison in wet expansion presents the same trend. Following, there are presented the figures for operation with equal mass flow to initial operation.

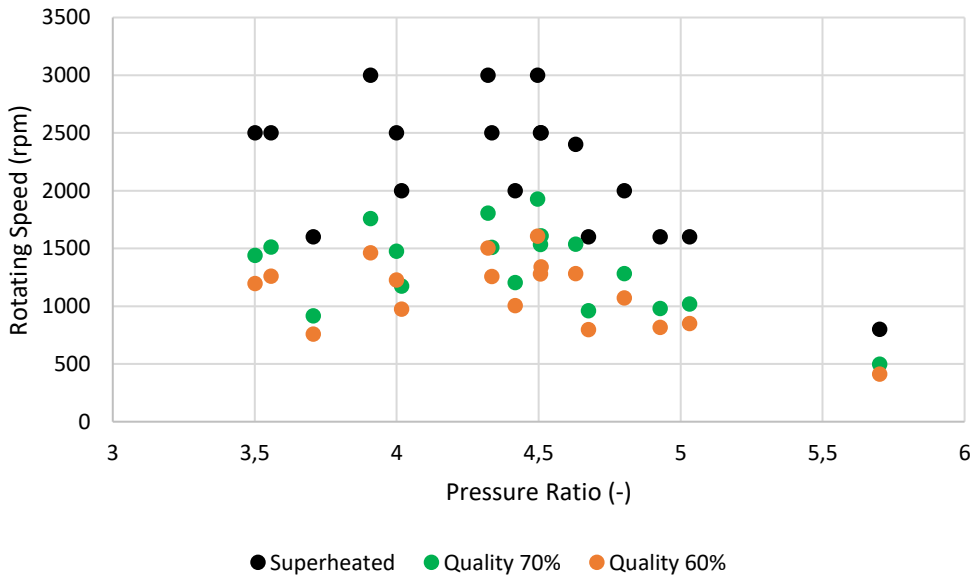

Figure 79: Comparison of shaft power with pressure ratio for different vapor quality at intake.

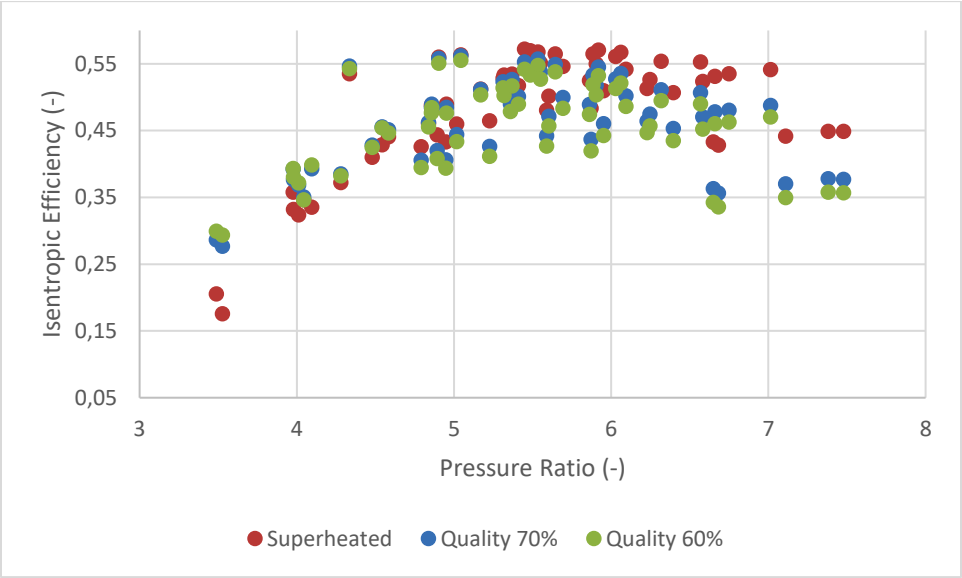

Figure 80: Isentropic efficiency with pressure ratio for dry and wet expansion for equal mass flow to initial operation

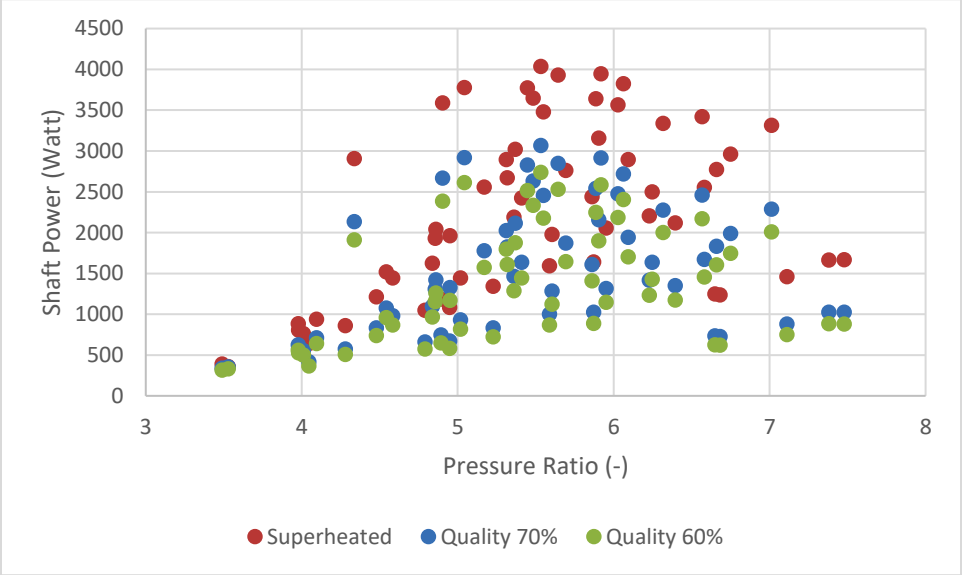

Figure 81: Shaft Power with pressure ratio for dry and wet expansion for equal mass flow to initial operation

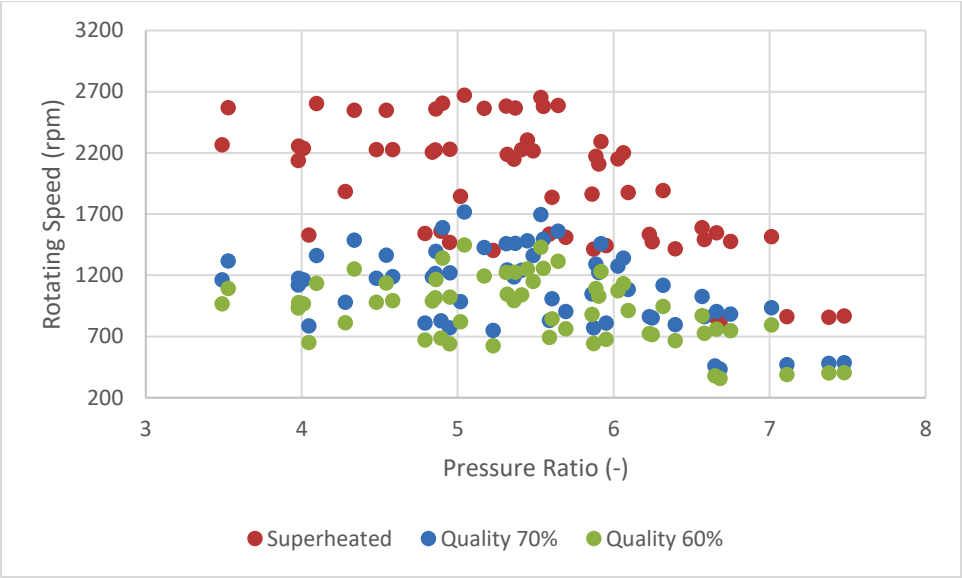

Figure 82: Comparison between calculated rotational speed for dry and wet expansion.

In figures above is observed that the efficiency is a little higher for low pressure ratios and as pressure ratio increases, it is constantly lower. Both in evolution of isentropic efficiency and produced shaft power, the deviation of dry and wet expansion increases with the increase of the pressure ratio.

In conclusion, in expansion in two-phase area using the semi-empirical model, in case of imposing the same shaft speed to dry operation, the results are not reliable. In case of imposing same mass flow to initial operation and obtain by the model the shaft speed the results tend to be more reliable. The obtained shaft speed in all cases is less than dry expansion and is getting lower as the vapor quality at inlet decreases. Regarding to isentropic efficiency, it is also lower compared to dry expansion, with an exception. In pressure ratios lower than 4-4.5, it is observed an increased efficiency. This effect can occur due to under-expansion of the superheated vapor in lower pressure ratios and in case of wet expansion this phenomenon is eliminated due to lower mass of vapor, hence is feasible to be fully expanded. Also, in all expander models the shaft power in wet expansion is less than dry expansion and this drop is constantly increasing with the pressure ratio.

4.2 Calibration of liquid flooded expansion in scroll expander

Bell et al. [21] experimentally investigated a test-rig with flooded scroll machines to measure the performance of the liquid flooded Ericsson cycle. The working fluid which was used was dry nitrogen and the flooding fluid was alkyl-benzene refrigeration oil.

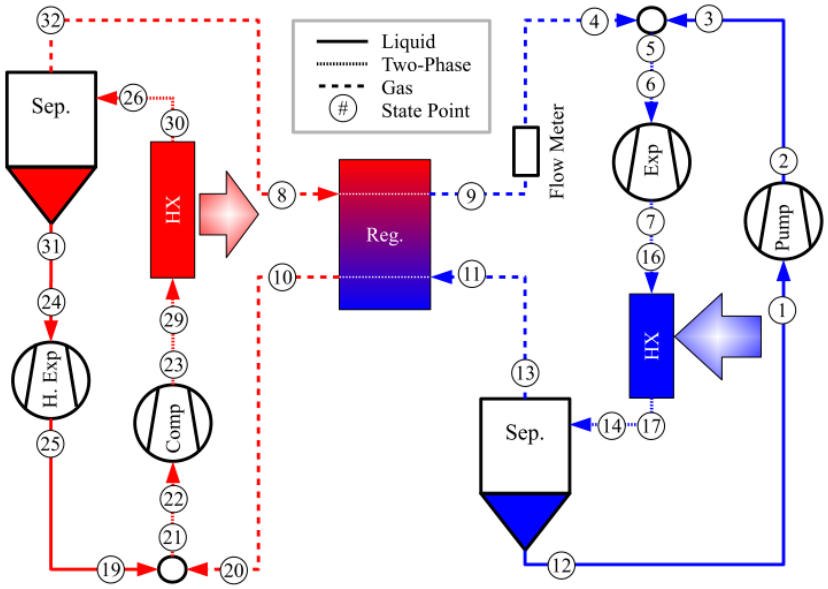

Figure 83: Schematic diagram of Ericsson cycle test-rig [21].

A mix of oil and gas enters in compressor (point 22) and is pumped to point 23 where is cooled in a heat exchanger and comes out in gas state point 30. Then, gets separated and the oil is expanded in low pressure to state point 25. The gas from separation in state 32 enters the regenerator and is cooled to state point 9. The it is adiabatically mixed with cool oil from state point 3 and enters the expander in two phase condition. Then, expands in state point 16, where is heated in heat exchanger and enters in the separator. The oil flows in low pressure (state 1) to be pumped in high pressure (state 2). The gas in state 13 is warmed in regenerator in state point 10. The flooded expander achieved an isentropic efficiency of 66% with the oil fraction up to 76%.

In Figure 84, is depicted the overall isentropic efficiency as a function of oil mass fraction. Generally, as oil fraction increases the isentropic efficiency drops. This effect is more intense as increases the rotating shaft speed.

This expander model was calibrated against semi-empirical model which was developed on this thesis. It used the mass flow rate of nitrogen and the calibration based on that. Despite the global error which occurred after the calibration had the value of 3.577%, it can be seen in figures below the fitting on measured value was not reliable.

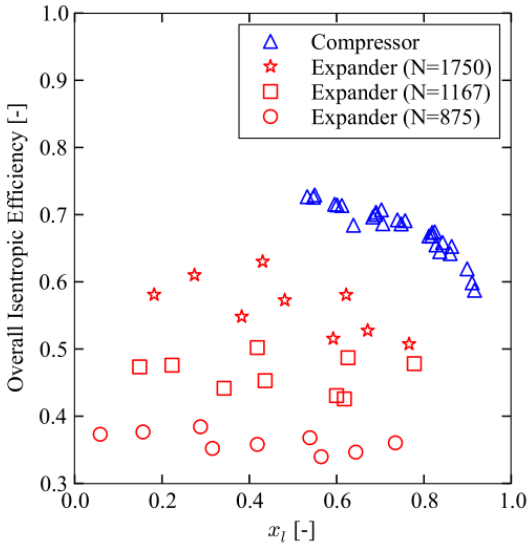

Figure 84: Experimental overall isentropic efficiency of scroll machines.

Table 8: Calibrated parameters for expander model [21]

	Calibrated Parameters	*Units*
$r_{v_{in}}$	2.15063	$(-)$
$AU_{amb,n}$	6.9932	(W/K)
$AU_{su,n}$	15.0078	(W/K)
$AU_{ex,n}$	34.92	(W/K)
A_{leak}	5.2032 E-06	m^2
T_{loss}	0.331363	$N \cdot m$
$V_{s_{exp}}$	7.4727 E-05	m^3
A_{su_n}	2.742 E-05	m^2
M_{dot_n}	0.06718	kg/s

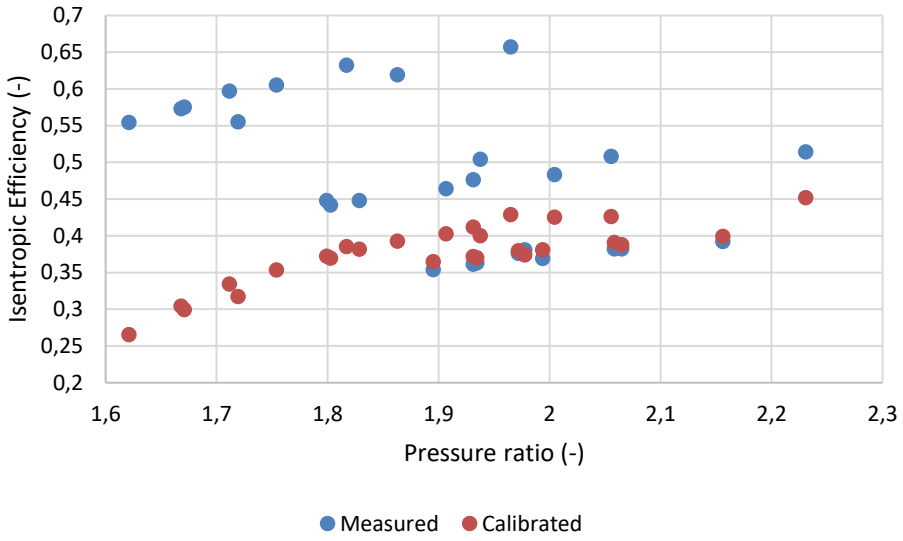

Figure 85: Isentropic efficiency as a function of pressure ratio for measured and calibrated data.

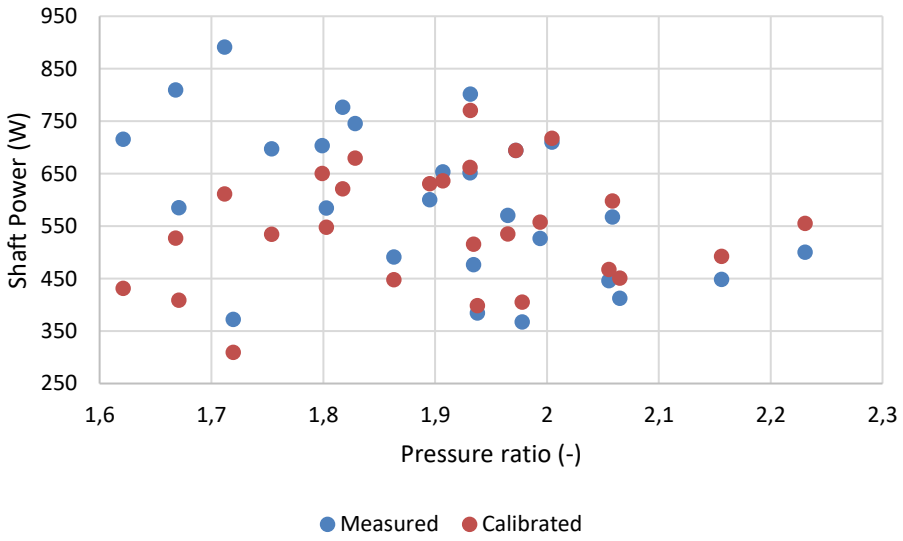

Figure 86: Shaft Power as a function of pressure ratio for measured and calibrated data.

As can be seen in Figure 85 and Figure 86, there is a large deviation between measured and calculated data with calibrated parameters. In lower pressure ratios the deviation is higher than in the case of higher pressure ratios. The overall isentropic efficiency error reaches the values of 52%, while for pressure ratio 1.97 can be observed the minimum error of 0.9%. The same trend is observed in evolution of shaft power, in which case for the minimum pressure ratio the error is 39.7%, while with increasing the ratio the error decreases. In the case of isentropic efficiency, there is a mean error value of 20% and in the case of shaft power 11.7%.

This suggests that the calibration is not reliable and these parameters which were obtained, cannot predict the performance of this liquid flooded expansion.

4.3 Wet expansion with R1234ze(E)

4.3.1 Lemort et al. [9] model with R1234ze(E) in wet expansion

The operation in two phase conditions was investigated in this case with R1234ze(E) as the working fluid. The values were obtained with the same supply conditions, for the case of constant mass flow to initial operation and with rotational speed as variable.

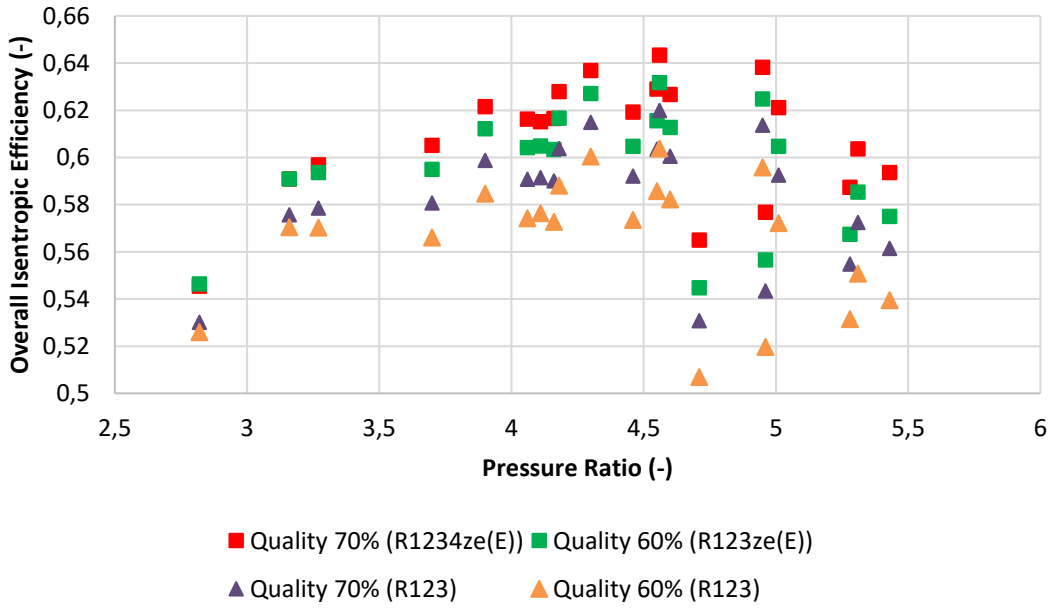

Figure 87: Comparison of overall isentropic efficiency in wet expansion between refrigerants R123 and R1234ze(E)

As observed in Figure 87, the isentropic efficiency in the case of operation with R1234ze(E) is higher than R123. Specifically, the increase is in range of 2.6% to 6.4% in the case of 70% vapor quality supply. In the case of 60% quality, the efficiency with R1234ze(E) compared to R123 is much higher and it ranges between 3.6%-7.5%. The increase of deviation follows the increase of pressure ratio.

The produced shaft power is also higher with refrigerant R1234ze(E) compared to R123, according to Figure 88. As the pressure ratio increases, the deviation increases too. In the case of 70% inlet vapor quality, the deviation is 14%-17.8% , while in the operation with 60% inlet vapor quality, the increase is 14.8%-18.6%.

This performance suggests that both the overall isentropic efficiency and the produced shaft power is better for wet expansion with R1234ze(E) as working fluid than R123.

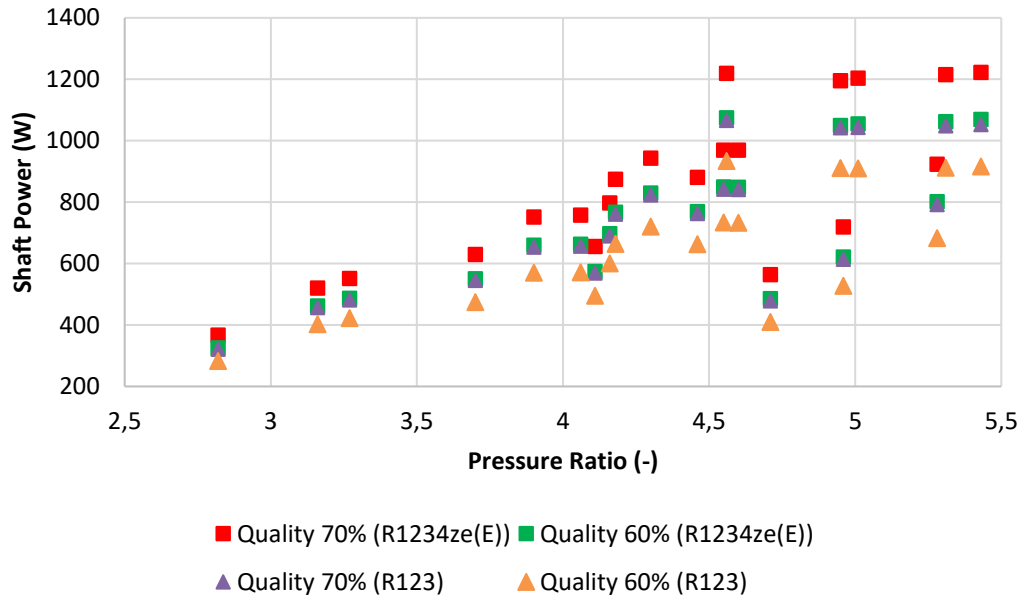

Figure 88: Comparison of produced shaft power in wet expansion between refrigerants R123 and R1234ze(E)

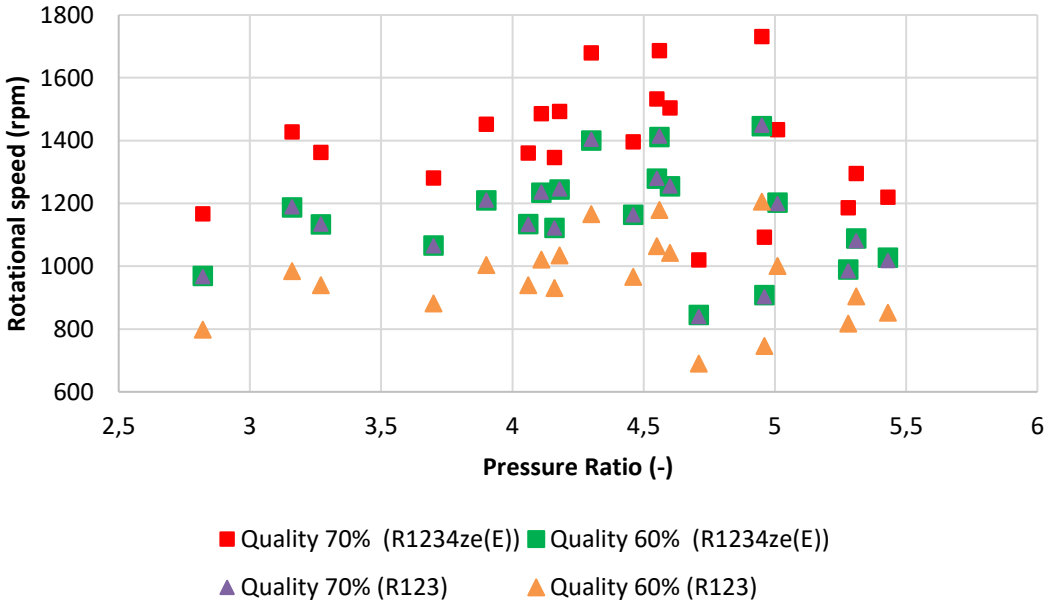

Figure 89: Comparison of rotational speed in wet expansion between refrigerants R123 and R1234ze(E)

4.3.2 Miao et al. [10] model with R1234ze(E) in wet expansion

In this expander model has been conducted a comparison with tested operation data for wet expansion with R123 and R1234ze(E). The data was calculated for constant mass flow to initial operation and varying rotational speed.

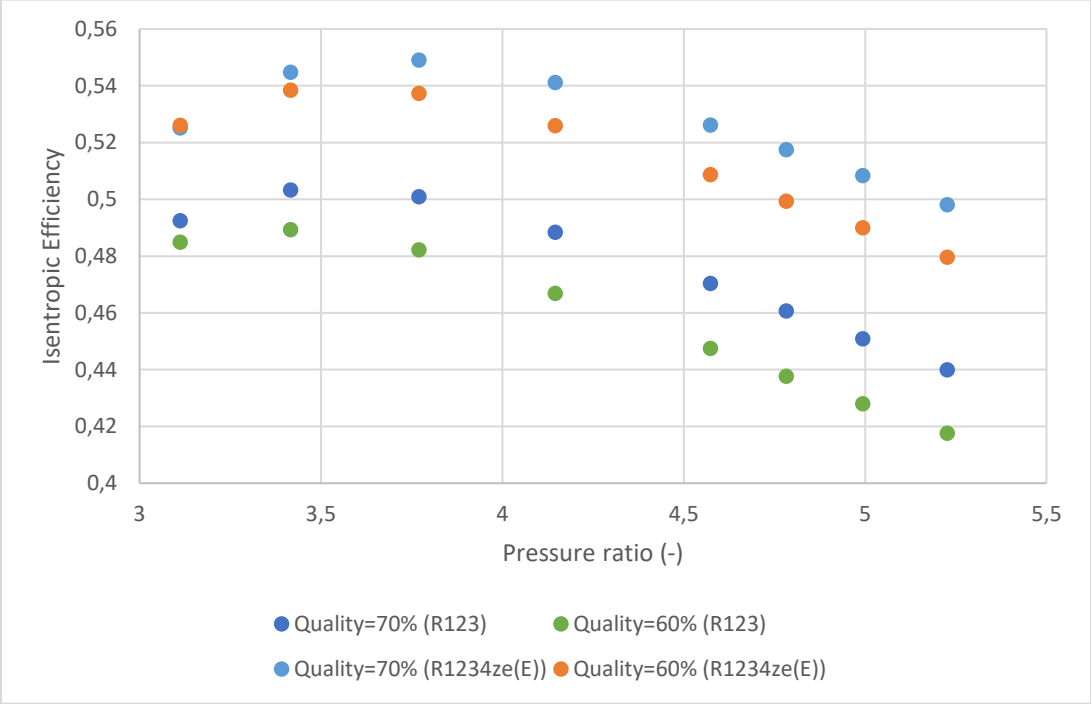

Figure 90: Comparison of overall isentropic efficiency in wet expansion between refrigerants R123 and R1234ze(E)

In Figure 90, it can be seen that the efficiency in operation with R1234ze(E) is higher compared to R123. In the case of 70% inlet vapor quality, in pressure ratio 3.1 the efficiency is 6.6% higher than operation with R123. As the pressure ratio increases, the deviation also increases and reaches the values of 13.2%. In the case of 60% inlet vapor quality, it observed the same trend with increase in range of 8.5% to 14.9%. In general, the efficiency with R1234ze(E) as working fluid is higher compared to R123.

In shaft power can be seen also an increase by changing working fluid to R1234ze(E). Figure 91, presents that the shaft power is higher in all operating points with an increasing deviation as increases the pressure ratio. Specifically, in the case of 70% inlet vapor quality, the deviation ranges between 18.3% to 24.2% and in the case of 60% quality, 20% to 25.6% increase.

In Figure 92, can be observed an increase in rotational speed, with approximately the same deviation between the two cases. This effect caused due to refrigerants' properties and not to the expander model.

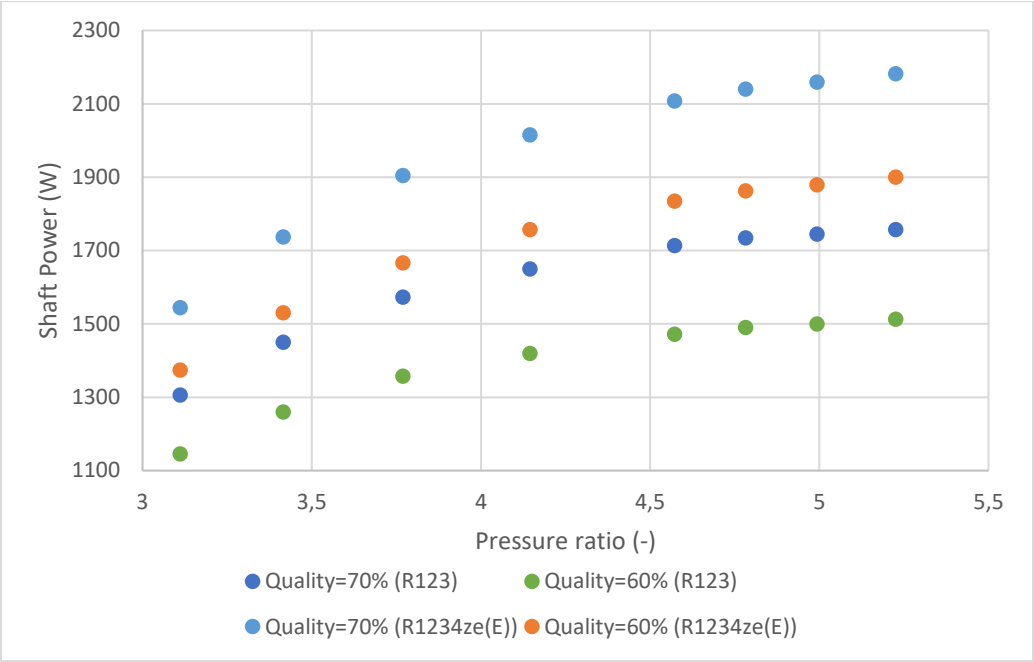

Figure 91: Comparison of produced shaft power in wet expansion between refrigerants R123 and R1234ze(E)

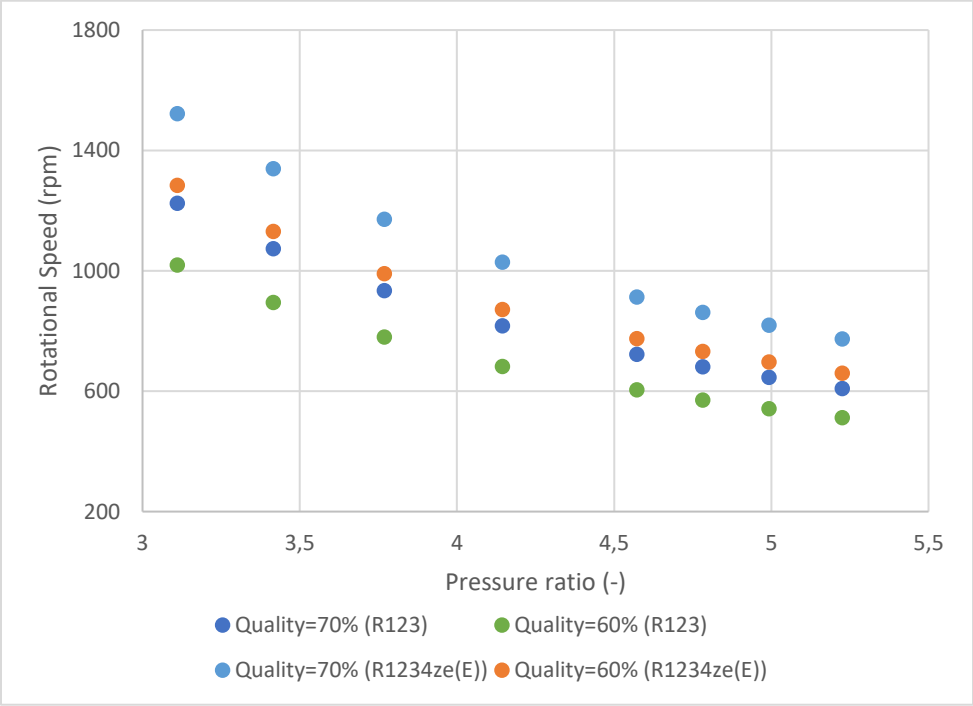

Figure 92: Comparison of obtained rotational speed in wet expansion between refrigerants R123 and R1234ze(E)

4.3.3 Ziviani et al. [11] model with R1234ze(E) in wet expansion

This test-rig was using as working fluid R245fa and was investigated above for wet expansion. Below, is compared the operation in two-phase region with R245fa and R1234ze(E) as working fluids. The same supply conditions with initial operation were used.

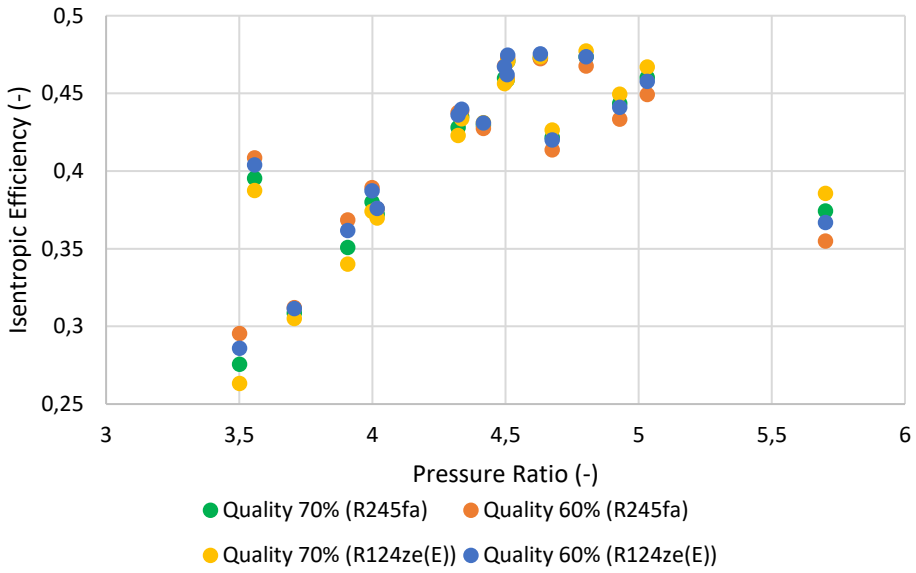

Figure 93: Comparison of overall isentropic efficiency speed in wet expansion between refrigerants R123 and R1234ze(E)

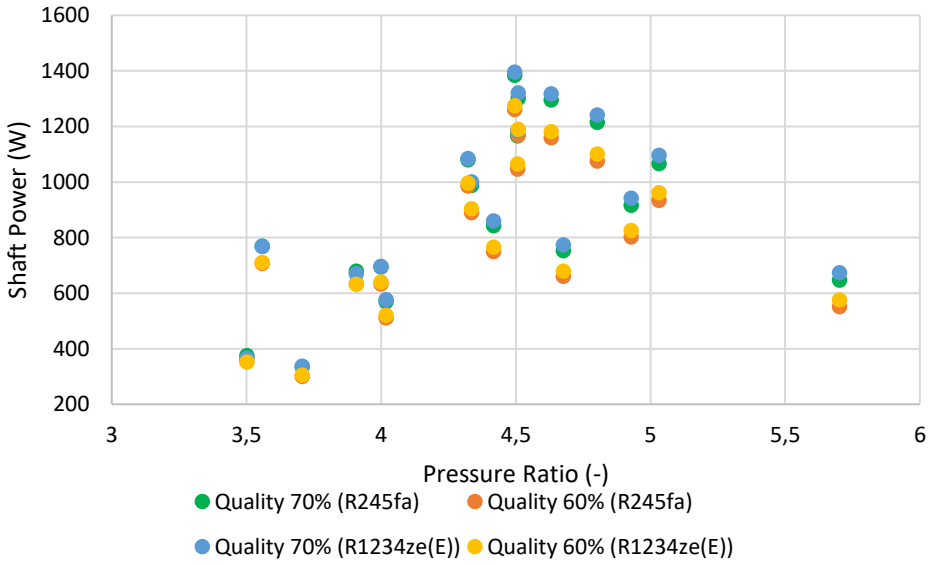

Figure 94: Comparison of shaft power in wet expansion between refrigerants R123 and R1234ze(E)

In Figure 93, is presented the comparison of isentropic efficiency between operation with R245fa and R1234ze(E). Generally, the efficiency with R1234ze(E) is higher compared to initial operation, with an increase which does not exceed 3% in case of 70% inlet vapor quality and 3.4% in the case of 60% quality. A few operation points in high pressure ratios present a decrease in efficiency about 4.5% and 3.2%, respectively.

The produced shaft power, in Figure 94, increased with the replacement of the refrigerant. The increase is higher in higher pressure ratios and the maximum increase is 4.2% and 4.3% for 70% and 60% inlet vapor quality, respectively. In lower pressure ratios the produced shaft power is almost equal.

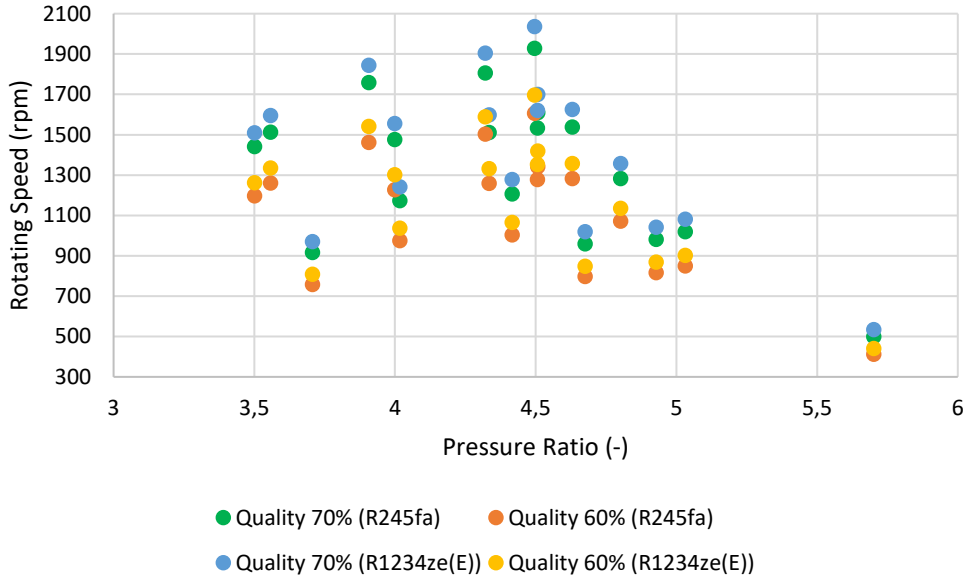

Figure 95: Comparison of obtained rotational speed in wet expansion between refrigerants R123 and R1234ze(E)

In Figure 95, can be observed a constant increase in estimated rotational speeds by replacing the refrigerant. The increase is in range of 4.7%-6.8% in the case of 70% quality and 5.3%-7% in the case of 60%.

5. Discussion

This work investigated the reliability of the semi-empirical expander model in single- and two-phase flows. The results have shown that this model has a satisfying predictability of expander performance. However, to have a complete view of the expander it is necessary to be created a deterministic model. The advantage of semi-empirical model is that it can be created easily and compare different types of volumetric expanders with the same model by changing the parameters.

In single-phase flows, in terms of isentropic efficiency, was presented a deviation that does not exceed 10% for Lemort et al. [9] model and a minimum deviation of 0.85%. In comparison with Ziviani et al. [11] the deviation in isentropic efficiency between measured and calibrated data was in range of 1%-37.5% with an average values of 13.7%. It was observed that the highest values of deviation were presented on boundary operation points in which either the pressure ratio or the rotating speed was too low. The produced shaft power had an average deviation between measured and calibrated data in both studies a value that does not exceed 12.5%. The highest deviation among the investigated studies was found on the filling factor, in which the average deviation was up to 17%.

In operation with the low-GWP refrigerants, R1234ze(E) and R1233zd(E), the analysis showed a better performance than the initial operation and these fluids are appropriate to replace the old refrigerants. The operation with R1234ze(E) had an increased efficiency of up to 4.7% as calculated for Miao et al. [10] model. In produced shaft power was calculated a maximum increase of 8.7% for the same model.

In two-phase flow conditions, due to lack of measured data, it cannot be exported a safe conclusion for the expander's performance. The semi-empirical model calculated, in general, lower isentropic efficiencies than operation with single-phase flow. In fact, as the vapor quality was decreasing the isentropic efficiency was decreasing too. The operation was evaluated with 70% inlet vapor quality and the decrease was in range of 2.3%- 12% for Miao et al. [10], based on the input data that was chosen to used. In case of 60% inlet vapor quality, the decrease was in range of 3.4%-16.3% for the same ORC system. Also, a decrease was presented on produced shaft power which reached the 47.5% for a vapor quality 60%.

The parameters calibration in flooded expansion system [21], as in paragraph 4.2, the results have shown that the semi-empirical model failed to predict the expander's performance. So, it can be concluded that the model cannot be calibrated by using data in two-phase flow.

To summarize all the above, the semi-empirical model is a fast and easy way to calculate the first estimation of expanders performance. The experiments in wet expansion is in early stages, as a result, there are not any experimental data available in the literature. So as a future work, is suggested to be used experimental data for a single-phase expansion in order to calibrate the parameters. After that, the model will be used to calculate the performance in two-phase region

and comparing with two-phase expansion measurements for the same expansion machine. In this way, the reliability of the semi-empirical model can be checked on two-phase flow conditions. Also, the working fluid could be changed, in order to be checked the prediction of the semi-empirical model with other working fluids.

In the case of a mixed flow, in which both liquid and vapor exist, the semi-empirical model takes into account only the expansion of the vapor. That was the reason why in the calibration of the system with flooded expansion the prediction has failed. In order to improve the model, either a safety factor has to be added in the calculated values or an external function be created which calculates the effect of the liquid's expansion. Then, the produced power from both the vapor and the liquid expansion, which would have been calculated separately, would be summed by considering a weighting factor. In overall, the most important step towards the evaluation of the semi empirical model on two-phase expansion is its comparison against detailed experimental data or well-defined CFD models.

6. List of Tables

7. List of Figures

8. References

[1] O. Dumont, A. Parthoens, R. Dickes, and V. Lemort, “Experimental investigation and optimal performance assessment of four volumetric expanders (scroll, screw, piston and roots) tested in a small-scale organic Rankine cycle system,” Energy, vol. 165, pp. 1119–1127, Dec. 2018, doi: 10.1016/j.energy.2018.06.182.

[2] S. Quoilin, M. V. D. Broek, S. Declaye, P. Dewallef, and V. Lemort, “Techno-economic survey of Organic Rankine Cycle (ORC) systems,” Renewable and Sustainable Energy Reviews, vol. 22, pp. 168–186, Jun. 2013, doi: 10.1016/j.rser.2013.01.028.

[3] Z. Zhang, Y. Ma, M. Li, and L. Zhao, “Recent advances of energy recovery expanders in the transcritical CO2 refrigeration cycle,” p. 11.

[4] K. Braimakis and S. Karellas, “Energetic optimization of regenerative Organic Rankine Cycle (ORC) configurations,” Energy Conversion and Management, vol. 159, pp. 353–370, Mar. 2018, doi: 10.1016/j.enconman.2017.12.093.

[5] K. Qiu and E. Entchev, “Development of an organic Rankine cycle-based micro combined heat and power system for residential applications,” Applied Energy, vol. 275, p. 115335, Oct. 2020, doi: 10.1016/j.apenergy.2020.115335.

[6] S. H. Kang, “Design and preliminary tests of ORC (organic Rankine cycle) with two-stage radial turbine,” Energy, vol. 96, pp. 142–154, Feb. 2016, doi: 10.1016/j.energy.2015.09.040.

[7] U. Muhammad, M. Imran, D. H. Lee, and B. S. Park, “Design and experimental investigation of a 1kW organic Rankine cycle system using R245fa as working fluid for low-grade waste heat recovery from steam,” Energy Conversion and Management, vol. 103, pp. 1089–1100, Oct. 2015, doi: 10.1016/j.enconman.2015.07.045.

[8] S. Eyerer, F. Dawo, J. Kaindl, C. Wieland, and H. Spliethoff, “Experimental investigation of modern ORC working fluids R1224yd(Z) and R1233zd(E) as replacements for R245fa,” Applied Energy, vol. 240, pp. 946–963, Apr. 2019, doi: 10.1016/j.apenergy.2019.02.086.

[9] V. Lemort, S. Quoilin, C. Cuevas, and J. Lebrun, “Testing and modeling a scroll expander integrated into an Organic Rankine Cycle,” Applied Thermal Engineering, vol. 29, no. 14–15, pp. 3094–3102, Oct. 2009, doi: 10.1016/j.applthermaleng.2009.04.013.

[10] Z. Miao, J. Xu, and K. Zhang, “Experimental and modeling investigation of an organic Rankine cycle system based on the scroll expander,” Energy, vol. 134, pp. 35–49, Sep. 2017, doi: 10.1016/j.energy.2017.06.001.

[11] D. Ziviani, N. A. James, F. A. Accorsi, J. E. Braun, and E. A. Groll, “Experimental and numerical analyses of a 5 kWe oil-free open-drive scroll expander for small-scale organic Rankine cycle (ORC) applications,” Applied Energy, vol. 230, pp. 1140–1156, Nov. 2018, doi: 10.1016/j.apenergy.2018.09.025.

[12] Z. Liu, M. Wei, P. Song, S. Emhardt, G. Tian, and Z. Huang, “The fluid-thermal-solid coupling analysis of a scroll expander used in an ORC waste heat recovery system,” Applied Thermal Engineering, vol. 138, pp. 72–82, Jun. 2018, doi: 10.1016/j.applthermaleng.2018.04.048.

[13] D. Ziviani et al., “Employing a Single-Screw Expander in an Organic Rankine Cycle with Liquid Flooded Expansion and Internal Regeneration,” Energy Procedia, vol. 129, pp. 379–386, Sep. 2017, doi: 10.1016/j.egypro.2017.09.239.
[14] B. Lei et al., “Development and experimental study on a single screw expander integrated into an Organic Rankine Cycle,” Energy, vol. 116, pp. 43–52, Dec. 2016, doi: 10.1016/j.energy.2016.09.089.
[15] F. Ayachi, E. B. Ksayer, P. Neveu, and A. Zoughaib, “Experimental investigation and modeling of a hermetic scroll expander,” Applied Energy, vol. 181, pp. 256–267, Nov. 2016, doi: 10.1016/j.apenergy.2016.08.030.
[16] H. Tang, H. Wu, X. Wang, and Z. Xing, “Performance study of a twin-screw expander used in a geothermal organic Rankine cycle power generator,” Energy, vol. 90, pp. 631–642, Oct. 2015, doi: 10.1016/j.energy.2015.07.093.
[17] L. P. M. Colombo, A. Lucchini, and L. Molinaroli, “Experimental analysis of the use of R1234yf and R1234ze(E) as drop-in alternatives of R134a in a water-to-water heat pump,” International Journal of Refrigeration, vol. 115, pp. 18–27, Jul. 2020, doi: 10.1016/j.ijrefrig.2020.03.004.
[18] P. Życzkowski, M. Borowski, R. Łuczak, Z. Kuczera, and B. Ptaszyński, “Functional Equations for Calculating the Properties of Low-GWP R1234ze(E) Refrigerant,” Energies, vol. 13, no. 12, p. 3052, Jun. 2020, doi: 10.3390/en13123052.
[19] J. Yang, Z. Sun, B. Yu, and J. Chen, “Modeling and optimization criteria of scroll expander integrated into organic Rankine cycle for comparison of R1233zd(E) as an alternative to R245fa,” Applied Thermal Engineering, vol. 141, pp. 386–393, Aug. 2018, doi: 10.1016/j.applthermaleng.2018.06.001.
[20] E. W. Lemmon and I.H. Bell and M. L. Huber and M. O. McLinden, NIST Standard Reference Database 23: Reference Fluid Thermodynamic and Transport Properties-REFPROP, Version 10.0, National Institute of Standards and Technology. 2018.
[21] I. H. Bell, V. Lemort, E. A. Groll, J. E. Braun, G. B. King, and W. T. Horton, “Liquid flooded compression and expansion in scroll machines – Part II: Experimental testing and model validation,” International Journal of Refrigeration, vol. 35, no. 7, pp. 1890–1900, Nov. 2012, doi: 10.1016/j.ijrefrig.2012.07.008.